Removing extragalactic foregrounds in CMB lensing reconstruction

In collaboration with: Simone Ferraro, Emmanuel Schaan, Omar Darwish, Blake Sherwin

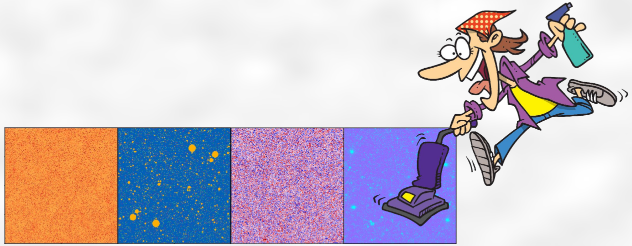

CMB lensing

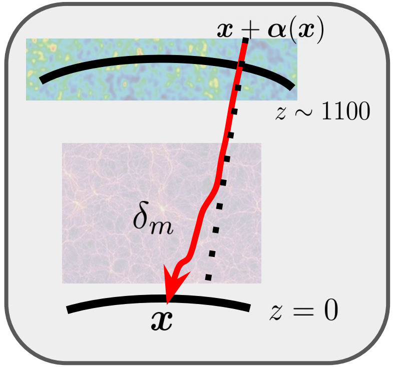

$$T^{\text{lensed}}(\boldsymbol{x}) = T^{\text{unlensed}}(\boldsymbol{x}+\boldsymbol{\alpha}(\boldsymbol{x}))$$

Conventionally measure lensing convergence

$$\boxed{\kappa = -\frac{1}{2}\boldsymbol{\nabla}\cdot\boldsymbol{\alpha}} \sim \int dz\, W^{\kappa}(z)\,\delta_m$$

Clean probe of late-time structure evolution: $\sigma_8(z)$, neutrino masses, gravitational slip, etc.

Why is this interesting now?
Rapid advances in sensitivity

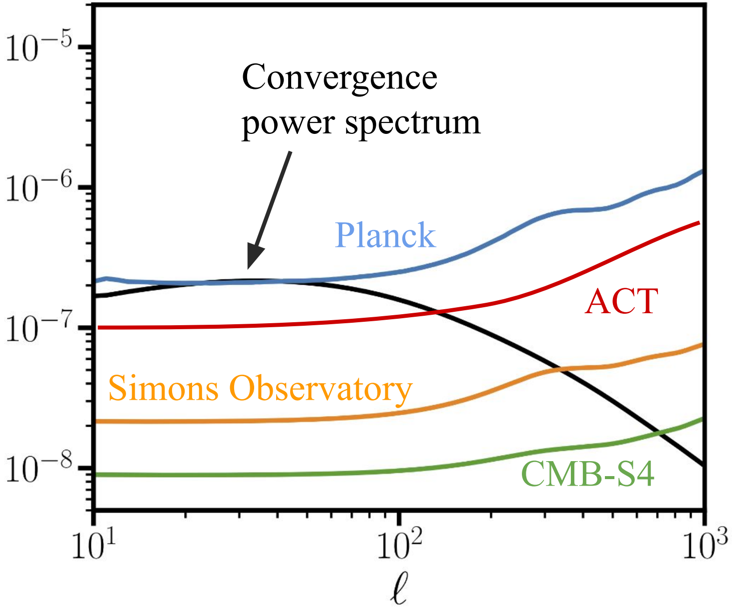

CMB lensing reconstruction – quadratic estimators (QE)

Unlensed CMB statistically isotropic

$$\langle T_{\boldsymbol{\ell}} T_{\boldsymbol{L}-\boldsymbol{\ell}} \rangle \propto \delta^D_{\boldsymbol{L}}$$

For a *fixed* lensing field, anisotropy is broken

$$\langle T_{\boldsymbol{\ell}} T_{\boldsymbol{L}-\boldsymbol{\ell}} \rangle_{\text{at fixed } \kappa_{\boldsymbol{L}}} = f^{\kappa}_{\boldsymbol{\ell},\boldsymbol{L}-\boldsymbol{\ell}} \, \kappa_{\boldsymbol{L}} + \cdots$$

$$f^{\kappa}_{\boldsymbol{\ell},\boldsymbol{L}-\boldsymbol{\ell}} \equiv \frac{2\boldsymbol{L}}{L^2} \cdot \left[\boldsymbol{\ell} C^0_{\ell} + (\boldsymbol{L}-\boldsymbol{\ell}) C^0_{|\boldsymbol{L}-\boldsymbol{\ell}|} \right]$$

Solve for κ!

$$\hat{\kappa}_{\boldsymbol{L}} = \frac{T_{\boldsymbol{\ell}} T_{\boldsymbol{L}-\boldsymbol{\ell}}}{f^{\kappa}_{\boldsymbol{\ell},\boldsymbol{L}-\boldsymbol{\ell}}}$$

Spatial averages = ensemble averages

$$\boxed{\hat{\kappa}_{\boldsymbol{L}} = N_{\boldsymbol{L}} \int_{\boldsymbol{\ell}} F^{\kappa}_{\boldsymbol{\ell},\boldsymbol{L}-\boldsymbol{\ell}} \, T_{\boldsymbol{\ell}} T_{\boldsymbol{L}-\boldsymbol{\ell}}}$$

Weights F are *arbitrary*, typically chosen to minimize variance (standard QE: Hu, Okamoto 2002)

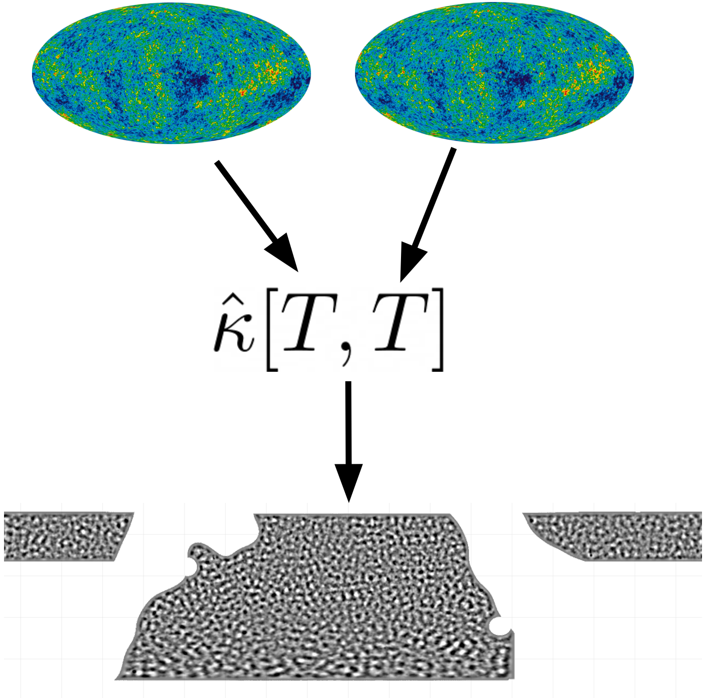

CMB lensing biases (extragalactic)

Standard QE runs into trouble when foregrounds are:

- **non-Gaussian**
- **correlated with the lensing convergence**

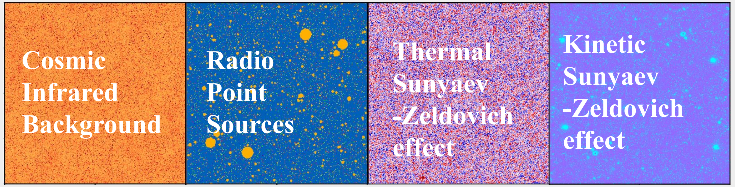

Sehgal et al. 2010

Suppose $\mathbf{T} = \mathbf{T}^{\mathbf{CMB}} + \mathbf{s}$, with s some foreground

- Bias to auto-correlation

$$\langle \hat{\kappa}[T,T]\hat{\kappa}[T,T]\rangle \sim C^{\kappa\kappa} + \underbrace{\langle \hat{\kappa}[T^{\mathrm{CMB}},T^{\mathrm{CMB}}]\hat{\kappa}[s,s]\rangle + \langle \hat{\kappa}[T^{\mathrm{CMB}},s]\hat{\kappa}[T^{\mathrm{CMB}},s]\rangle}_{\text{primary and secondary biases } \sim\langle \kappa s s\rangle} + \underbrace{\langle \hat{\kappa}[s,s]\hat{\kappa}[s,s]\rangle}_{\text{trispectrum bias}}$$

- Bias to cross-correlation

$$\langle \hat{\kappa}[T,T]g\rangle \sim C^{\kappa g} + \langle \hat{\kappa}[s,s]g\rangle$$

For ACT-like survey, extragalactic foregrounds can yield ~ **10σ** biases to auto and cross (Schaan & Ferraro 2018)

Two remedies: (1) bias-hardening and (2) multifrequency techniques

(1) Bias hardening – theory

Basic idea: build a QE for s, and subtract s from κ

- To build the source estimator, generalize the response function

$$\langle TT \rangle = f\ \kappa + \cdots \quad \longrightarrow \quad f^{\kappa} = \frac{\langle TT\kappa \rangle}{\langle \kappa\kappa \rangle}$$

- For a source

$$\langle ss \rangle = f^{s}\ s \quad \longrightarrow \quad f^{s} = \frac{\langle sss \rangle}{\langle ss \rangle}$$

from which we build the minimum variance source QE

Can evaluate using halo model for Poisson sources with identical profiles

No assumptions about trispectrum (or higher order statistics) needed!

- In the presence of a single foreground $\langle TT \rangle = f^{\kappa}\ \kappa + f^{s}\ s$

Bias hardening: take linear combination that nulls bias

$$\boxed{\begin{pmatrix} \hat{\kappa}^{\mathrm{BH}}_{\boldsymbol{L}} \\ \hat{s}^{\mathrm{BH}}_{\boldsymbol{L}} \end{pmatrix} = \begin{pmatrix} 1 & N^{\kappa}_{\boldsymbol{L}}\mathcal{R}_{\boldsymbol{L}} \\ N^{s}_{\boldsymbol{L}}\mathcal{R}_{\boldsymbol{L}} & 1 \end{pmatrix}^{-1} \begin{pmatrix} \hat{\kappa}_{\boldsymbol{L}} \\ \hat{s}_{\boldsymbol{L}} \end{pmatrix}}$$

Namikawa, Hanson, Takahashi (2013)
Osborne, Hanson, Dore (2014)
Sailer, Schaan, Ferraro (2020)

Easy to generalize to N foregrounds (just a bigger matrix)

Bias hardening – results

Lower bias, lower noise ☺

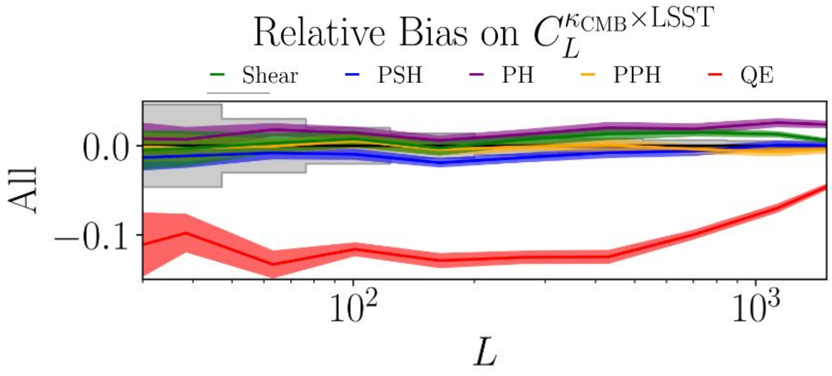

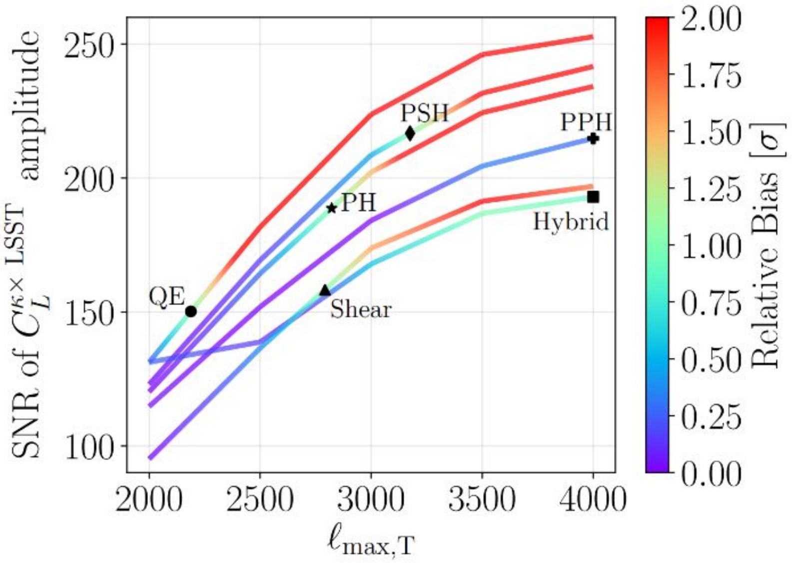

150 GHz map, SO-like map noise
Biases computed using Sehgal simulations (Sehgal et al. 2010)

Sailer Schaan Ferraro (2020)

(2) Multifrequency techniques

Spectral dependence of e.g. tSZ and CIB are known

Traditional approach: take linear combinations of CMB maps at different frequencies to "deproject" foregrounds

$$\hat{T}_{\boldsymbol{\ell}} = \boldsymbol{w}_{\ell}^T \boldsymbol{T}_{\boldsymbol{\ell}}$$

Some "not-so-obvious" problems

- Deprojecting tSZ boosts CIB
- Deprojecting CIB boosts tSZ

Need to deproject both? Huge noise price!

Can we compromise?

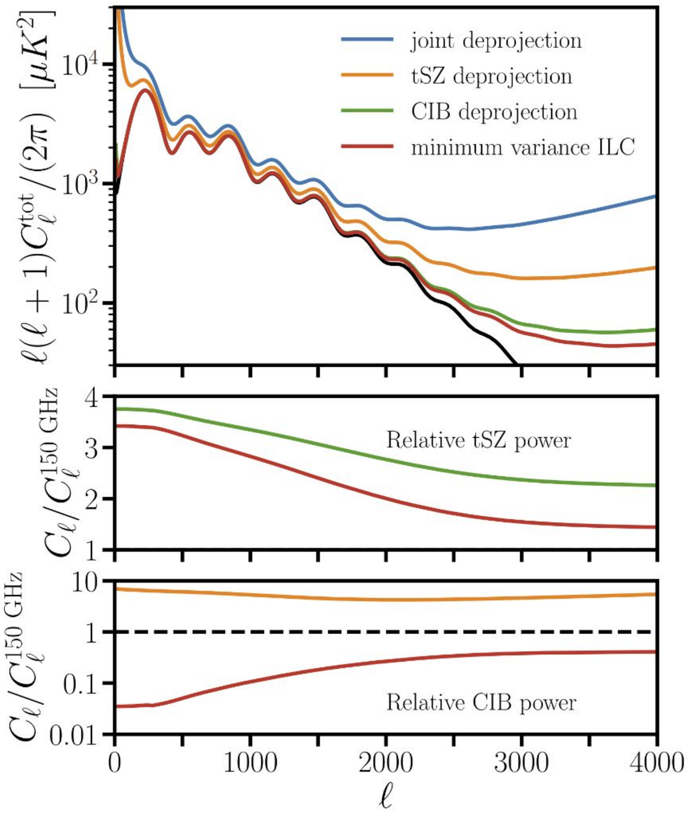

Sailer, Schaan, Ferraro, Darwish, Sherwin 2021

Multifrequency techniques

Very simple compromise – draw a line:

$$\boldsymbol{w}_\ell(t) = t\boldsymbol{X}_\ell + (1-t)\boldsymbol{w}_\ell^{\rm ILC}$$

Empirically find, for SO-like instrument, t~0.2 to reduce bias/noise < ½

Only need to pay a ~10% cost in noise, instead of a factor of 2

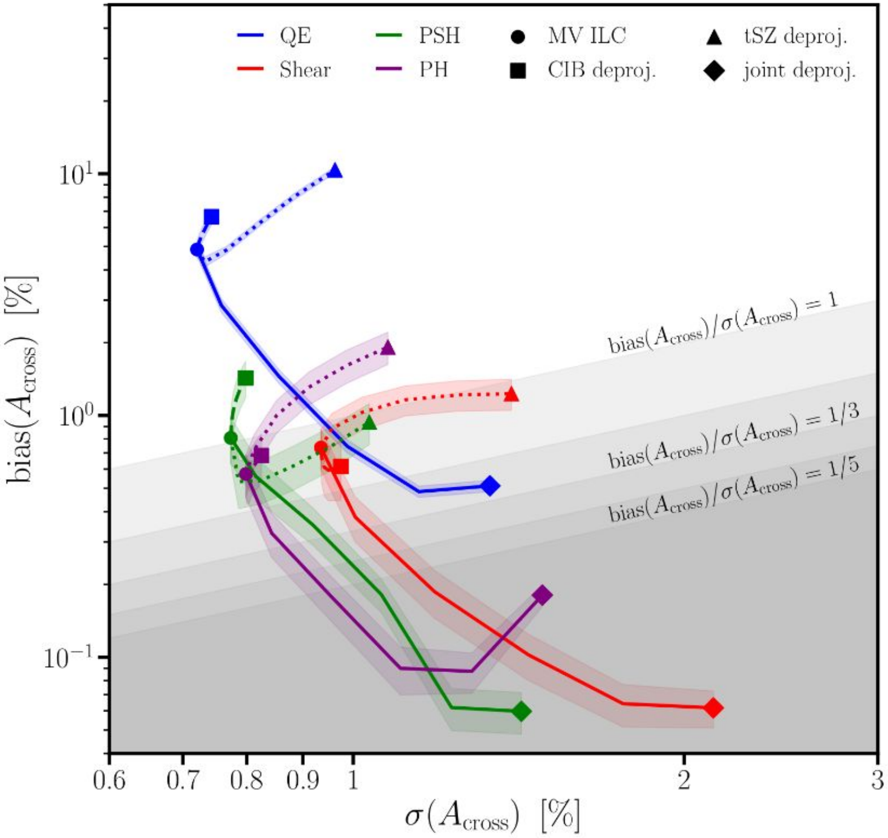

Sailer, Schaan, Ferraro, Darwish, Sherwin (2021)

Summary

- Extragalactic foregrounds bias standard QE by ~ **10σ**
- Naive approach (deproject CIB and tSZ) increases noise by **2x**
- Bias-hardening + partial deprojection: unbiased at ~**10%** noise cost

Outlook/future

- Generalize bias-hardening to polarization (in prep.)
- DESI x ACT

Forecast for Recovery of r in CMB-Bharat: *Dust complexities and optimum range of frequency*

CMB
भारत
CMB BHĀRAT: AN INDIAN COSMOLOGY CONSORTIUM

Cosmology From Home 2022

Aparajita Sen
IISER Thiruvananthapuram, India

CMB-Bharat

- A next generation satellite mission proposed to indian space agency .
- Detection of CMB B-Mode among key scientific goals
- CMB-Bharat aims to detect r=0.001 at a confidence level of 3σ

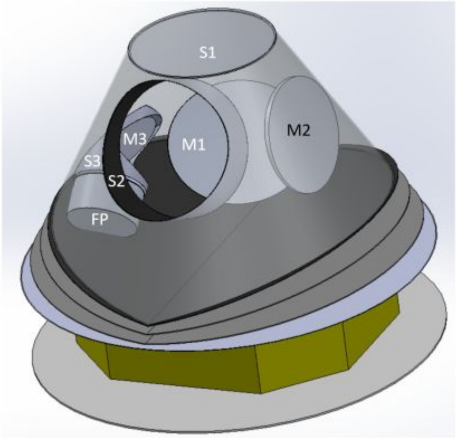

Frequency Bands: 28-850 GHz
Resolution: 5-1.8 arcmin

The Challenges in Detection of B-mode

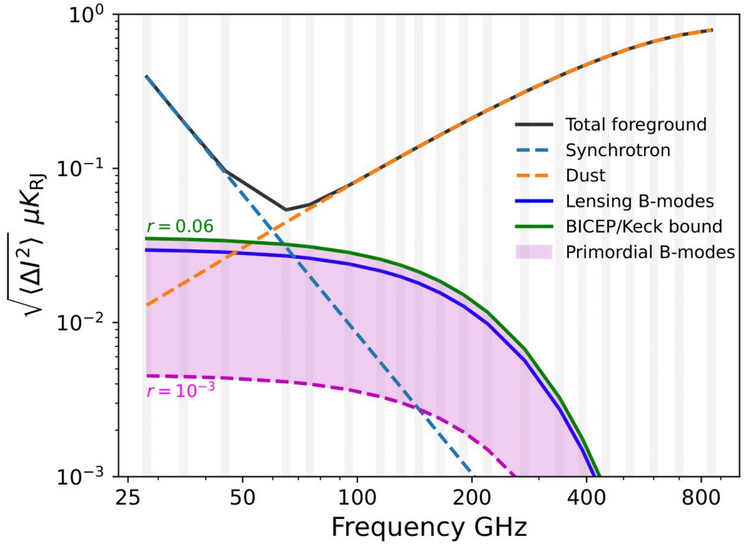

High level of foregrounds: Increase the frequency range of observations.

Contamination from lensing: Delensing methods

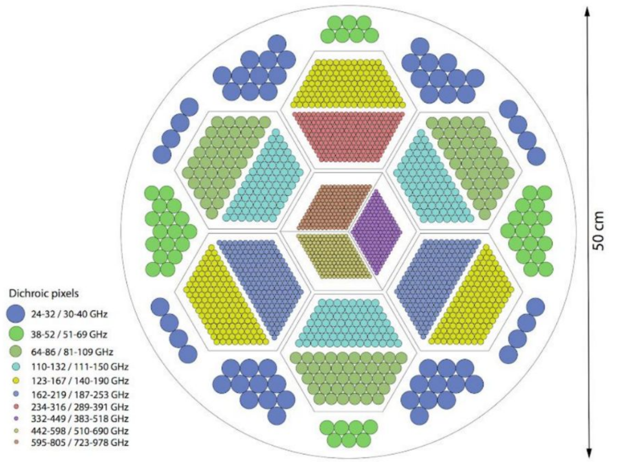

Overview

This Talk is based on the following two works:

- **B-mode forecast of CMB-Bhārat,**

  Debabrata Adak, Aparajita Sen, Soumen Basak, Jacques Delabrouille, Tuhin Ghosh, Aditya Rotti, Ginés Martínez-Solaeche, Tarun Souradeep,*Monthly Notices of the Royal Astronomical Society*, Volume 514, Issue 2, August 2022, Pages 3002–3016

- **Optimum Range of Frequency for Thermal Dust Removal in CMB-Bhārat,**

  Aparajita Sen, Debabrata Adak, Soumen Basak, Tuhin Ghosh. (Manuscript under preparation)

Overview:

- Test the ability of CMB-Bharat to detect CMB-B-mode
- We consider a range of foreground components.
- We also account for complexities in dust and synchrotron modelling.
- Frequency bands higher than 100GHz are dominated by thermal dust.
- How to improve the performance of component separation techniques?
- Increase the frequency range for dust observations.
- Is this true for CMB-Bharat frequency configuration?

Thermal Dust Models

The thermal dust emission is empirically modelled Modified Black Body Spectra at a single temperature

$$I_\nu = A_D^I \left(\frac{\nu}{\nu_0}\right)^{\beta_d} B_\nu(T_d).$$

This modelling does not account for line-of-sight effects, variation in dust composition and size and the galactic magnetic field

Some of these effects leads to frequency decorrelation.

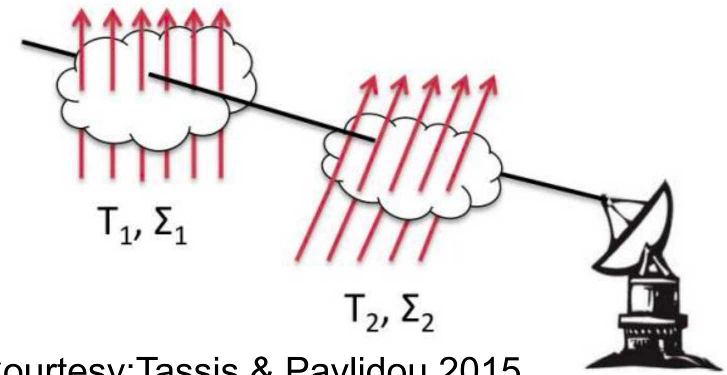

Courtesy:Tassis & Pavlidou,2015

Complex Thermal Dust Models

- **The MKD-Dust model**: 3-dimensional modelling of dust which accounts for variation in dust properties along line-of-sight. *Martınez-Solaeche et.al, 2018*, Karakci & Delabrouille (2018)

$$I_\nu = \int_0^\infty dr \frac{d\tau(r,\nu_0)}{dr} \left(\frac{\nu}{\nu_0}\right)^{\beta(r)} B_\nu(T(r))$$

- **TD-dust model**: Generated from 3 phases of HI cloud. (*Ghosh et.al.2017 & Adak et.al. 2017*)
- **Physical dust model**: Accounts for physical properties of the dust grains (*Hensley&Draine 2017*)

r forecast : Baseline model

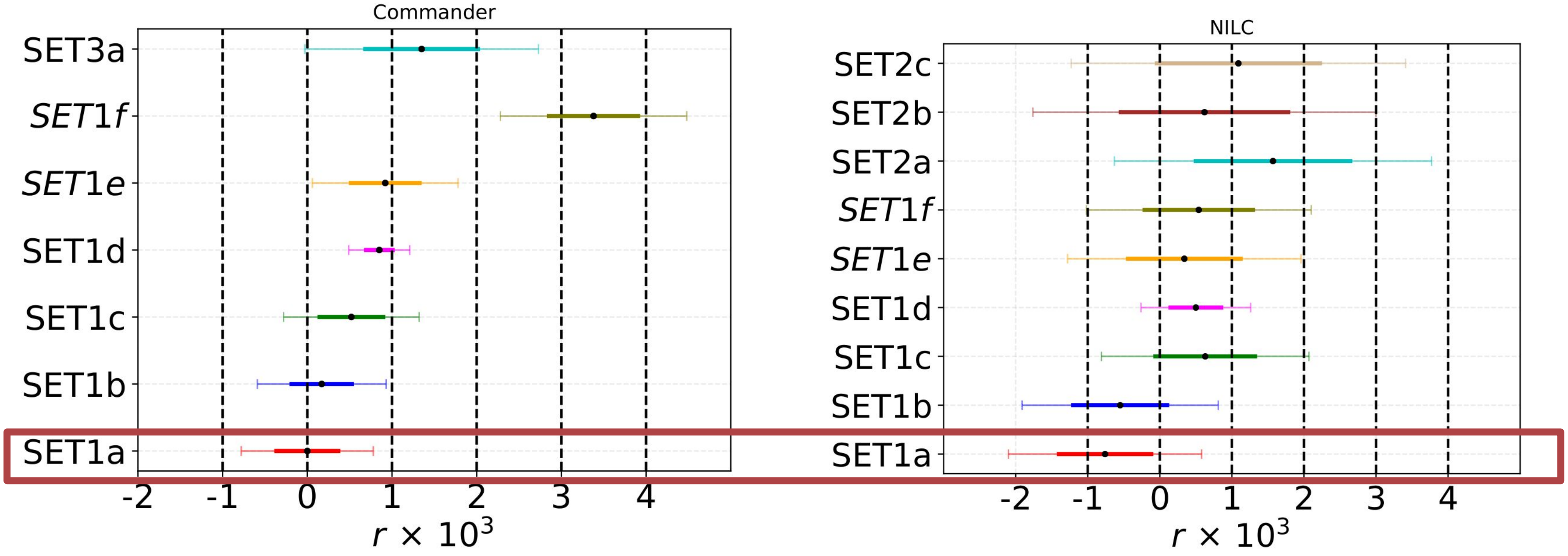

uncertainty= 0.0004-0.0007

r forecast : Dust Complexity

Sim.ID	NILC			Commander		
	$r_{mp} \times 10^3$	$\sigma(r_{mp})\times 10^3$	χ^2/dof	$r_{mp} \times 10^3$	$\sigma(r_{mp})\times 10^3$	χ^2/dof
SET1a	-0.76	0.67	0.60	-0.08	0.39	0.95
SET2a	1.57	1.10	1.11	47.45	1.48	33.72
SET2b	0.62	1.19	1.91	51.06	1.56	33.92
SET2c	1.09	1.16	1.90	34.82	1.43	25.57
SET3a	-	-	-	1.35	0.69	4.02
SET3b		-	-	188.41	5.93	123.0

MKD DUST

TD-DUST

Optimum range frequency channels

What is the frequency range at for which will ensure optimal removal of thermal dust component?

Henseley & Bull 2018 has shown that in some cases it is more beneficial to limit the observations at lower frequencies ~200-500 GHz.

Analysis done on single pixel of sky, parametric component separation

We analyse for CMB-Bharat frequency channels for the given noise budget

Analysis done on full sky, Blind component separation method used.

Results: Change in bias on r

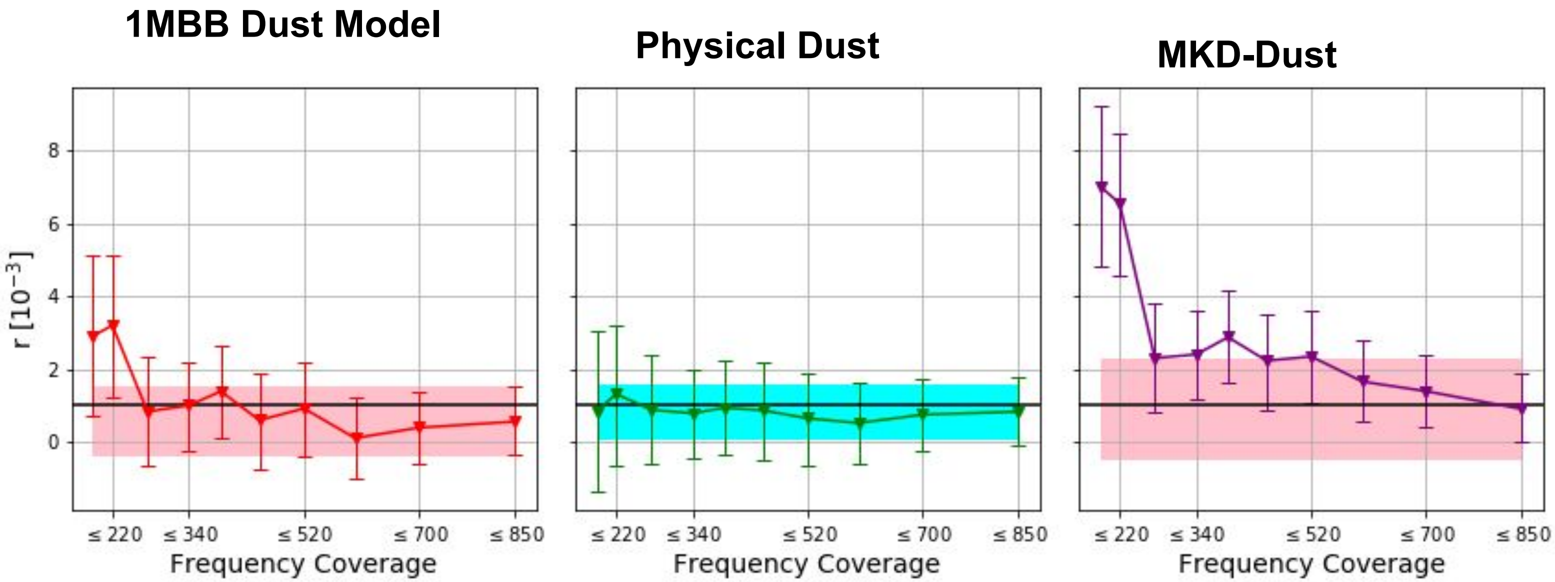

Results: Change in sensitivity of the instrument

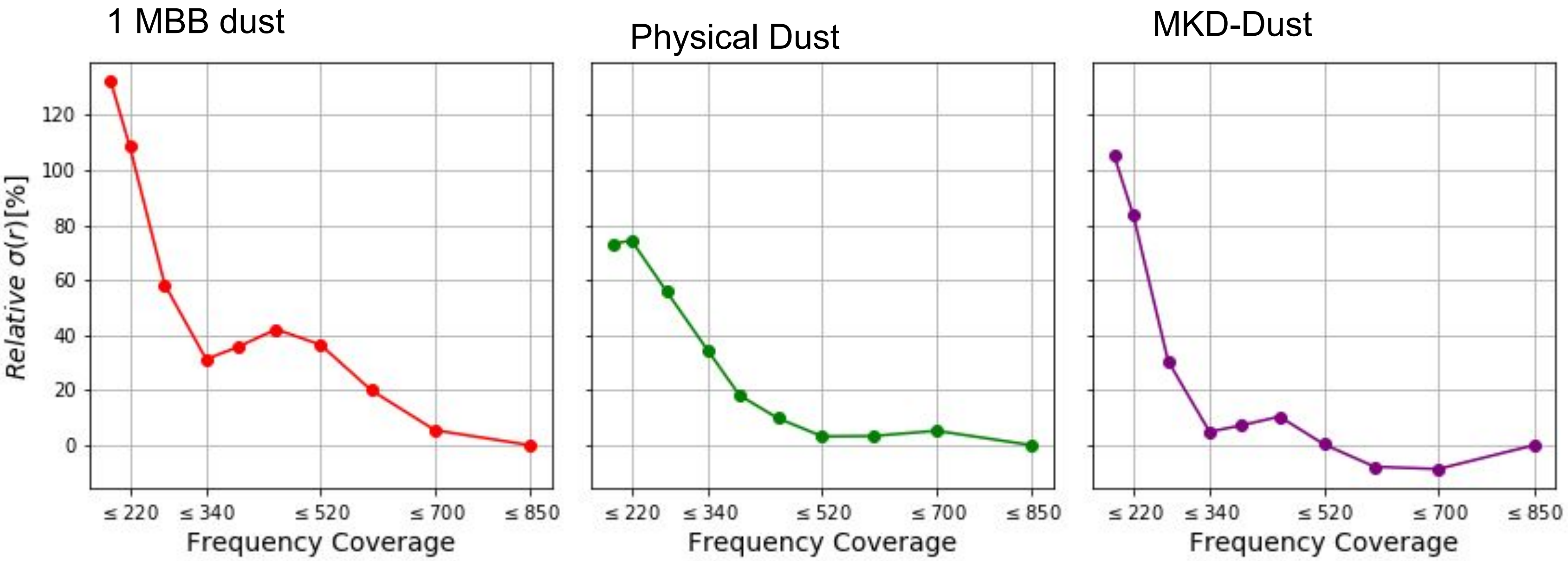

Conclusions

- The configuration of CMB-Bharat can recover $r \sim 0.001$.
- The bias in r increases in case of complex dust models such as the MKD-dust.
- Parametric methods are not suitable for frequency decorrelated dust models.
- Thermal dust observations upto 500 GHz is adequate for minimizing its contamination.

Thank You for Your Attention

E and B modes of the CMB y-type distortions: Polarised kinetic Sunyaev-Zeldovich effect.

ICTP Summer School on Cosmology 2022

Aritra Kumar Gon
Rishi Khatri

tifr

MAX-PLANCK-GESELLSCHAFT

July 2022

Electron peculiar velocities at second order generate E and B mode polarisation: The pkSZ effect

- Free electrons produced during reionisation, have peculiar velocities $(\mathbf{v})$.
- In the electron rest frame, the CMB is not isotropic. Has a quadrupolar anisotropy $\propto \mathbf{v}^2$.
    - Non-linear nature of Relativistic Doppler shift.
    - A non-linear relation between temperature and intensity in the Planck spectrum
- Thomson Scattering generates linear polarisation in the CMB.
- First predicted by Sunyaev and Zeldovich in 1980. (MNRAS,190:413-420)
- Previous studies (Renaux-Petel et. al. arXiv:1213.4448) (Kamionkowski et. al. arXiv: 2203.12503)

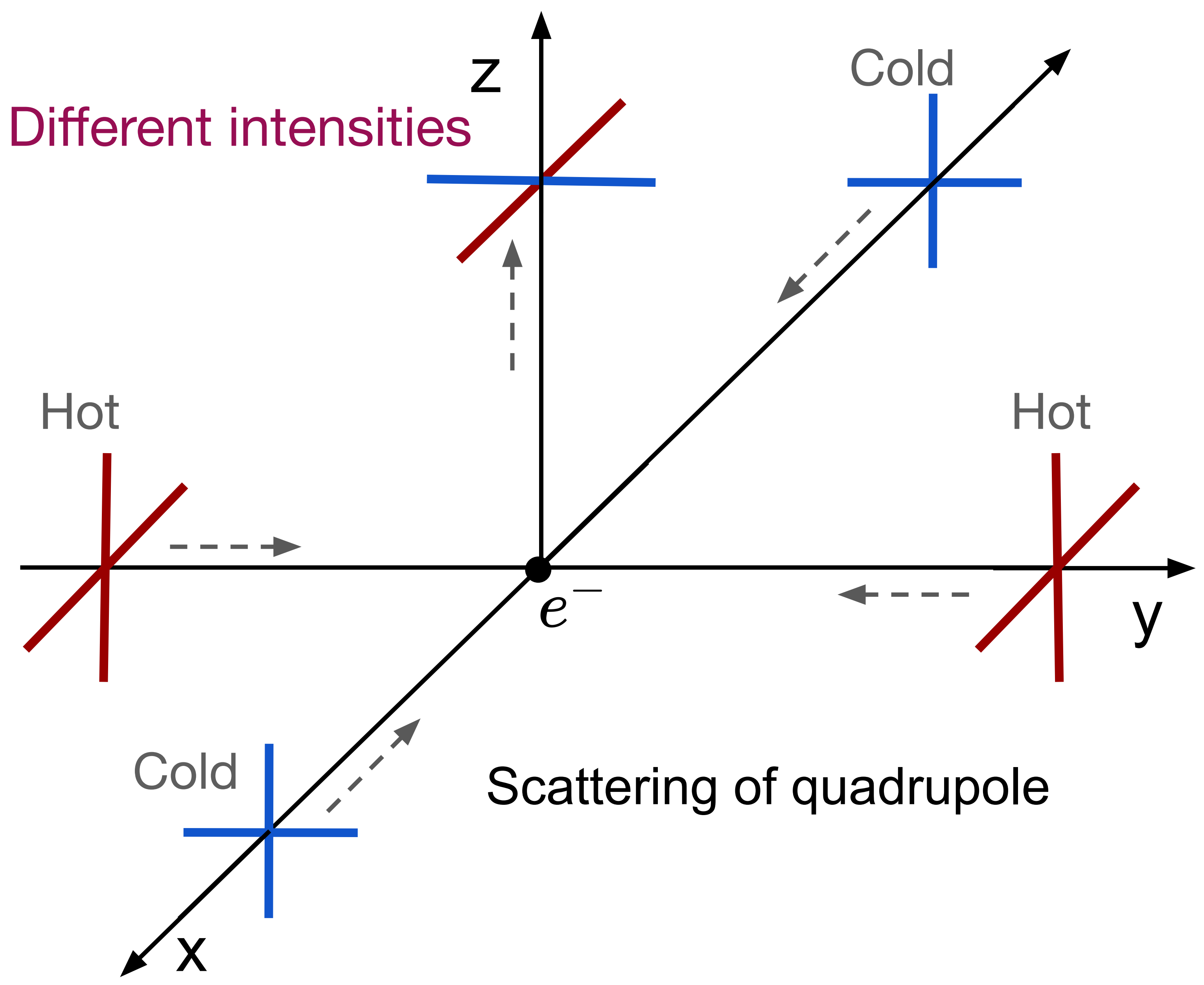

Beating the cosmic variance with pkSZ effect

★Full sky angular power spectra of the E and B modes

★Sensitive to reionisation central redshift, width and the matter power spectrum.

★Spectrum consists of y-type distortions part.

★Differentiates it from primary CMB signals with blackbody spectrum and other SZ-type signals, which are unpolarised.

★Free from the cosmic variance of the primary CMB polarisation signal and lensing B modes.

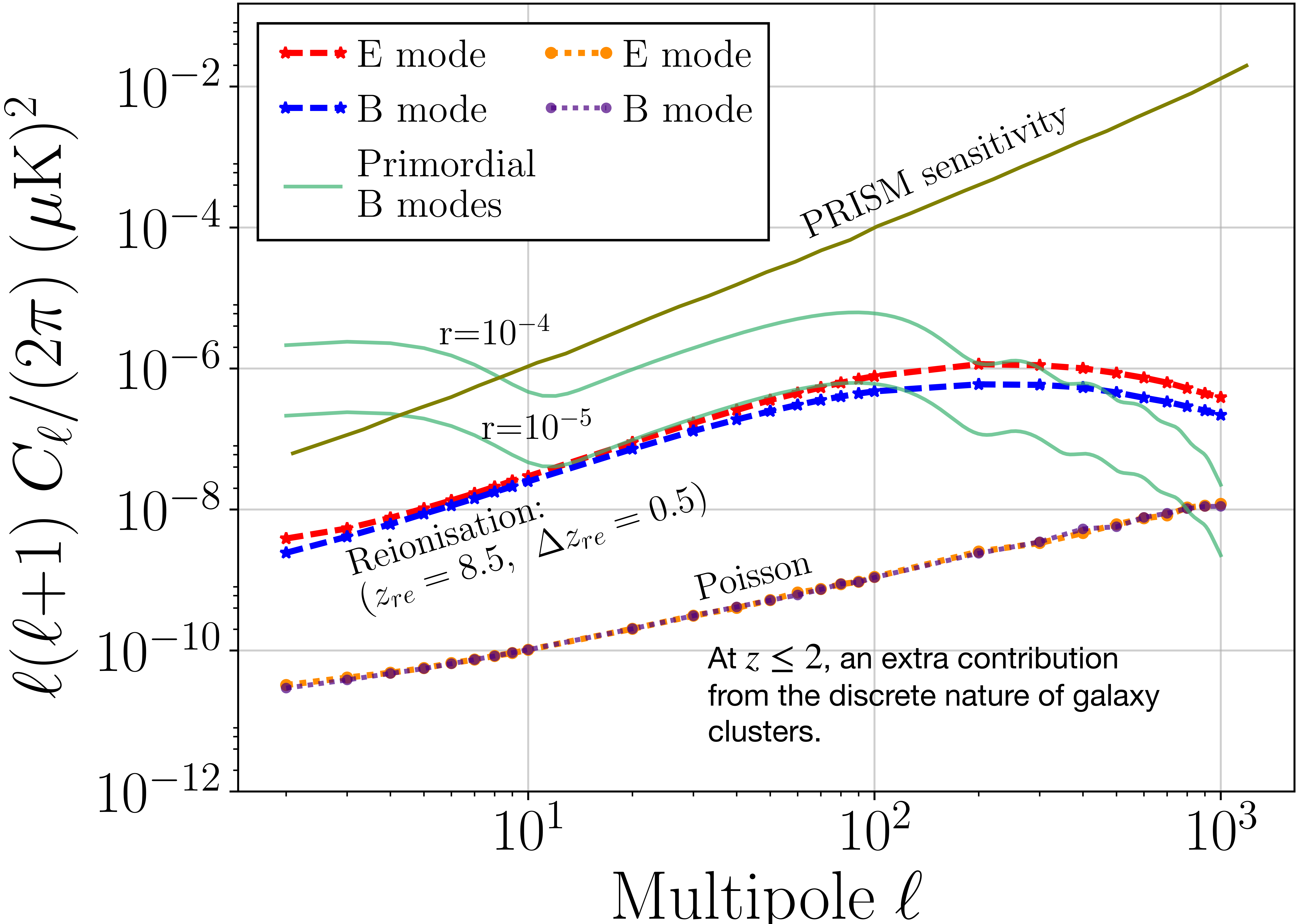

The scattered spectrum has a y-type distortion

- Photons from different blackbody spectra with different temperatures mix.
- Scattered spectrum not only has a differential blackbody but also a y-type distortion also.

$$\left(\frac{\delta I}{I} \equiv \mathcal{I}_{\rm sc}\right)\Big|_{\rm (quadrupolar)} = 2\left(\mathbf{v}\cdot\hat{\mathbf{n}}'\right)^2 g(x) + \frac{1}{2} y(x) \left(\mathbf{v}\cdot\hat{\mathbf{n}}'\right)^2$$

$$g(x) = \frac{xe^x}{(e^x-1)} \qquad y(x) = \frac{xe^x}{(e^x-1)}\left(x\frac{e^x+1}{e^x-1} - 4\right)$$

Planck Spectrum: $n_\nu(x) = \dfrac{1}{(e^x-1)}$ $\quad x = \dfrac{h\nu}{k_B T_0}$

- Distinguishable from the primary polarisation signals which only have a blackbody spectrum.
- Differentiable from other y-type signals, such as the thermal SZ effect which are unpolarised.

Polarisation field and angular power spectra

- The polarisation field :

$$\left(\mathcal{Q} \pm i\mathcal{U}\right)\left(\hat{\mathbf{n}}\right) \equiv P_{\pm}\left(\hat{\mathbf{n}}\right)$$

$$a_{\ell m} = \int P_{+}\left(\hat{\mathbf{n}}\right)\ {}_2Y^*_{\ell m}\left(\hat{\mathbf{n}}\right) d^2\hat{\mathbf{n}}$$

1. Polarisation field is a spin-2 field.
2. Electron number density - only a function of time.
3. Transverse velocity.

- Construct spin-0 fields related to the polarisation field.

$$e_{\ell m} = \frac{1}{2}\left(a_{\ell m} + (-1)^m a^*_{\ell -m}\right) \qquad b_{\ell m} = \frac{-i}{2}\left(a_{\ell m} - (-1)^m a^*_{\ell -m}\right)$$

- The E and B mode power spectra :

$$\langle e_{\ell m} e^*_{\ell' m'} \rangle = C_\ell^{EE}\ \delta_{\ell,\ell'}\ \delta_{mm'}$$

$$\langle b_{\ell m} b^*_{\ell' m'} \rangle = C_\ell^{BB}\ \delta_{\ell,\ell'}\ \delta_{m,m'}$$

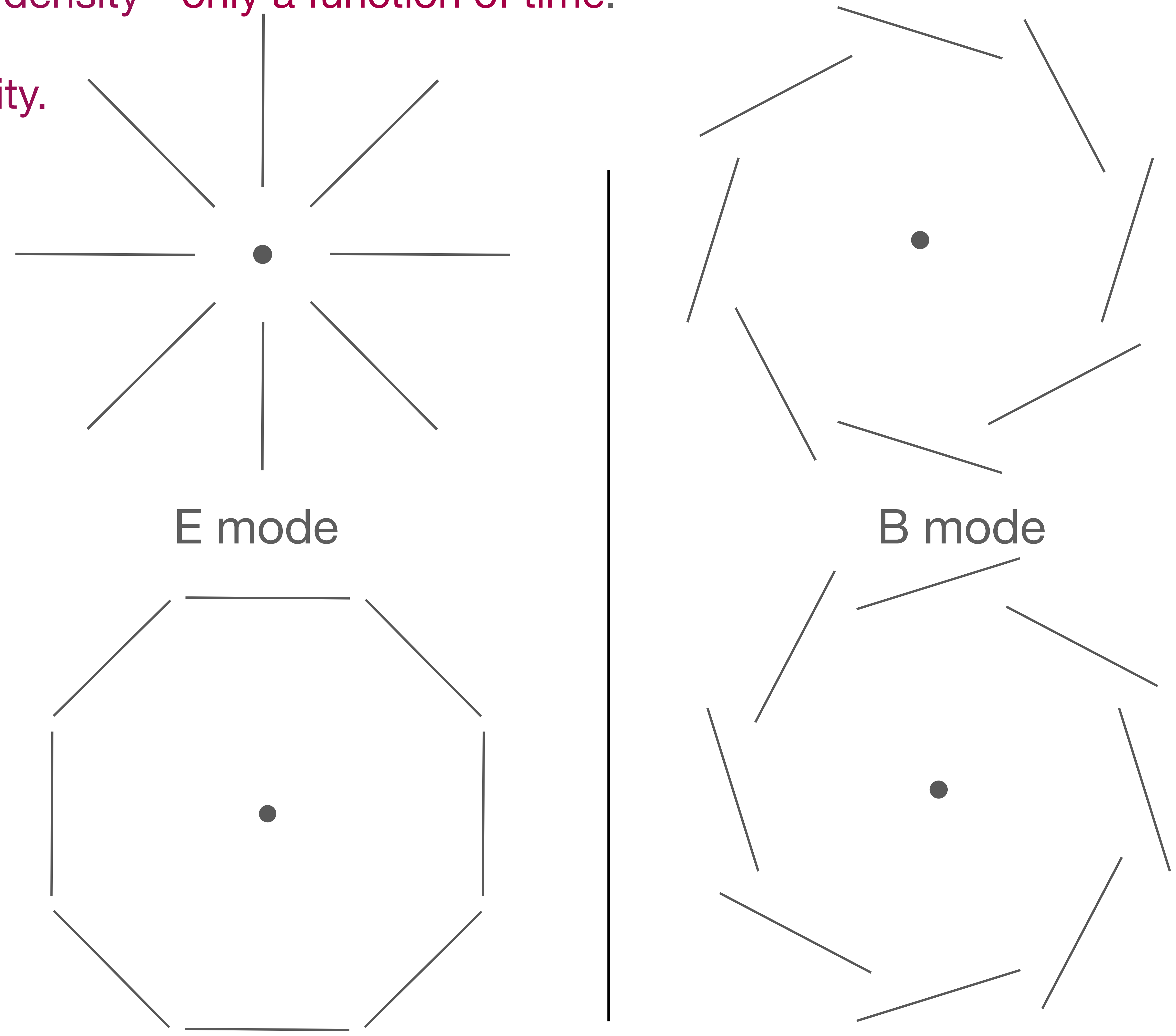

The power spectra at second order is a complicated function.

$$C_\ell^{BB} = \frac{T_{CMB}^2}{2}\left[(4\pi)\left(\frac{4\pi}{3}\right)^2\sqrt{\frac{3}{2\pi}}\frac{\sqrt{6}\sigma_T}{10}\right]^2 \sum_{\lambda,\lambda'=-2}^{2}(-1)^{(\lambda+\lambda')}\int_0^\chi d\chi\, e^{-\tau(\chi)}\,a(\chi)\int_0^\chi d\chi'\, e^{-\tau(\chi')}\times$$

$$a(\chi')\mathrm{n_e}(\chi)\mathrm{n_e}(\chi')\sum_{\substack{L,M\\L',M'}}\sum_{\substack{p_1,p_2\\p_1',p_2'}} i^{(L-L')}\begin{pmatrix}1 & 1 & 2\\ p_1 & p_2 & -\lambda\end{pmatrix}\begin{pmatrix}1 & 1 & 2\\ p_1' & p_2' & -\lambda'\end{pmatrix}\int\!\!\int\frac{k_1^2dk_1\,k_2^2dk_2}{(2\pi)^6}\times$$

$$P_{uu}(k_1)P_{uu}(k_2)\,j_L(k\chi)\,j_{L'}(k'\chi')\int d\Omega_{\mathbf{k}_1}\int d\Omega_{\mathbf{k}_2}\;Y^*_{L,M}(\hat{\mathbf{k}})Y_{L',M'}(\hat{\mathbf{k}})Y^*_{1p_1}(\hat{\mathbf{k}}_1)Y^*_{1p_2}(\hat{\mathbf{k}}_2)\times$$

$$Y_{1p_1'}(\hat{\mathbf{k}}_1')Y_{1p_2'}(\hat{\mathbf{k}}_2')\,A_{\ell m}^{\lambda LM}\,A_{\ell m}^{\lambda' L' M'}\left(1-(-1)^{(L+\ell)}\right)\left(1-(-1)^{(L'+\ell')}\right)$$

Wigner 3j symbols

Matter Velocity power spectrum

Spherical Bessel functions

Where $A_{\ell m}^{\lambda LM} = \sqrt{\frac{5(2L+1)(2\ell+1)}{4\pi}}(-1)^{(m)}\begin{pmatrix}L & 2 & \ell\\ 0 & -2 & 2\end{pmatrix}\begin{pmatrix}L & 2 & \ell\\ M & \lambda & -m\end{pmatrix}.$

pKSZ effect is sensitive to the redshift of central reionization

- The power spectra increase with the increase in the central redshift of reionisation
  - Increasing the central redshift increases the total Thomson optical depth

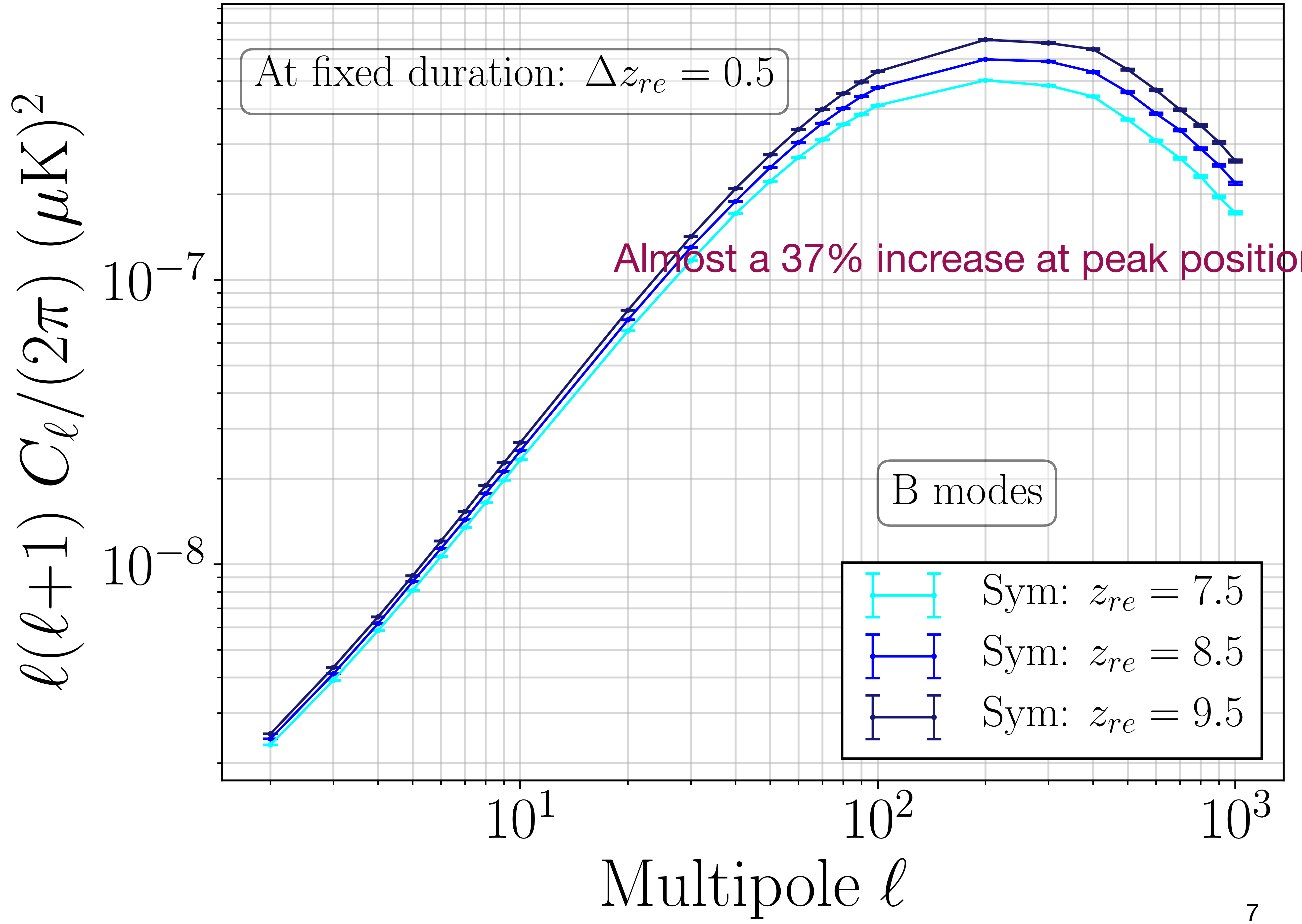

Almost a 37% increase at peak position between $z_{\rm re} = 7.5$ to $z_{\rm re} = 9.5$

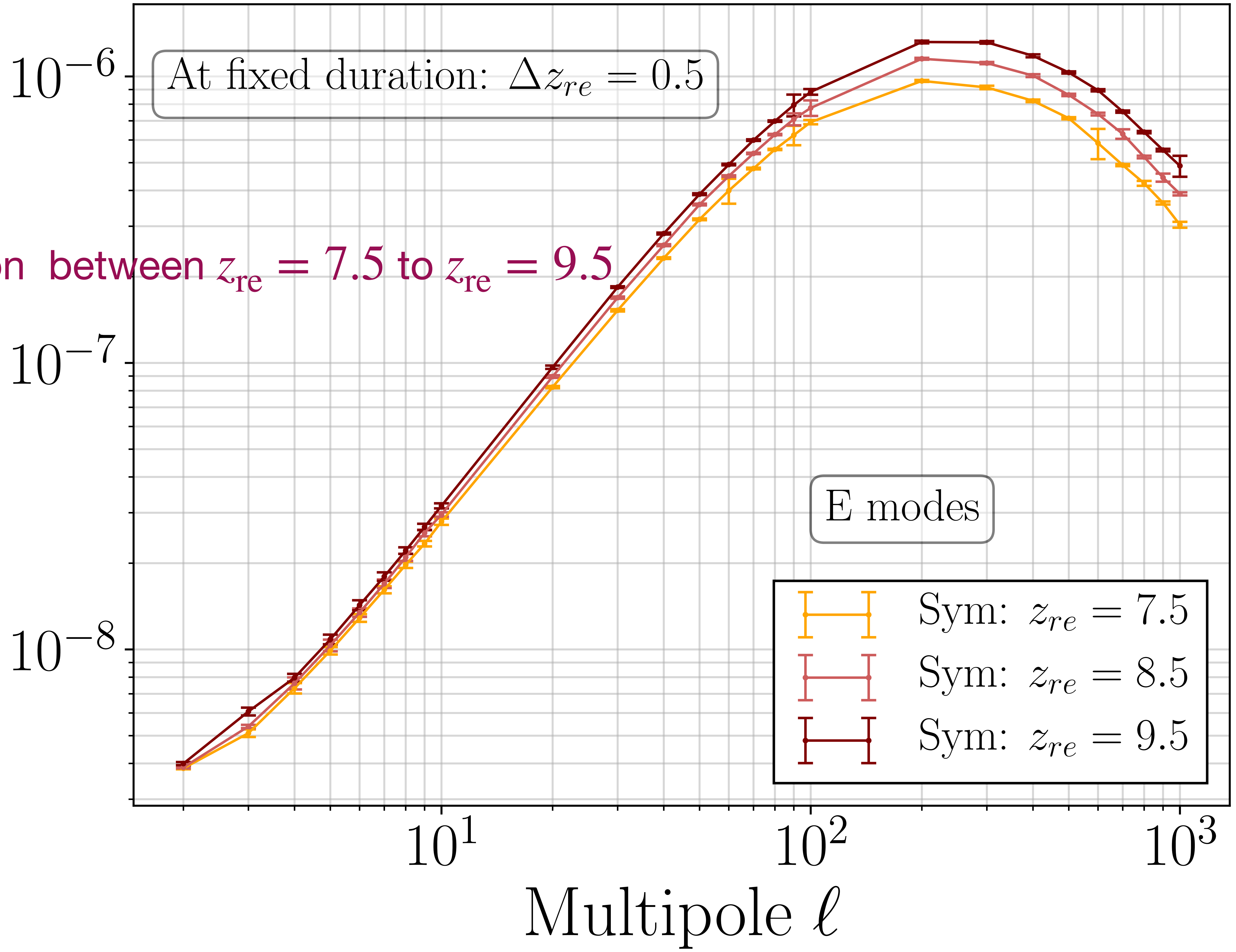

pkSZ effect is sensitive to the reionisation width

- Changing the width at a fixed central redshift has a negligible effect on the optical depth
- The power spectra still decrease with the increase in the duration of reionisation.

$$\text{Width} = z_{99\%} - z_{10\%}$$

pkSZ effect is sensitive to the reionisation width

- Changing the width at a fixed central redshift has a negligible effect on the optical depth
- The power spectra still decrease with the increase in the duration of reionisation.

$$\text{Width} = z_{99\%} - z_{10\%}$$

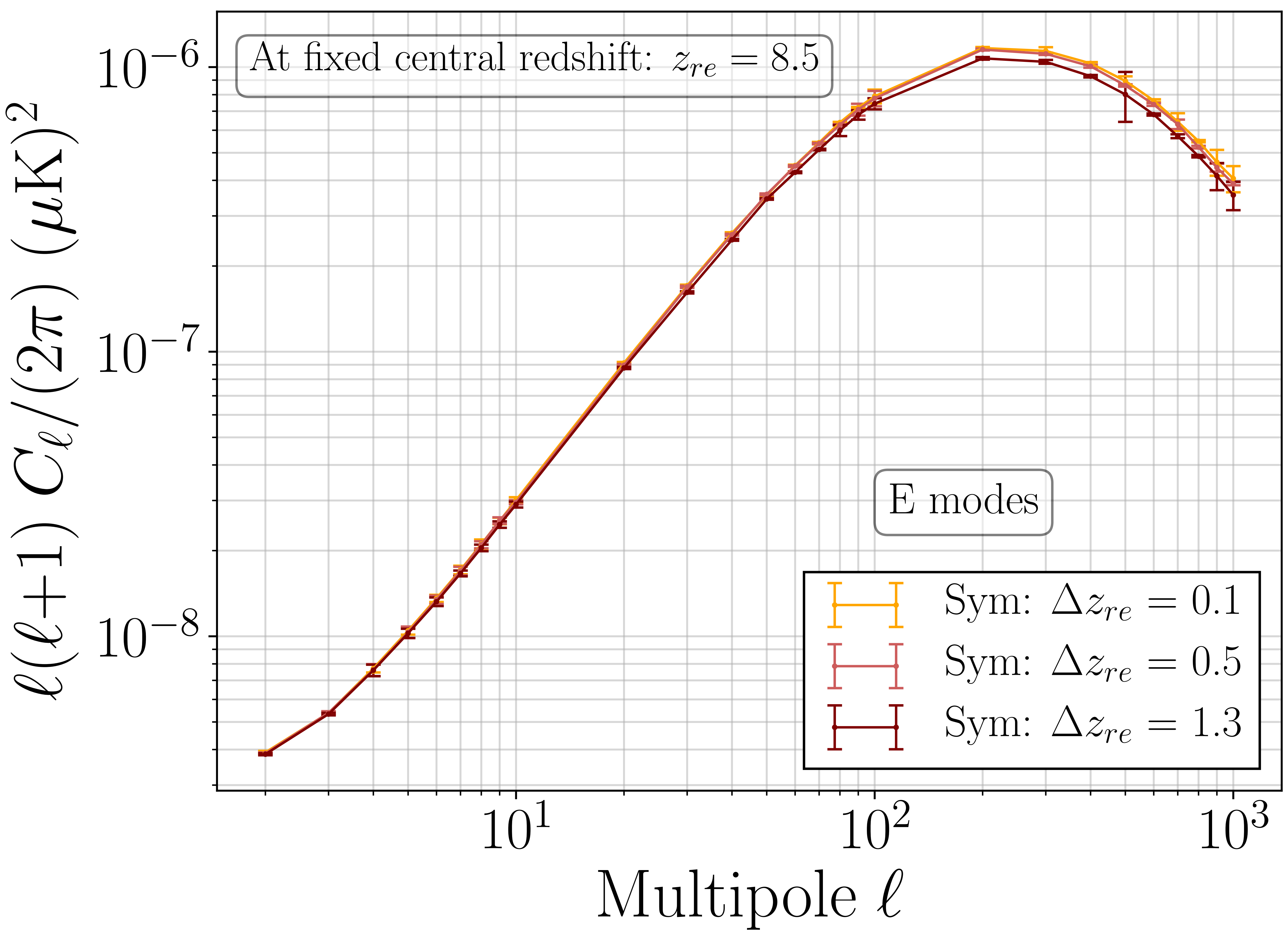

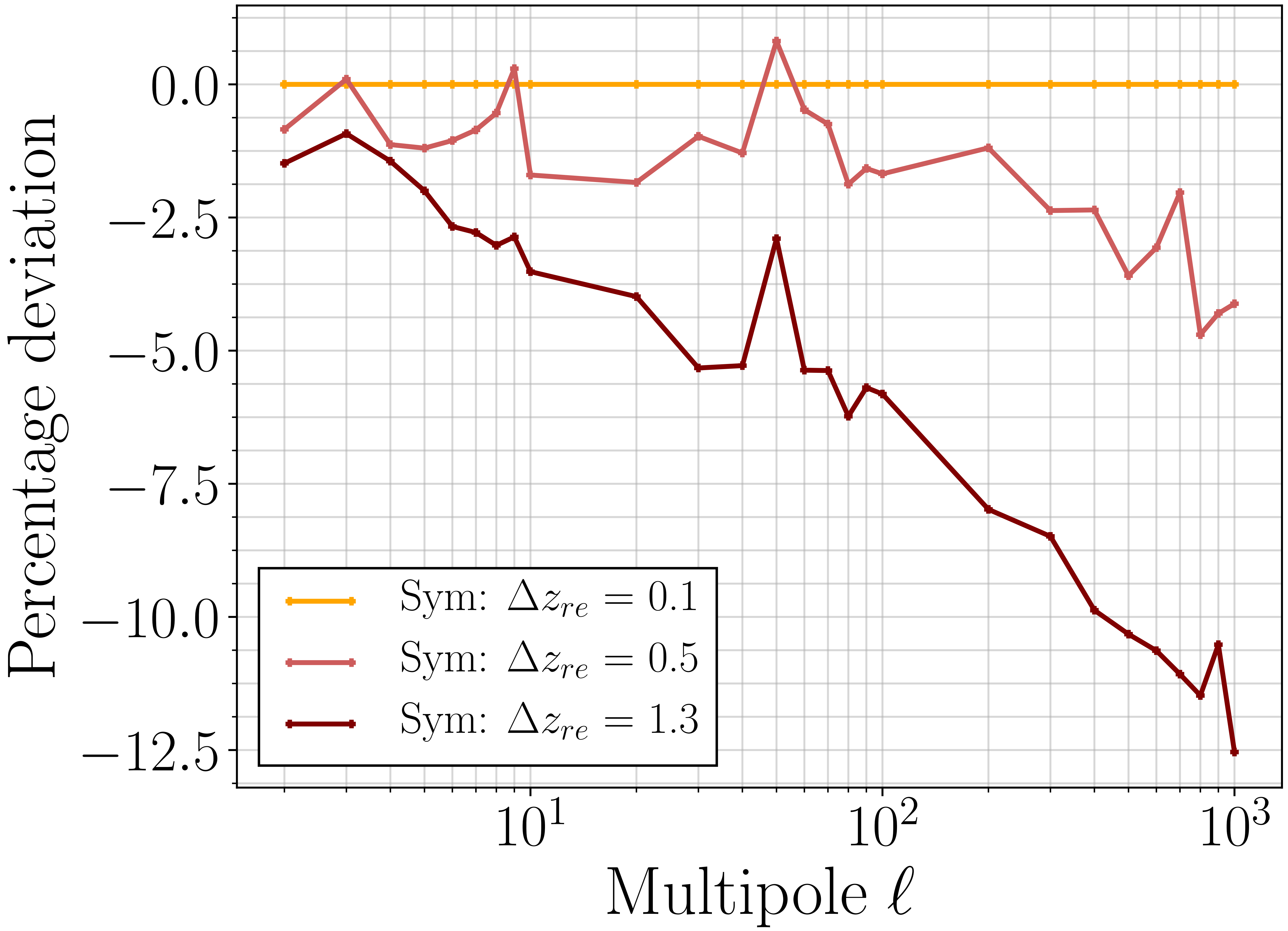

E modes greater than the B modes

Scalar ($\lambda = 0$), Vector ($\lambda = 1$) and Tensor ($\lambda = 2$) Decomposition

Auto-correlations

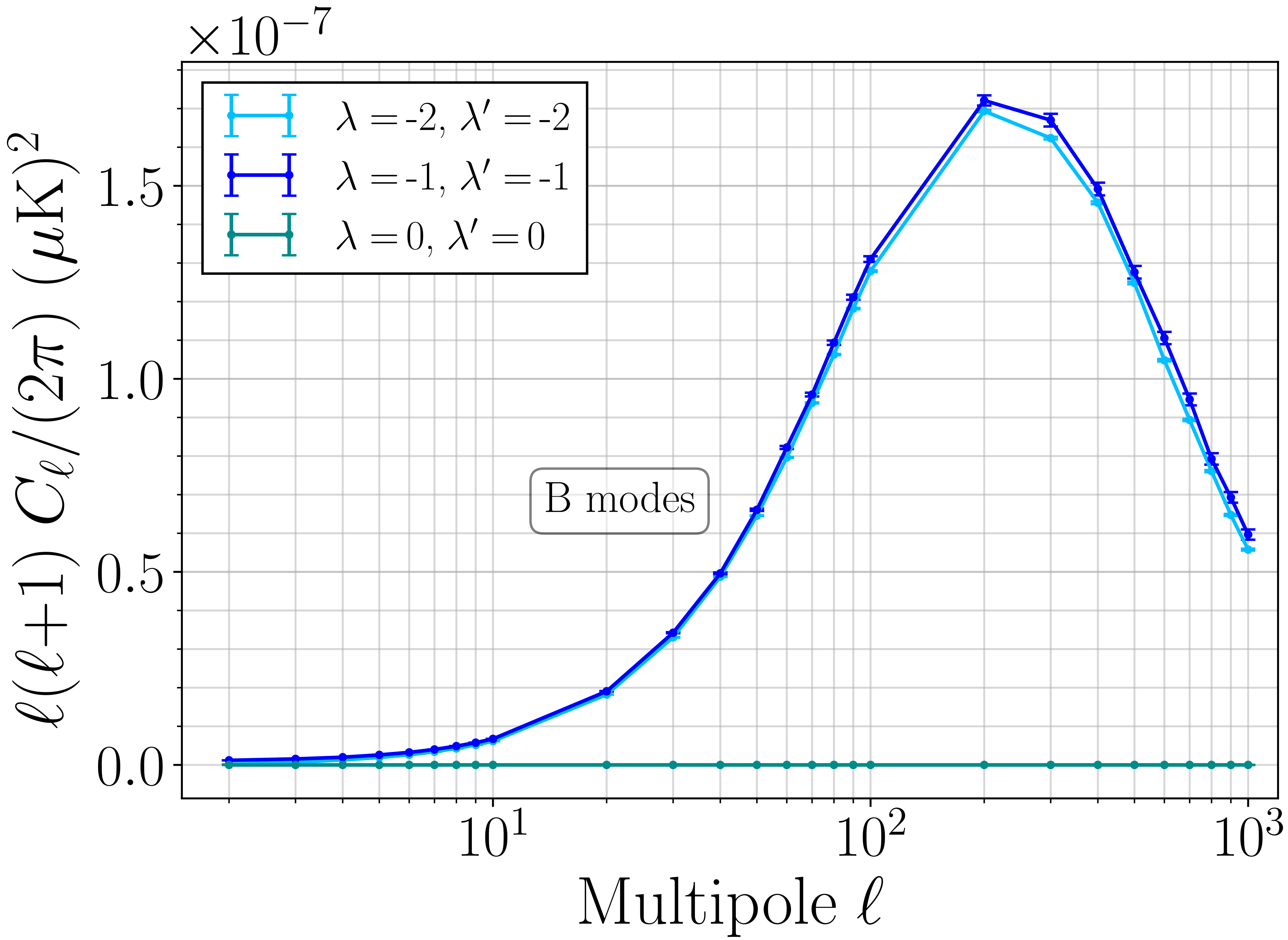

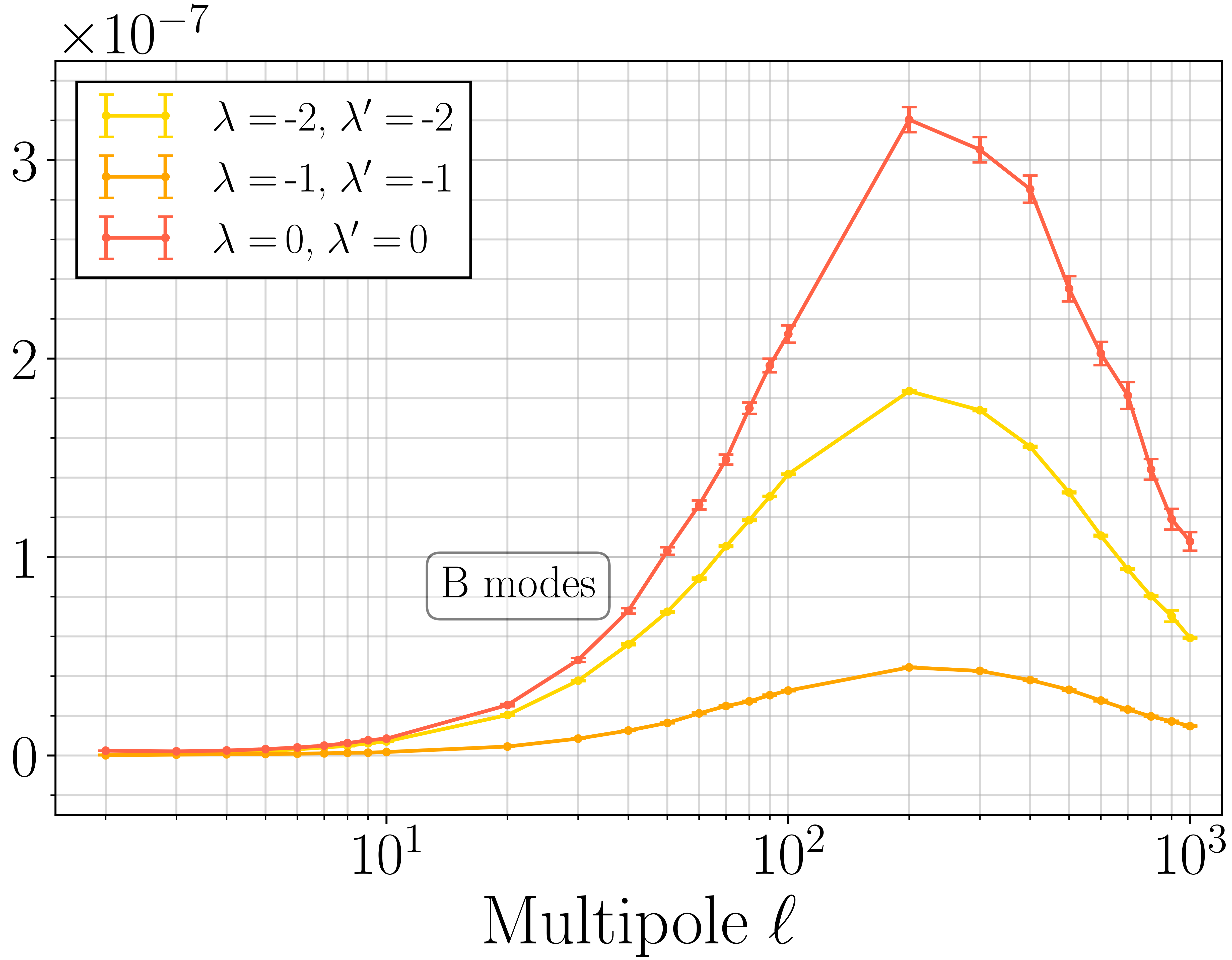

Concluding Remarks

★ Full sky angular power spectra of the E and B modes

★ Sensitive to reionisation central redshift, width and the matter power spectrum.

★ Spectrum consists of y-type distortions part.

★ Differentiates it from primary CMB signals with blackbody spectrum and other SZ-type signals, which are unpolarised.

★ Free from the cosmic variance of the primary CMB polarisation signal and lensing B modes.

Email: aritra.gon@tifr.res.in

Thank You !!

Secondary polarisation of CMB: The pkSZ effect

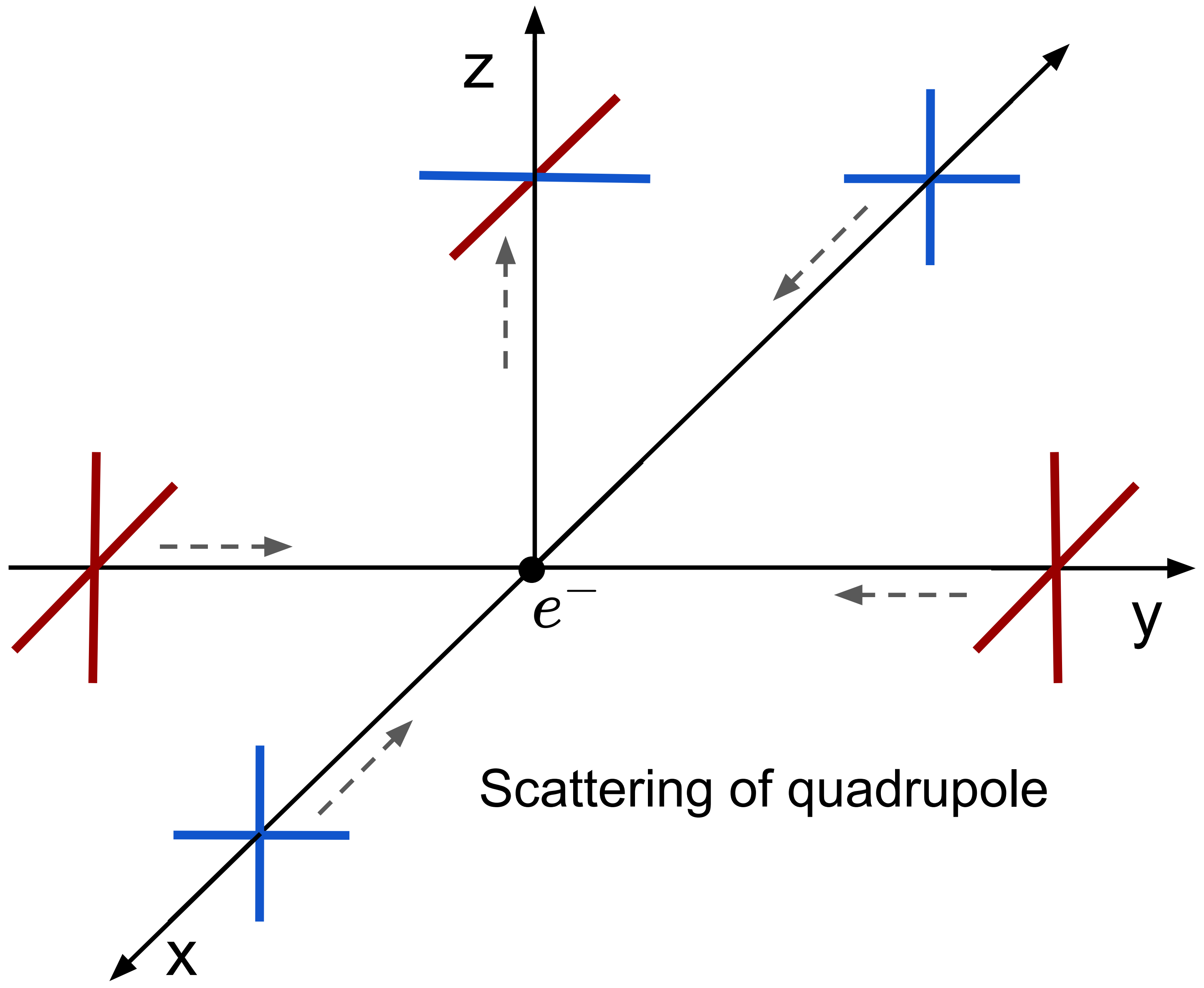

- Free electrons produced during reionisation, have a bulk peculiar velocity $(\mathbf{v})$.
- In the electron rest frame, the CMB is not isotropic, in particular, has a quadrupolar anisotropy $\propto \mathbf{v}^2$.
  - Non-linear nature of Relativistic Doppler shift.
  - A non-linear relation between temperature and intensity in the Planck spectrum
- Thomson Scattering in presence of a quadrupolar anisotropy generates polarisation in the CMB.
- First predicted by Sunyaev and Zeldovich in 1980. (MNRAS,190:413-420)

$$T\left(\mathbf{r}, \hat{\mathbf{n}}', \eta\right) = \frac{T_0(\eta)}{\gamma\left(1 + \mathbf{v}(\mathbf{r}, \eta)\cdot\hat{\mathbf{n}}'\right)} = T_0(\eta)\left[1 + \underbrace{\frac{1}{2}v^2 - \mathbf{v}\cdot\hat{\mathbf{n}}' + \left(\mathbf{v}\cdot\hat{\mathbf{n}}'\right)^2 + \mathcal{O}\left(\left(\mathbf{v}\cdot\hat{\mathbf{n}}'\right)^3\right) + \cdots}_{\theta(\mathbf{r}, \hat{\mathbf{n}}', \eta)}\right]$$

$$\delta n_\nu = \frac{1}{2h\nu^3}\delta I_\nu = \left(\theta + \theta^2\right)\left(T\frac{\partial n_{pl}}{\partial T}\right)\Bigg|_{T_0} + \frac{\theta^2}{2}\left(T^4\frac{\partial}{\partial T}\left(\frac{1}{T^2}\frac{\partial n_{pl}}{\partial T}\right)\right)\Bigg|_{T_0} + \mathcal{O}(\theta^3)\ \cdots$$

Polarisation field and Power spectra

- The polarisation field :

$$(\mathcal{Q} \pm i\mathcal{U})(\hat{\mathbf{n}}) \equiv P_{\pm}(\hat{\mathbf{n}}) = -\frac{\sqrt{6}\sigma_{\mathrm{T}}}{10}\int_0^{\chi} d\chi\, a(\chi)\, e^{-\tau(\chi)}\, \mathrm{n_e}(\chi) \sum_{\lambda=-2}^{2} {}_{\pm 2}Y_{2\lambda}(\hat{\mathbf{n}}) \int d^2\hat{\mathbf{n}}'\, Y_{2\lambda}^{*}(\hat{\mathbf{n}}')\left(\mathbf{v}(\mathbf{r},\chi)\cdot\hat{\mathbf{n}}'\right)^2.$$

→ Electron number density - only a function of time.

→ Shows that polarisation is a spin-2 field.

→ Source term - integral over all incoming photon direction. Extracts the quadrupole.

$$a_{\ell m} = \int P_{+}(\hat{\mathbf{n}})\, {}_2Y_{\ell m}^{*}(\hat{\mathbf{n}})\, d^2\hat{\mathbf{n}}$$

- We define to define spin 0 fields related to the polarisation field through spin raising and lowering operator.

$$\mathcal{E}(\hat{\mathbf{n}}) = \frac{1}{2}\left[\left(\eth^{*}\right)^2 P_{+}(\hat{\mathbf{n}}) + (\eth)^2 P_{-}(\hat{\mathbf{n}})\right] = \sum_{\ell,m} e_{\ell m}\sqrt{\frac{(\ell+2)!}{(\ell-2)!}}\, Y_{\ell m}(\hat{\mathbf{n}})$$

$$\mathcal{B}(\hat{\mathbf{n}}) = -\frac{i}{2}\left[\left(\eth^{*}\right)^2 P_{+}(\hat{\mathbf{n}}) - (\eth)^2 P_{-}(\hat{\mathbf{n}})\right] = \sum_{\ell,m} b_{\ell m}\sqrt{\frac{(\ell+2)!}{(\ell-2)!}}\, Y_{\ell m}(\hat{\mathbf{n}})$$

$$b_{\ell m} = \frac{-i}{2}\left(a_{\ell m} - (-1)^m a_{\ell -m}^{*}\right) \qquad e_{\ell m} = \frac{1}{2}\left(a_{\ell m} + (-1)^m a_{\ell -m}^{*}\right)$$

- The E and B mode power spectra :

$$\langle e_{\ell m} e_{\ell' m'}^{*}\rangle = C_{\ell}^{EE}\, \delta_{\ell,\ell'}\, \delta_{mm'} \qquad \langle b_{\ell m} b_{\ell' m'}^{*}\rangle = C_{\ell}^{BB}\, \delta_{\ell,\ell'}\, \delta_{m,m'}$$

y-type E and B mode power spectra are sensitive to the matter power spectrum

- We selected an asymmetric reionisation history

$$X_e^{Sym}(z) = \left[\frac{(1+f)}{2}\left\{1+\tanh\left(\frac{q_{re}-q}{\Delta q_{re}}\right)\right\} + \frac{f}{2}\left\{1+\tanh\left(\frac{q_{re}^{HeII}-q}{\Delta q_{re}^{HeII}}\right)\right\}\right]$$

$$q(z) = (1+z)^{1.5} \qquad \Delta q_{re} = 1.5(\sqrt{1+z_{re}})\Delta z_{re}$$

$$f = \left(\frac{m_H}{m_{He}}\frac{X_{He}}{1-X_{He}}\right) \simeq 0.079$$

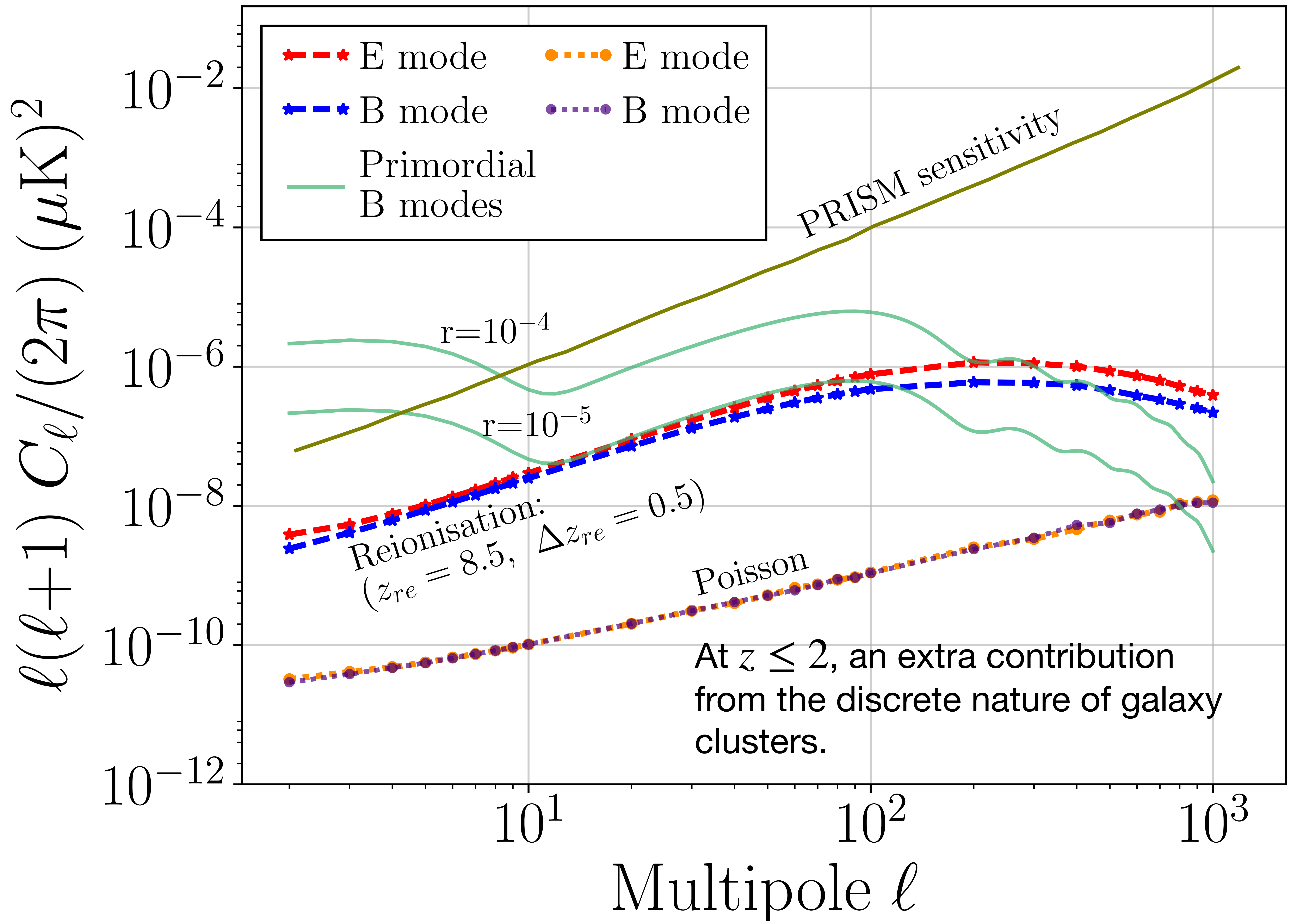

E modes greater than the B modes

Scalar, Vector and Tensor Decomposition

Cross-correlations

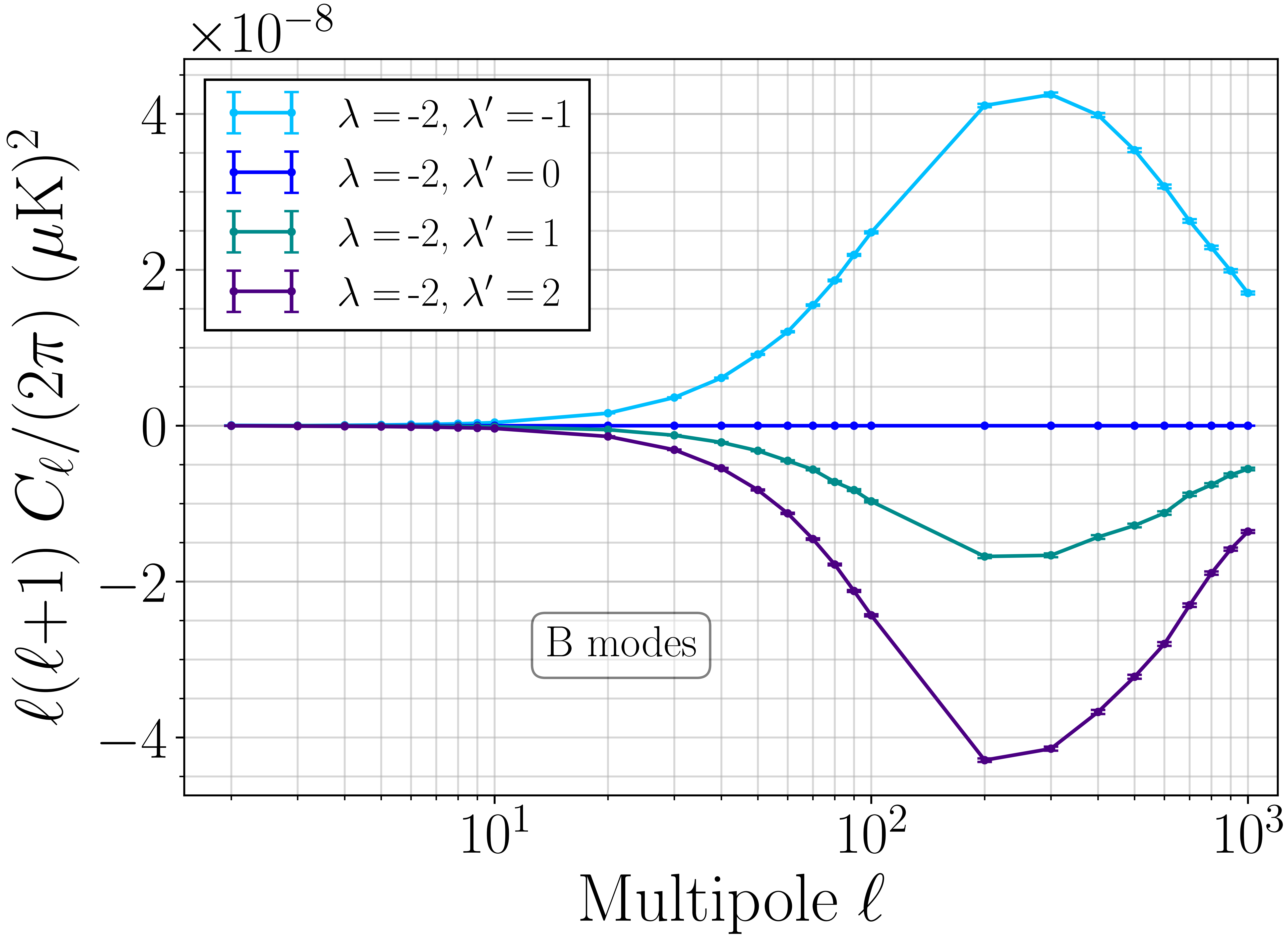

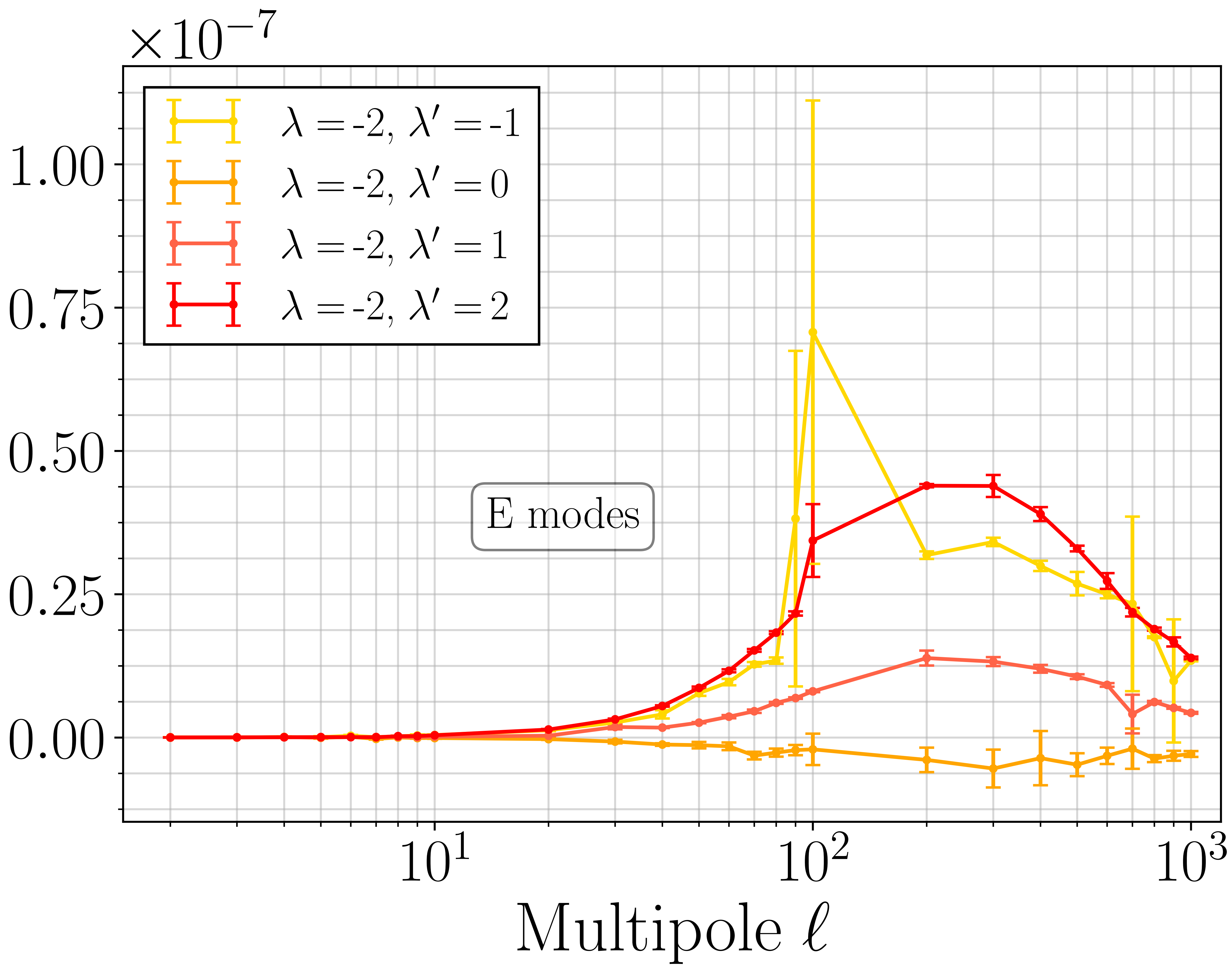

Thomson Scattering generates polarisation if the incoming radiation has a quadrupolar anisotropy

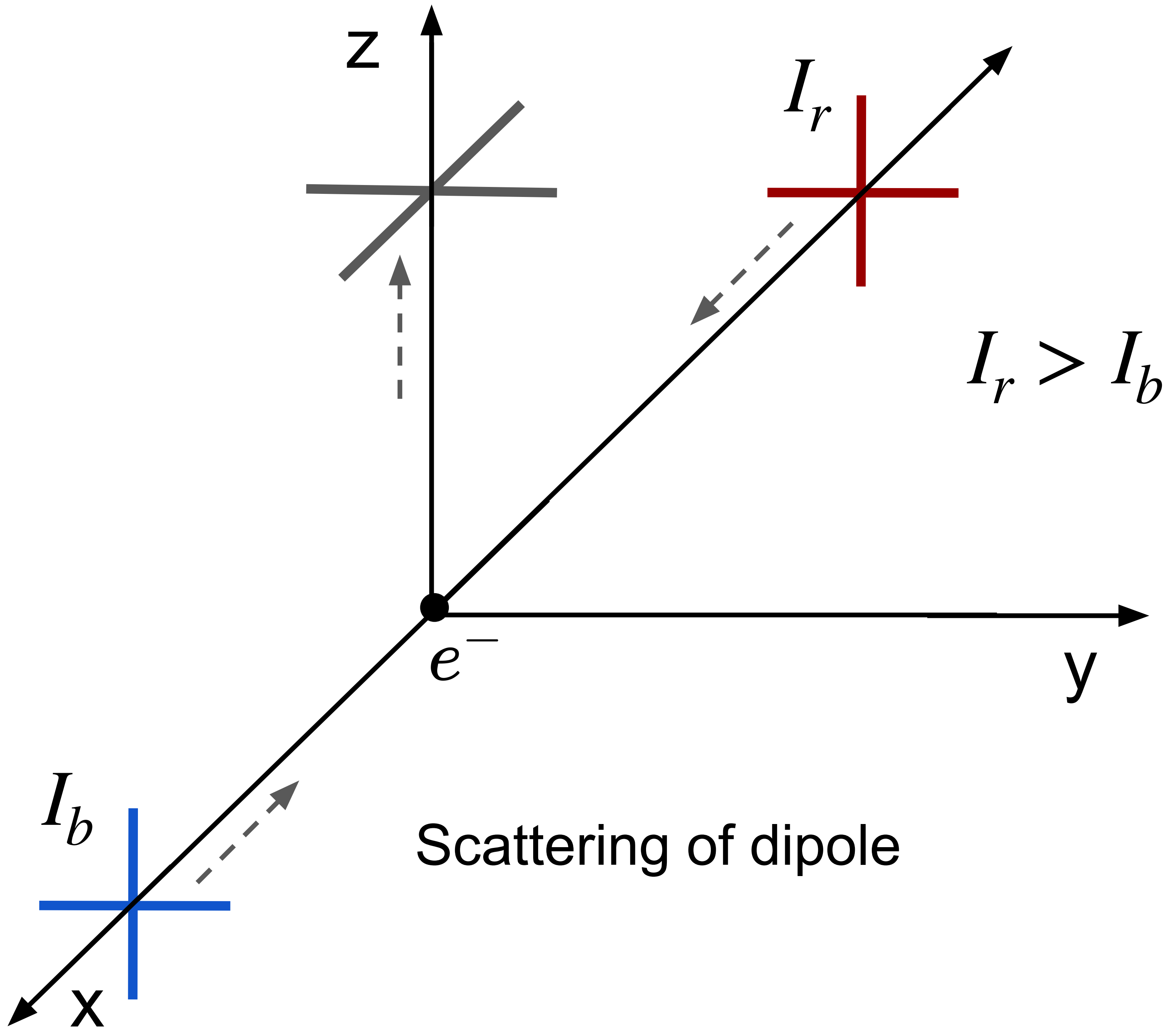

Scattering of dipole

$$\boxed{\sigma_T \propto \boldsymbol{\epsilon} \cdot \boldsymbol{\epsilon}'}$$

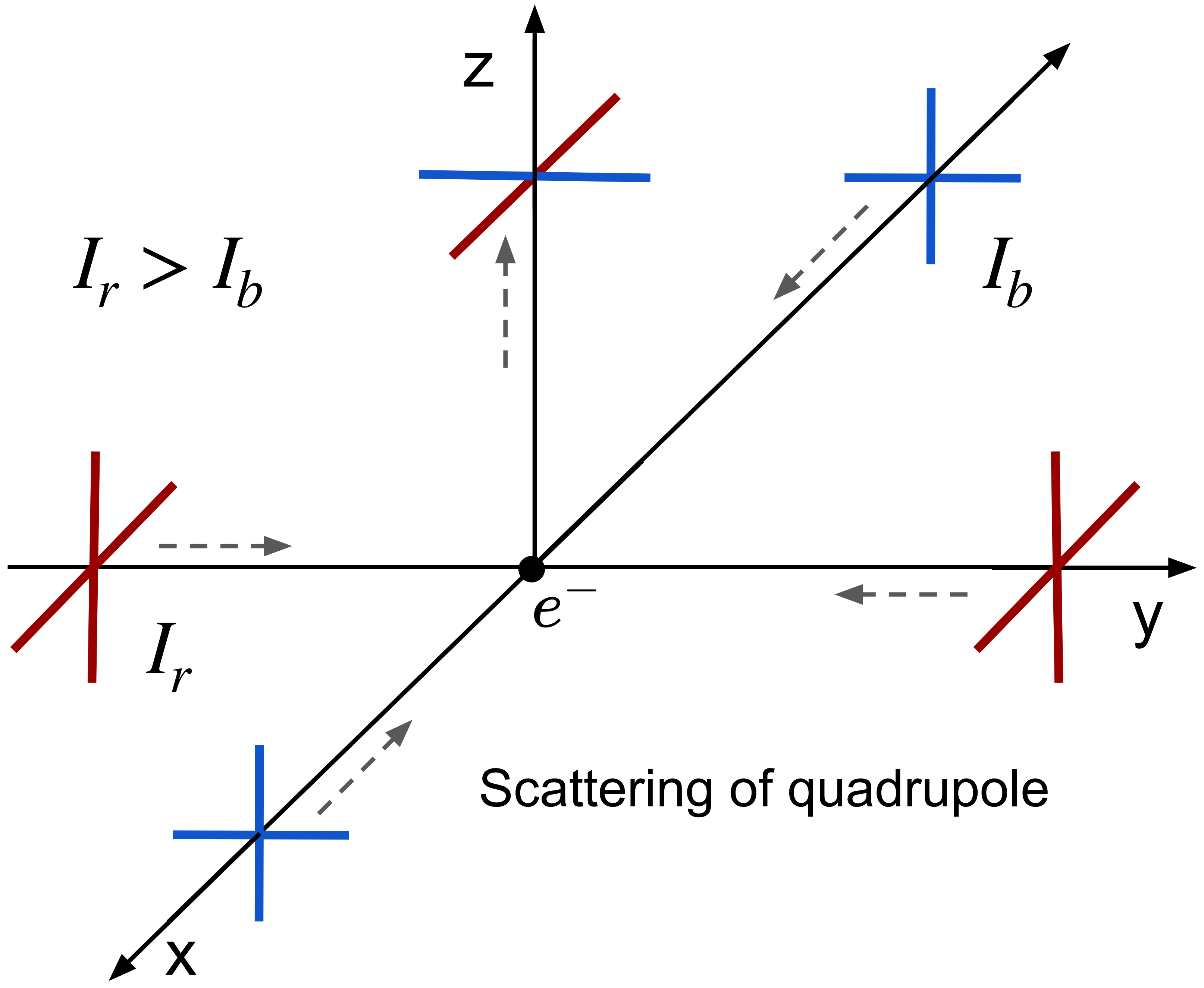

Scattering of quadrupole

$$\dot{\tau} = -\, n_e\, a(\chi)\, \sigma_T$$

Considering incoming radiation to be unpolarised

$$\boxed{P_{\pm}\left(\hat{\mathbf{n}}\right) = -\frac{\sqrt{6}\sigma_{\mathrm{T}}}{10}\int_0^{\chi} d\chi\, a(\chi)\, e^{-\tau(\chi)}\, \mathrm{n_e}(\chi) \sum_{\lambda=-2}^{2}\, {}_{\pm 2}Y_{2\lambda}\left(\hat{\mathbf{n}}\right) \int d^2\hat{\mathbf{n}}'\, Y^*_{2\lambda}\left(\hat{\mathbf{n}}'\right)\left(\mathbf{v}(\mathbf{r},\chi)\cdot\hat{\mathbf{n}}'\right)^2 .}$$

$Y^*_{2\lambda}\left(\hat{\boldsymbol{n}}'\right)$ will pick out the quadrupolar part in $\theta(\boldsymbol{r}, \hat{\boldsymbol{n}}')$

ICTP Summer School on Cosmology 2022

Interacting Dark Energy from Joint Analysis in Redshift-Space

Maria Tsedrik 1st year PhD
Supervisor: Dr. Alkistis Pourtsidou
Collaborators: Dr. Chiara Moretti, Dr. Pedro Carillho

THE UNIVERSITY of EDINBURGH

Motivation

- Inclusion of extended cosmologies into Stage-IV surveys' pipelines
- Validation tests in order to avoid false detection
- Parameter degeneracies
- Observables and their contribution

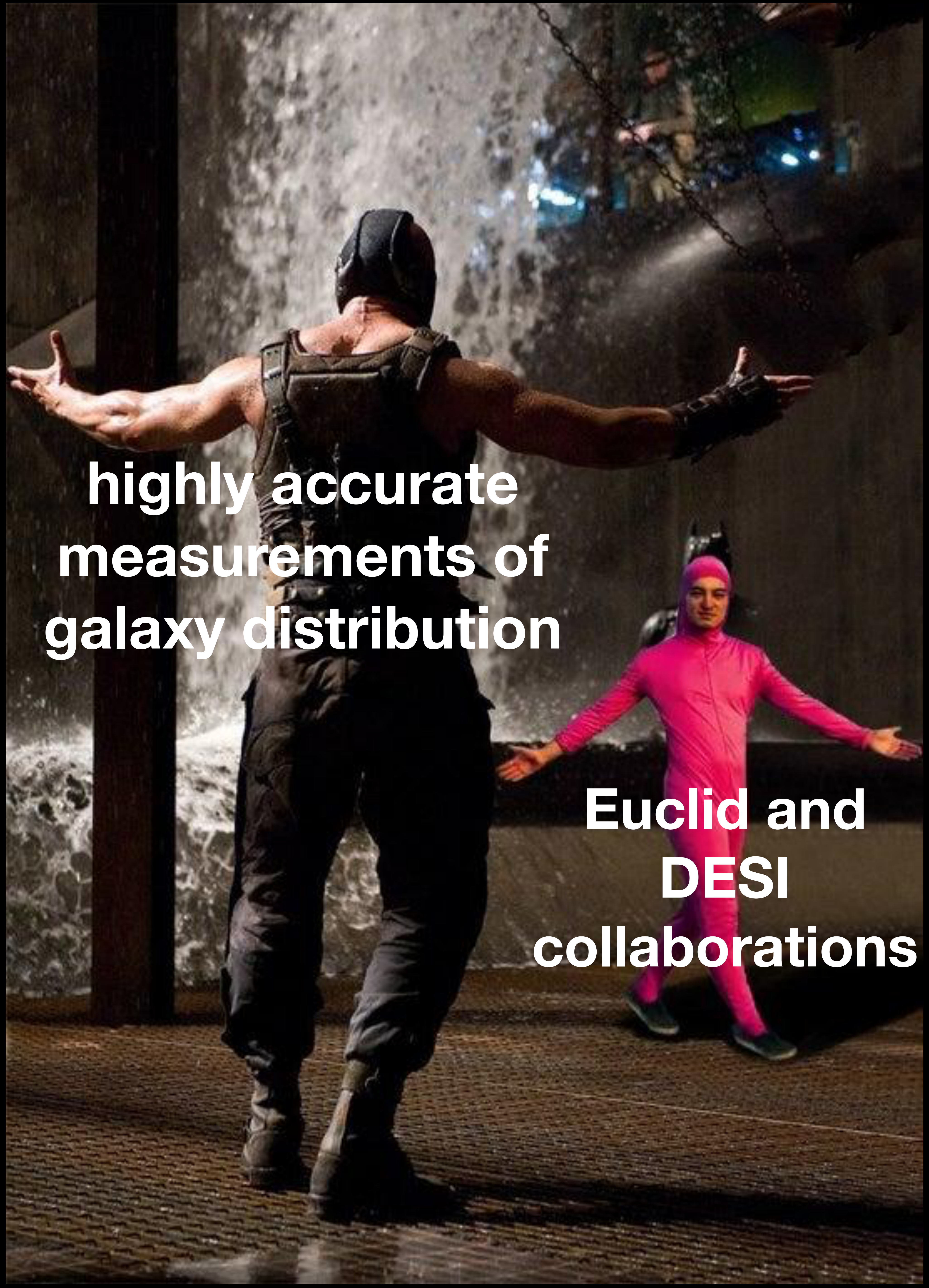

Likelihood Pipeline for Validation Tests

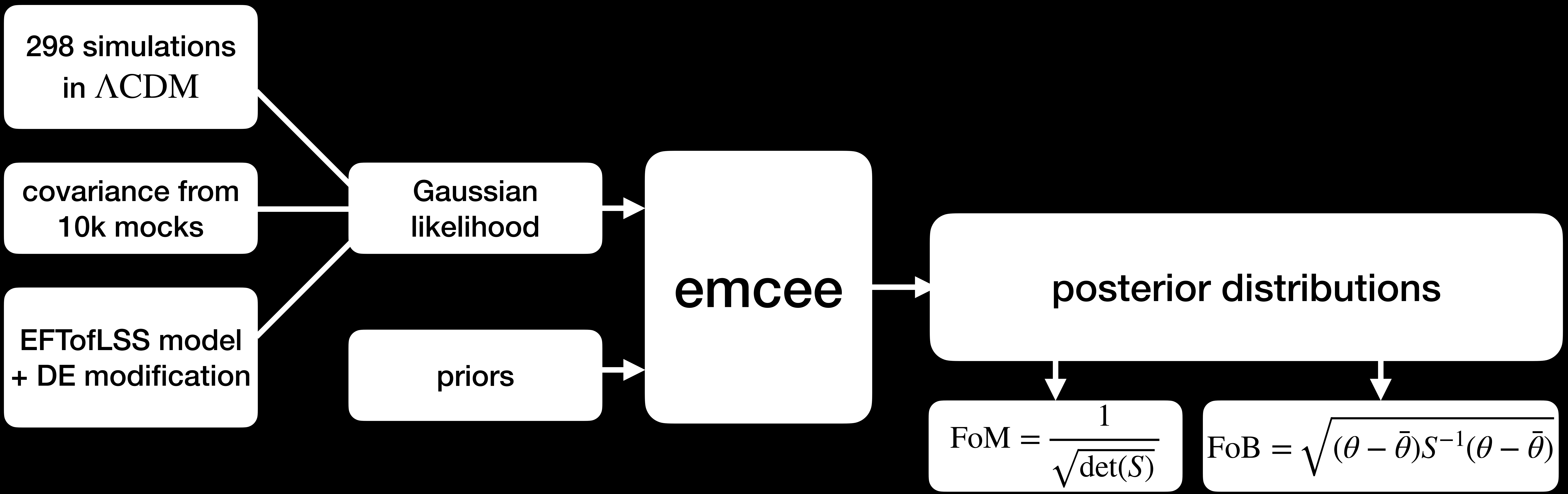

EFTofLSS: Power Spectrum (1-loop)

b_1 b_2 $b_{\mathcal{G}_2}$ b_{Γ_3}

Bias expansion

f

Growth Rate

$\tilde{c}_0$ $\tilde{c}_2$ $\tilde{c}_4$ $\tilde{c}_{\nabla^4\delta}$

Counterterms

α_P ϵ_{k^2}

Shot noise

$P_l(k)$ with $l \in \{0, 2, 4\}$

EFTofLSS: Bispectrum (tree-level)

b_1 b_2 $b_{\mathcal{G}_2}$

Bias expansion

f

Growth Rate

α_B

Shot noise

$B_l(k)$ with $l \in \{0, 2\}$

EFTofLSS: Power Spectrum (1-loop)

b_1 b_2 $b_{\mathcal{G}_2}$ b_{Γ_3}

Bias expansion

f

Growth Rate

$\tilde{c}_0$ $\tilde{c}_2$ $\tilde{c}_4$ $\tilde{c}_{\nabla^4\delta}$

Counterterms

α_P ϵ_{k^2} α_B

Shot noise

$P_l(k)$ with $l \in \{0, 2, 4\}$

$B_l(k)$ with $l \in \{0, 2\}$

Interacting Dark Energy

- Impulse transfer without energy transfer between DM and DE

- Only Euler equation is modified

$$\delta'' + \left(3 + (1+w)\xi\rho_\Lambda \frac{H_0}{H} + \frac{H'}{H}\right)\delta' - \frac{3\Omega_{\rm m} H_0^2}{2a^2H^2}\delta = 0$$

with $\rho_\Lambda = \rho_{\Lambda,0}\, a^{-3(1+w)}$,

$\Omega_{\rm m} = \Omega_{\rm m,0}\, a^{-3}$ and $\xi = \sigma/m_{DM}$

- w changes both the background cosmology and the perturbations, whereas $A = \xi\,(1+w)$ can only affect the latter

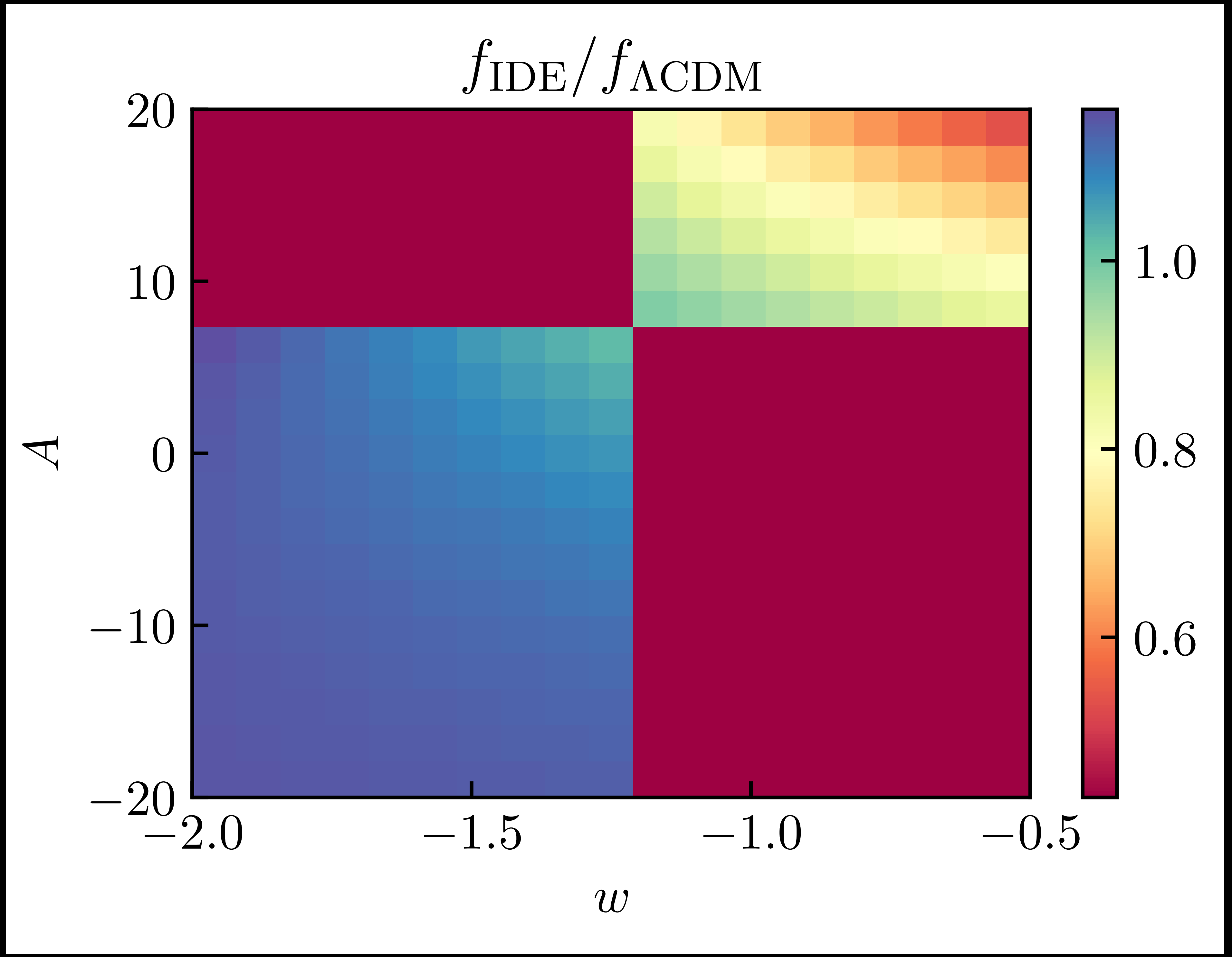

Validation Tests

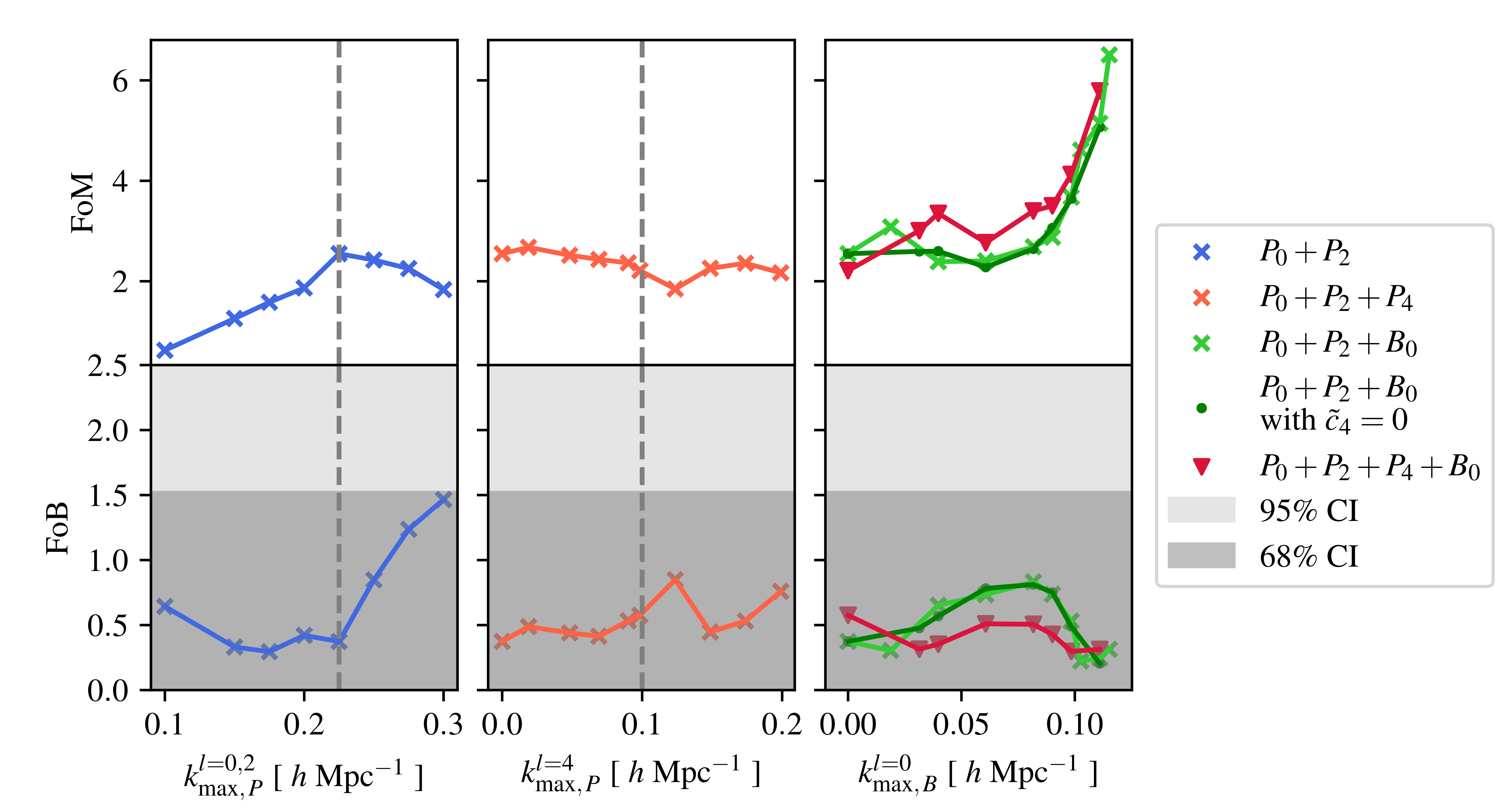

Validation Tests

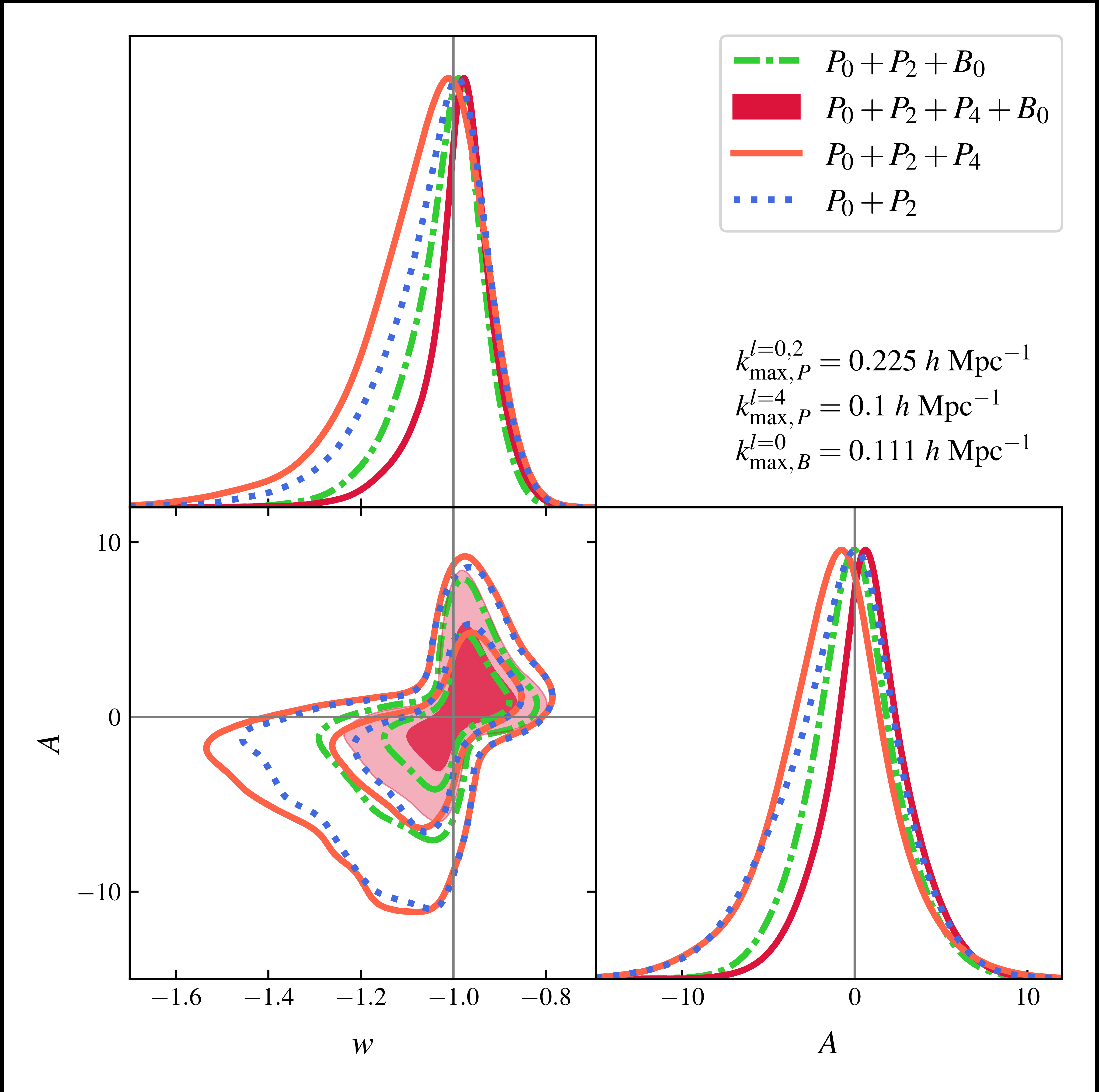

$w = -1.02 \pm 0.09,\ A = -0.08 \pm 2.65\,\mathrm{b\,GeV^{-1}}$

$w = -0.99 \pm 0.08,\ A = -0.78 \pm 2.51\,\mathrm{b\,GeV^{-1}}$

$w = -1.07 \pm 0.14,\ A = -1.26 \pm 3.46\,\mathrm{b\,GeV^{-1}}$

$w = -1.05 \pm 0.13,\ A = -0.91 \pm 3.57\,\mathrm{b\,GeV^{-1}}$

2054 triangles!!!

Improvement I: Bias Relations

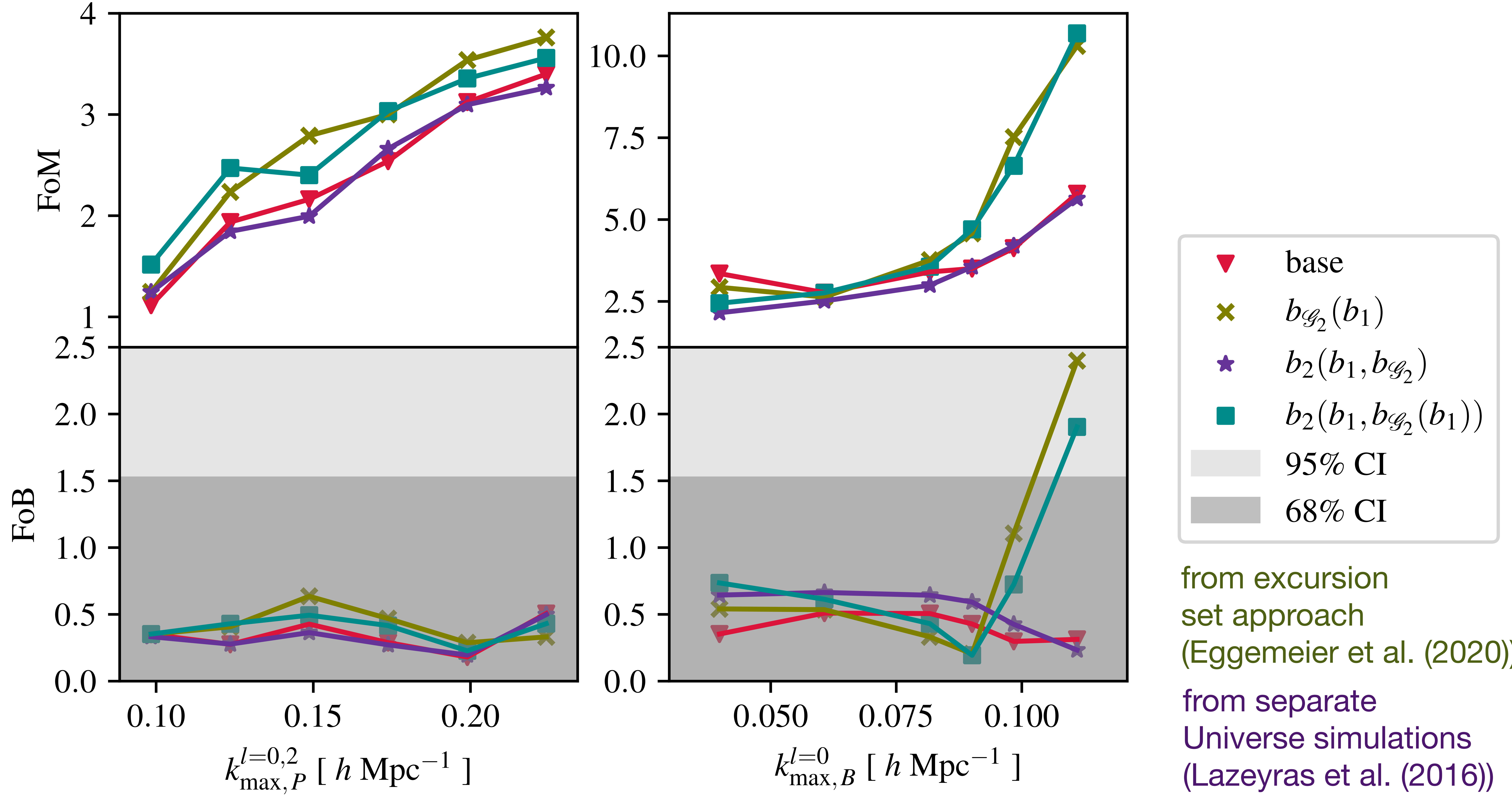

from excursion set approach (Eggemeier et al. (2020))

from separate Universe simulations (Lazeyras et al. (2016))

Improvement II: $+B_2$

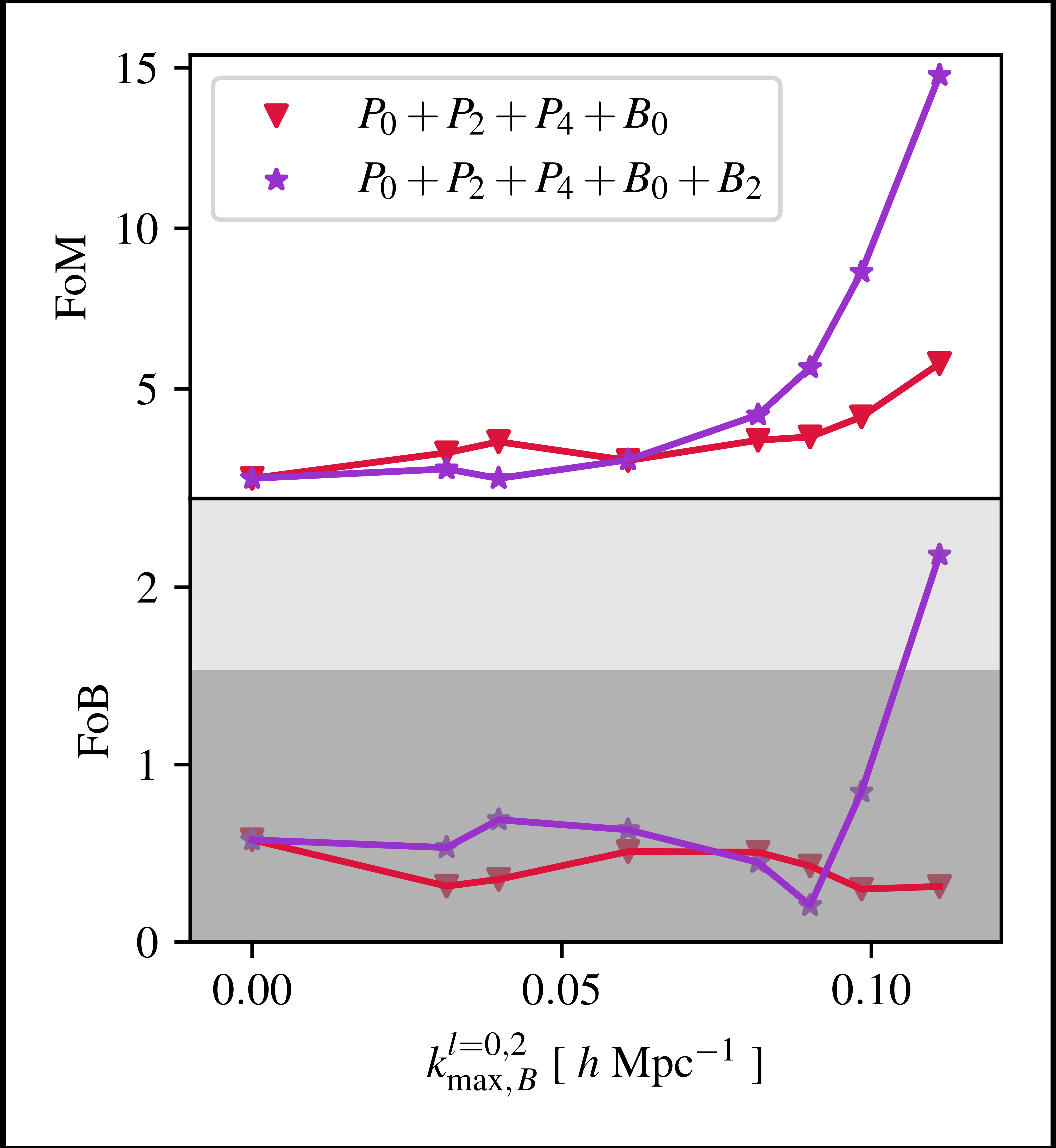

BOSS Data + Full Cosmology

Power Spectrum

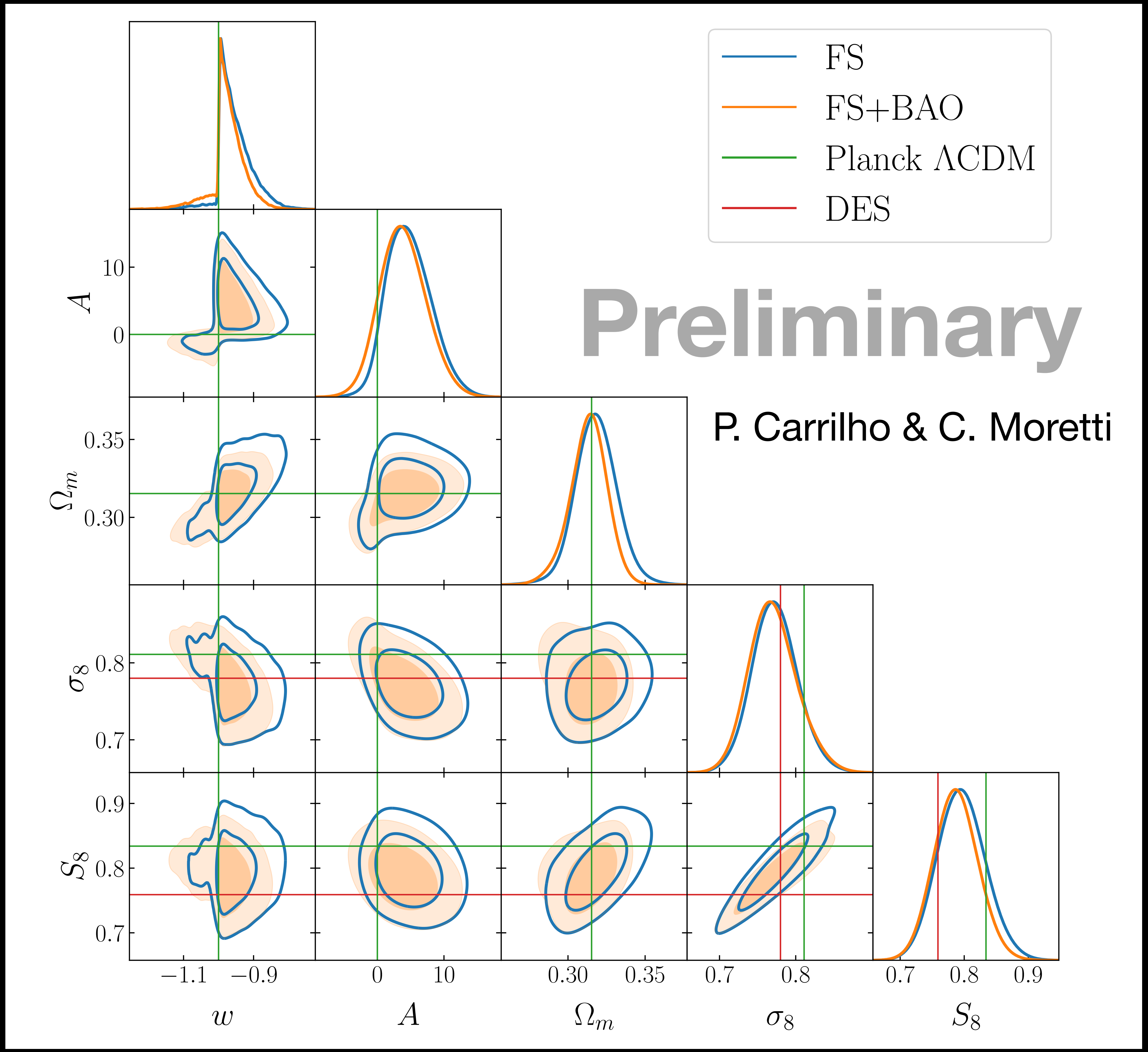

Power Spectrum + Bispectrum

Summary

- 30% improvement in constraints on IDE parameters if B_0 is included
- Same effect is achieved on more moderate scales if $b_{\mathcal{G}_2}$-relation is applied or B_2 is added to the analysis
- Similar improvements are observed in $w\mathrm{CDM}$ scenario

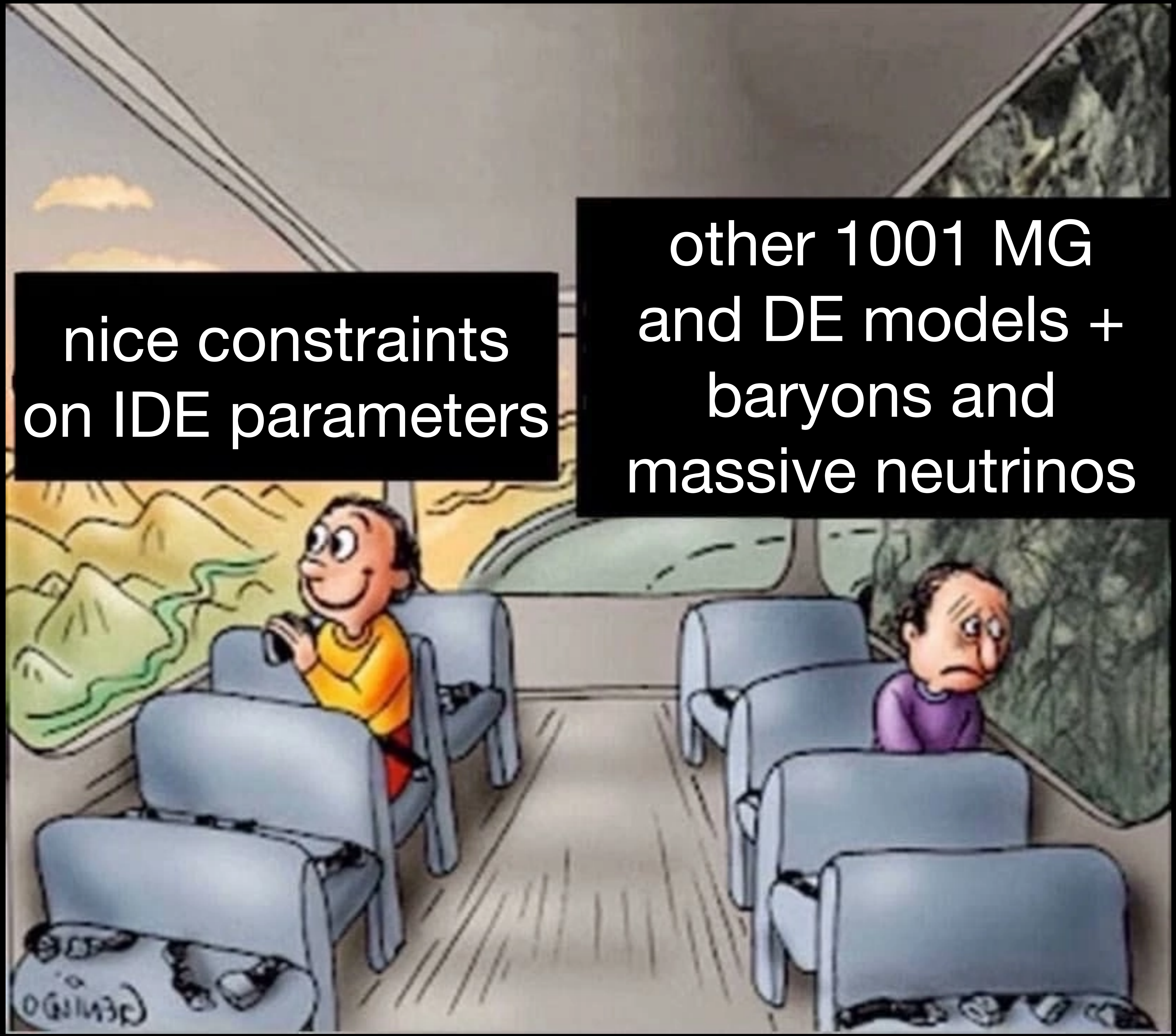

Binary system dynamics in the EFT approach

Summer School on Cosmology 2022

ICTP

Gabriel Luz Almeida (gabriel.luz@fisica.ufrn.br)
International Institute of Physics - UFRN, Brazil
PhD supervisor: Riccardo Sturani (ICTP-SAIFR)
In collaboration with Stefano Foffa (UNIGE)

The Abdus Salam International Centre for Theoretical Physics

12 July 2022

GW150914: First direct detection of gravitational waves

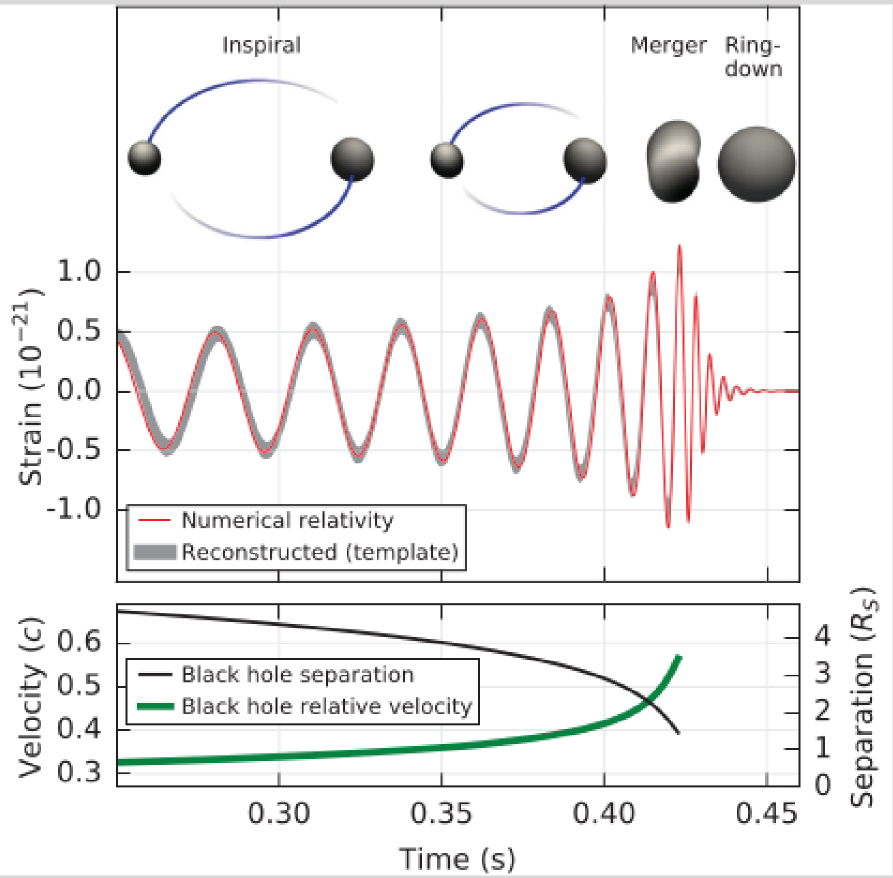

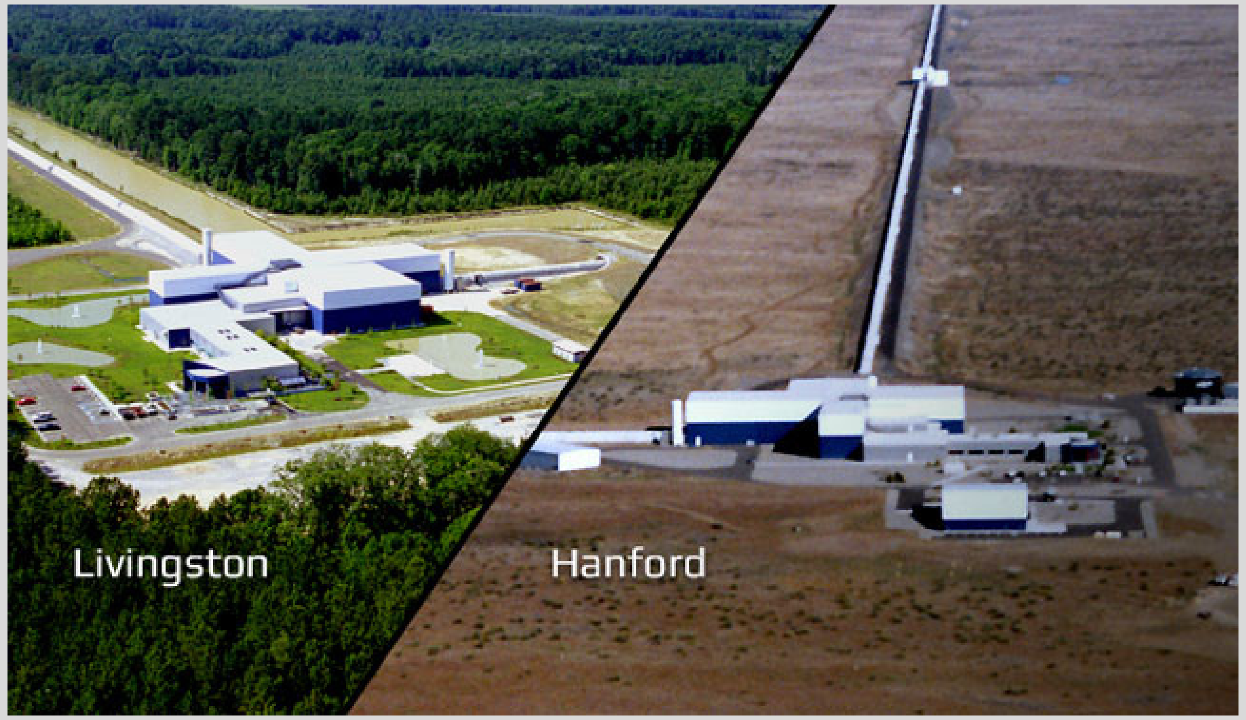

New window to observe the universe!

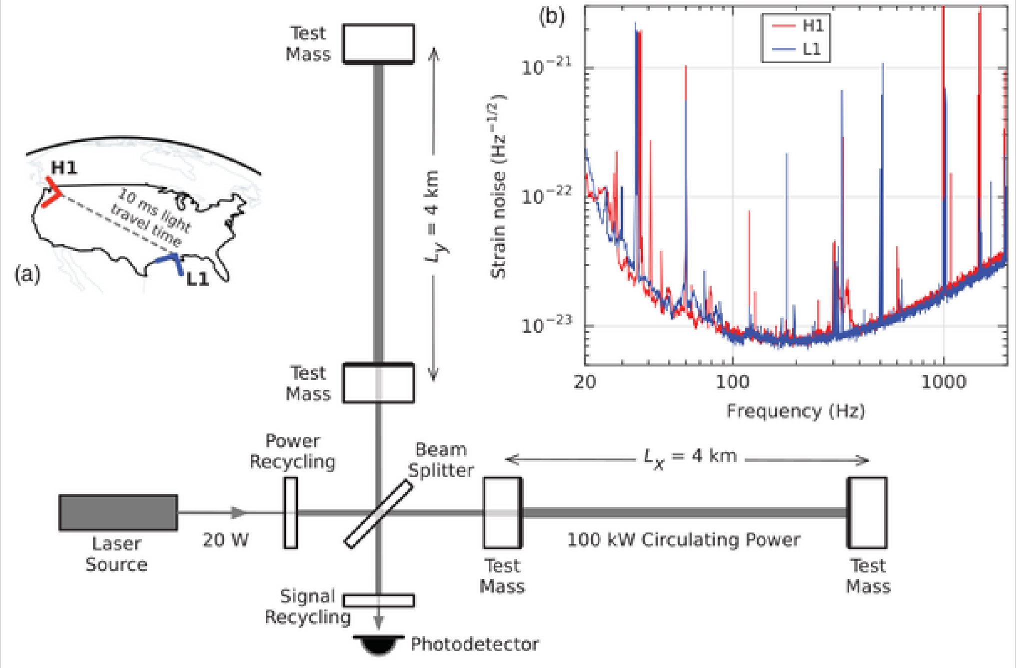

Today 90 GW events have been observed by the LVK Collaboration

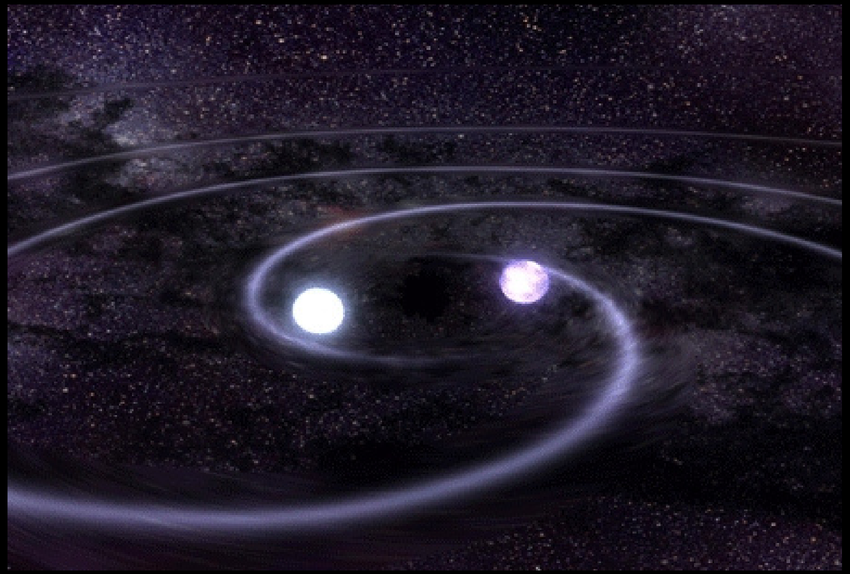
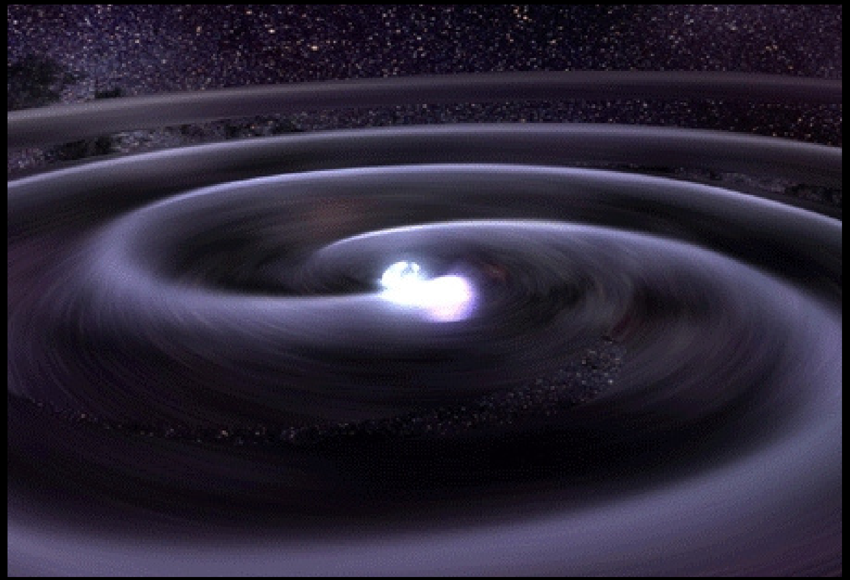
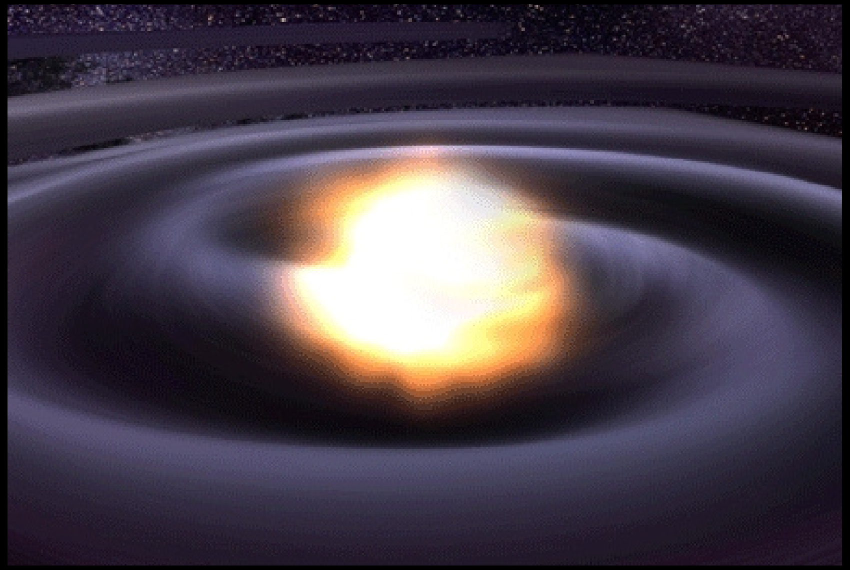

Morphology of the GW Signal

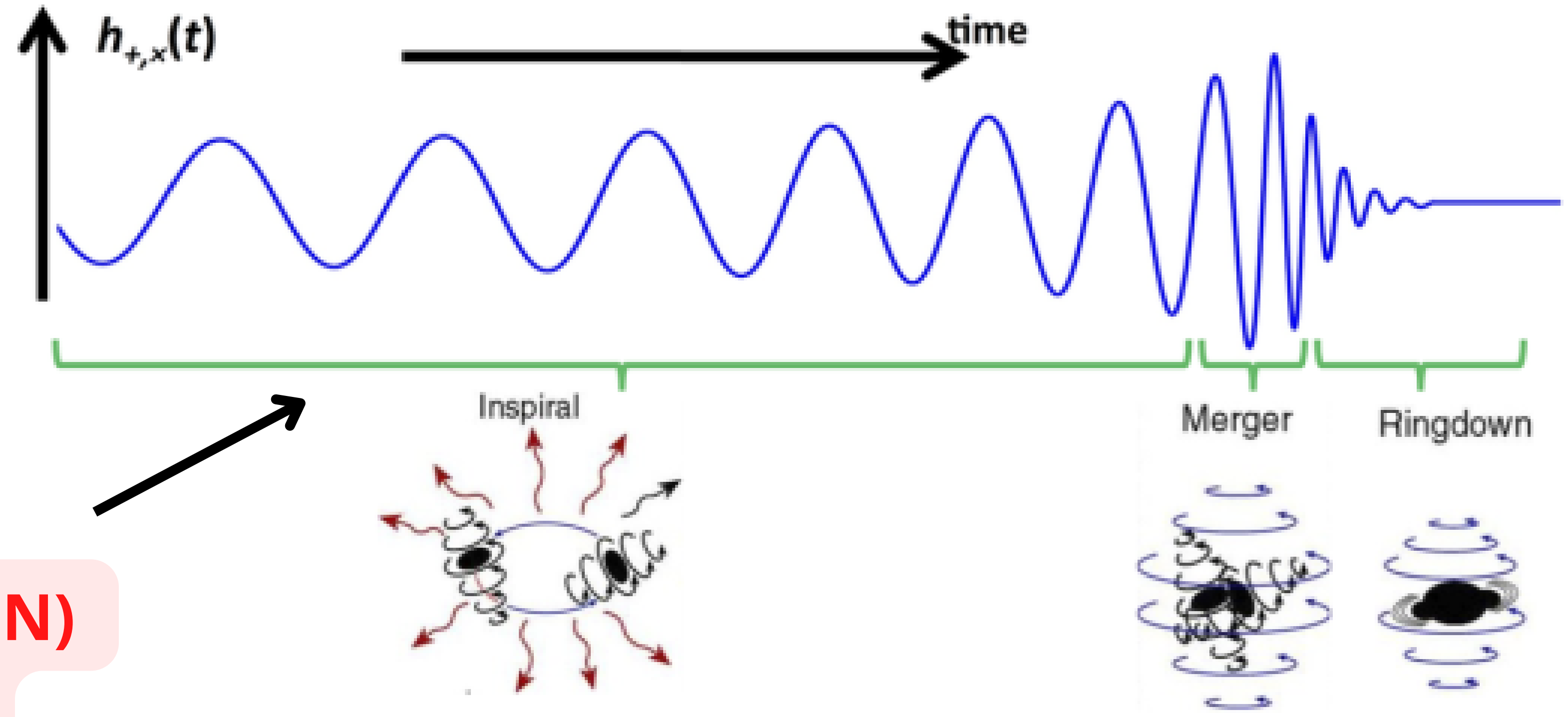

[www.soundsofspacetime.org]

Phases of the coalescence

Post-Newtonian (PN) approximation

$$\begin{cases} h_+ &= \dfrac{4}{d}(G\mathcal{M}_c)^{5/3}(\pi f_{gw})^{2/3}\left(\dfrac{1+\cos^2\iota}{2}\right)\cos(\Phi(t)) \\ h_\times &= \dfrac{4}{d}(G\mathcal{M}_c)^{5/3}(\pi f_{gw})^{2/3}\cos\iota\,\sin(\Phi(t)) \end{cases}$$

$$\Phi(t) = 2\int_{t_0}^{t} dt\,\omega(t) = -\frac{2}{G_N M}\int_{v(t_0)}^{v(t)} dv\,\frac{v^3}{P(v)}\frac{dE}{dv}\,,$$

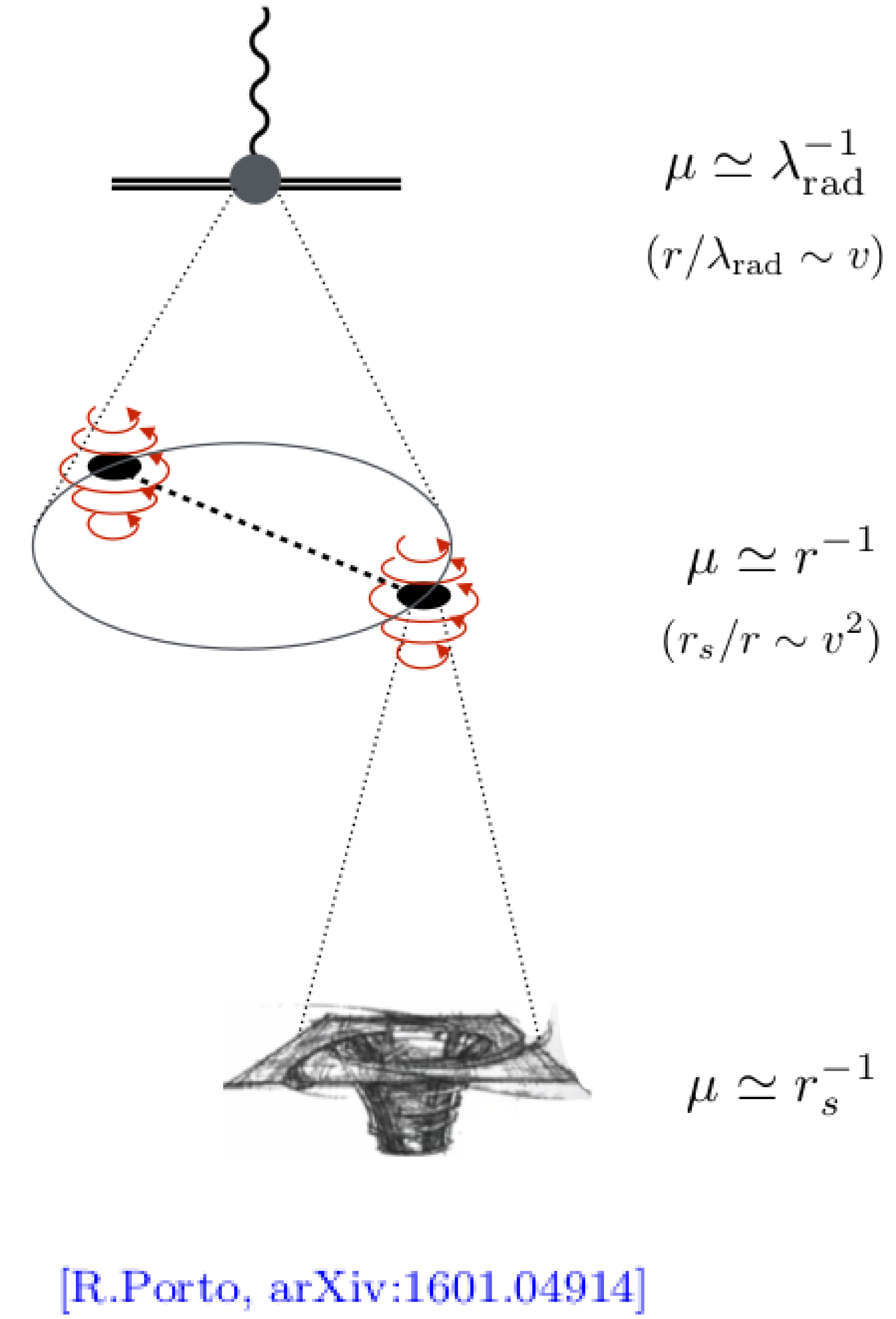

Hierarchy of scales and method of regions

Orbital scale: $v^2 \sim \dfrac{G_N m}{r} \quad \Rightarrow \quad r_s = 2G_N m \sim r v^2$

GW scale: $\lambda \sim r/v$

$$\boxed{r_s \sim r v^2 \sim \lambda v^3}$$

In the nonrelativistic regime, $v \ll 1$, hierarchy of scales:

$$\boxed{r_s \ll r \ll \lambda}$$

Method of regions: $h_{\mu\nu} = \underbrace{H_{\mu\nu}}_{\text{potential mode}} + \underbrace{\bar{h}_{\mu\nu}}_{\text{radiation mode}}$

$H_{\mu\nu}$: off-shell modes scaling as $(k^0, \mathbf{k}) \sim (v/r, 1/r)$

$\bar{h}_{\mu\nu}$: on-shell modes scaling as $(k^0, \mathbf{k}) \sim (v/r, v/r)$

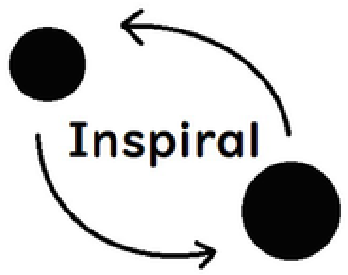

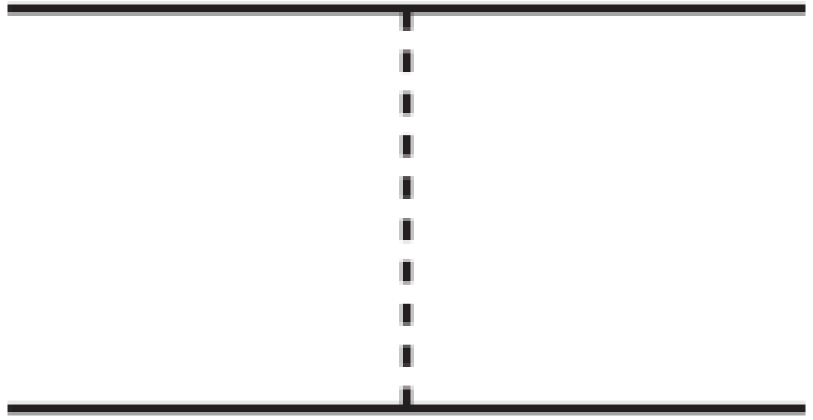

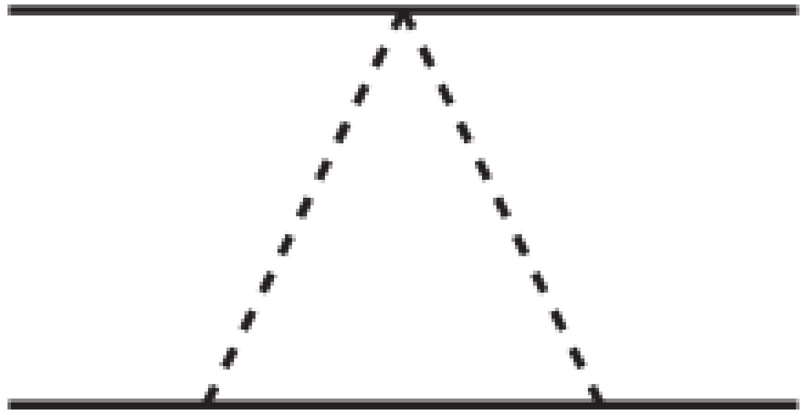

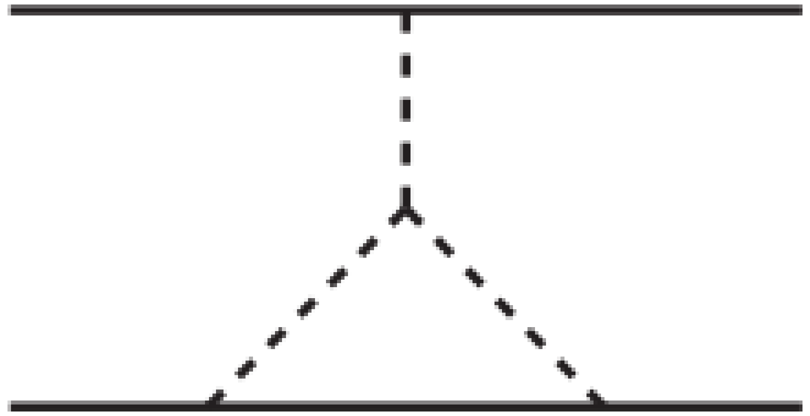

The Near Zone (Or Potential Zone)

Bulk action:

$$S_{\mathrm{EH}}[H_{\mu\nu}] = \frac{1}{16\pi G_N}\int d^4x\sqrt{-g}R[H_{\mu\nu}]$$

For the sources: (Wilsonian paradigm)

$$S_{\mathrm{pp}}[x_a(t), H_{\mu\nu}] = -m_a\int d\tau_a \underbrace{-\frac{1}{2}\int d\tau\, S^{\mu\nu}\omega_{\mu\nu}}_{\text{Spin d.o.f's.}} + \underbrace{c_E\int d\tau\, E_{\mu\nu}E^{\mu\nu} + c_B\int d\tau\, B_{\mu\nu}B^{\mu\nu}}_{\text{Finite size effects}} + \dots$$

Departure from instantaneity : implementation of the PN expansion

$$\frac{1}{k_0^2 - \mathbf{k}^2} = -\frac{1}{\mathbf{k}^2}\left(1 + \frac{k_0^2}{\mathbf{k}^2} + \frac{k_0^4}{\mathbf{k}^4} + \dots\right)$$

1PN correction to the Newtonian potential

$$L_{1PN} = \frac{1}{8}m_1v_1^4 + \frac{1}{8}m_2v_2^4 + \frac{G_Nm_1m_2}{2r}\left[3(v_1^2+v_2^2) - 7(v_1\cdot v_2) - \frac{(v_1\cdot r)(v_1\cdot r)}{r^2}\right] - \frac{G_N^2m_1m_2(m_1+m_2)}{2r^2}.$$

The Far Zone (Or Radiation Zone)

Integrating the potential modes

$$e^{iS_{\rm eff}[x_a,\bar{h}_{\mu\nu}]} = \int \mathcal{D}H_{\mu\nu}\exp\{iS_{\rm EH+GF}[H_{\mu\nu}+\bar{h}_{\mu\nu}] + iS_{\rm pp}[x_a(t), H_{\mu\nu}+\bar{h}_{\mu\nu}]\}$$

$$S_{\rm eff} = \frac{1}{2}\int d^4x\, T^{\mu\nu}\bar{h}_{\mu\nu}$$

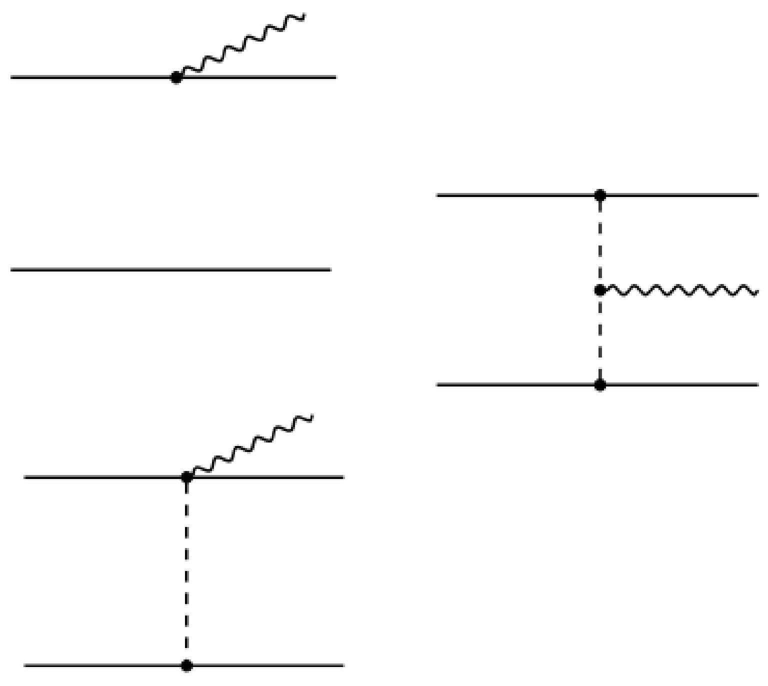

Multipole Expansion

$$(\,\lambda \gg r\,)$$

$$S_{\rm mult} = -E\int d\tau - \frac{1}{2}\int dx^\mu L_{ab}\omega_\mu^{ab}(\tau) + \frac{1}{2}\sum_{n=0}^{\infty}\int d\tau c_n^{(I)} I^{aba_1\ldots a_n}(\tau)\nabla_{a_1}\ldots\nabla_{a_n}E_{ab}(x)$$

$$+\frac{1}{2}\sum_{n=0}^{\infty}\int d\tau c_n^{(J)} J^{aba_1\ldots a_n}(\tau)\nabla_{a_1}\ldots\nabla_{a_n}B_{ab}(x)$$

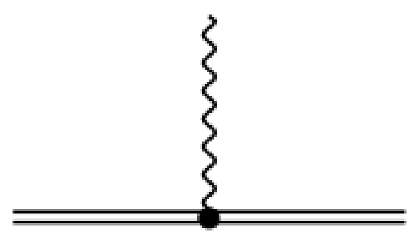

GW observables can be computed:

$$P = \frac{1}{2T}\sum_{\rm pol}\int\frac{d^3\mathbf{k}}{(2\pi)^3}|\mathcal{A}(\omega,\mathbf{k})|^2$$

$$i\mathcal{A}_0(\omega,\mathbf{k}) =$$

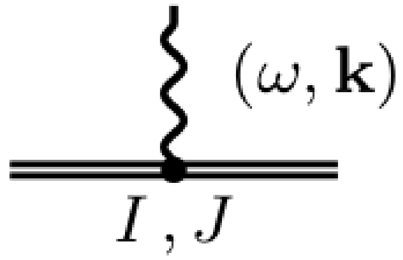

Nonlinear Effects: Emission and Radiation-Reaction

Tail

$i\mathcal{A}_{\text{tail}}(\omega, \mathbf{k}) =$ 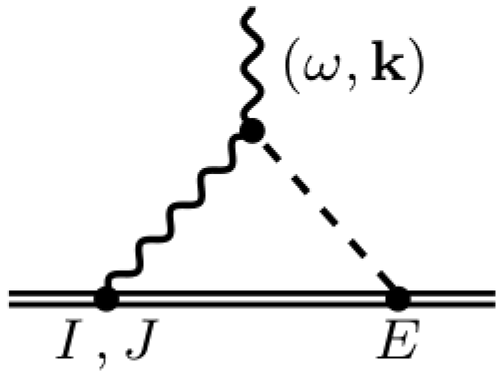

(G Almeida, S Foffa, R Sturani - 2021)

- IR and UV divergences
- Renormalization group evolution

Tail of tail

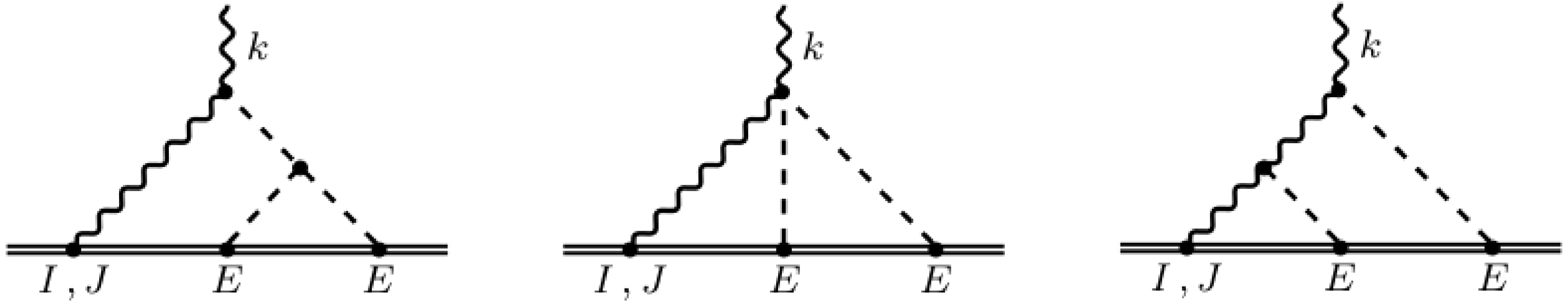

Self-energy diagrams

$iS_{\text{self}} =$ 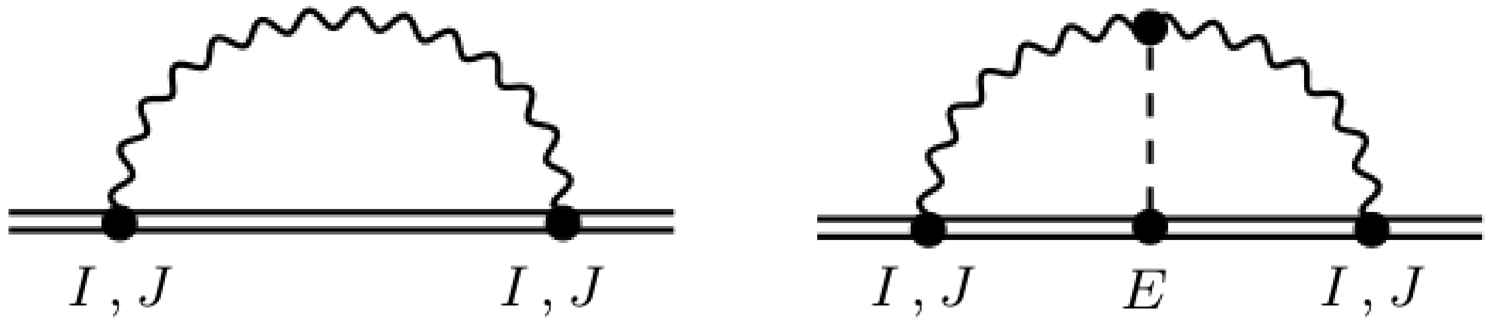

(G Almeida, S Foffa, R Sturani - 2021)

- $\mathrm{Im}(S_{\text{self}}) \Rightarrow$ Energy Flux
- $\mathrm{Re}(S_{\text{self}}) \Rightarrow$ Conservative contribution

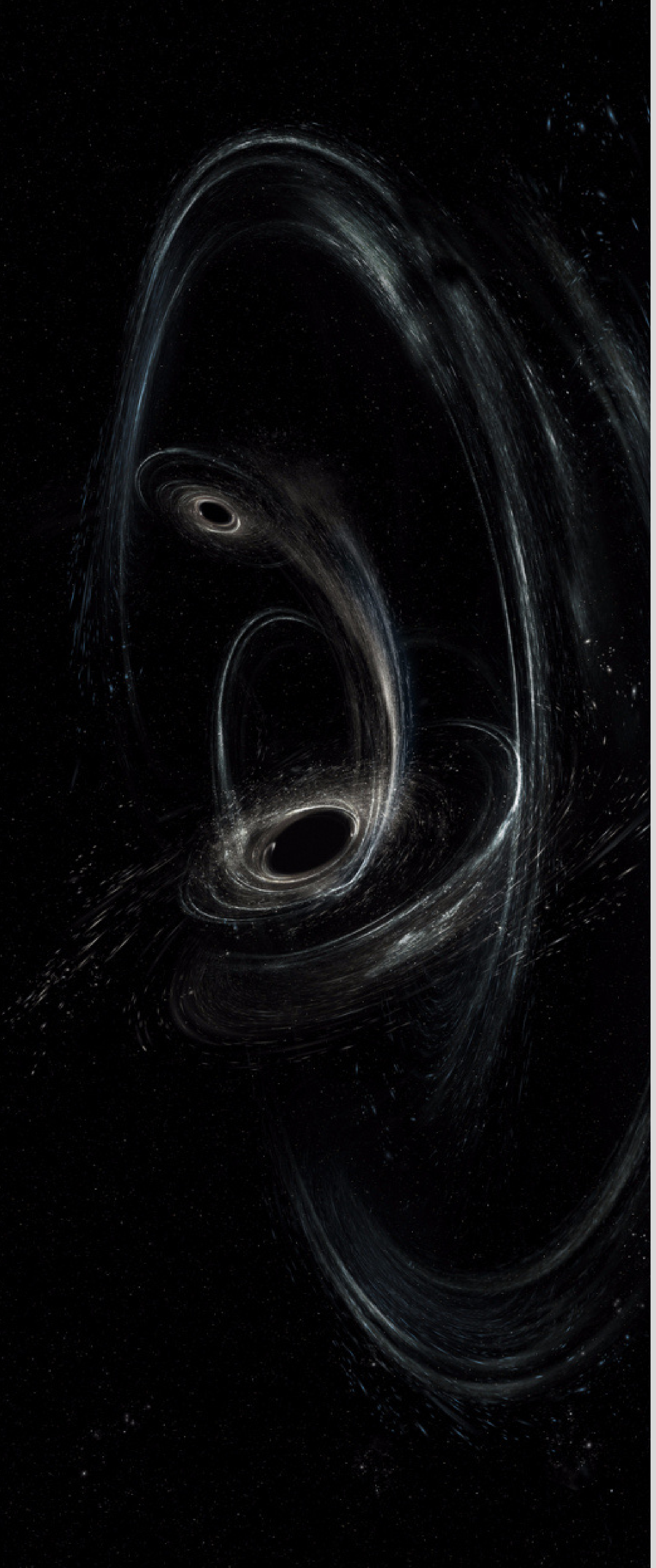

Final remarks

Advantages of studying the binary system dynamics in terms of EFTs

- Field theory techniques can be used
- Perturbative treatment using Feynman diagrams
- Separate description for conservative and dissipative dynamics
- IR and UV divergences can be understood in terms of the RG evolution

Current project

- The study of higher-order radiation-reaction effects that enter the 5PN conservative dynamics of the binary system.

(Astrophysically relevant since this is the order in which finite size effects start to appear and, hence, the strong field regime can be probed)

Sarah Libanore

The importance of clustering analysis in future Gravitational Wave surveys

ICTP Cosmology Summer School

July 12th, 2022

Sarah Libanore

prof Michele Liguori
dr Alvise Raccanelli
Lorenzo Valbusa Dall'Armi
Eleonora Vanzan
Matteo Peron
dr Andrea Ravenni
prof Michela Mapelli
dr Maria Celeste Artale

prof Ely D. Kovetz
dr Caner Ünal
dr Debanjan Sarkar

Sarah Libanore

Will be the *clustering*

of future *gravitational wave surveys*

an effective tool to

constrain cosmology and astrophysics?

Simulations

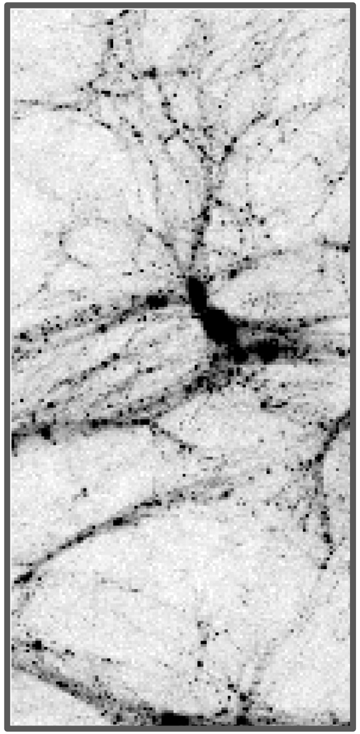

z = 0
EAGLE simulation
Dark Matter Halo sub-catalogue

clustering

Simulations

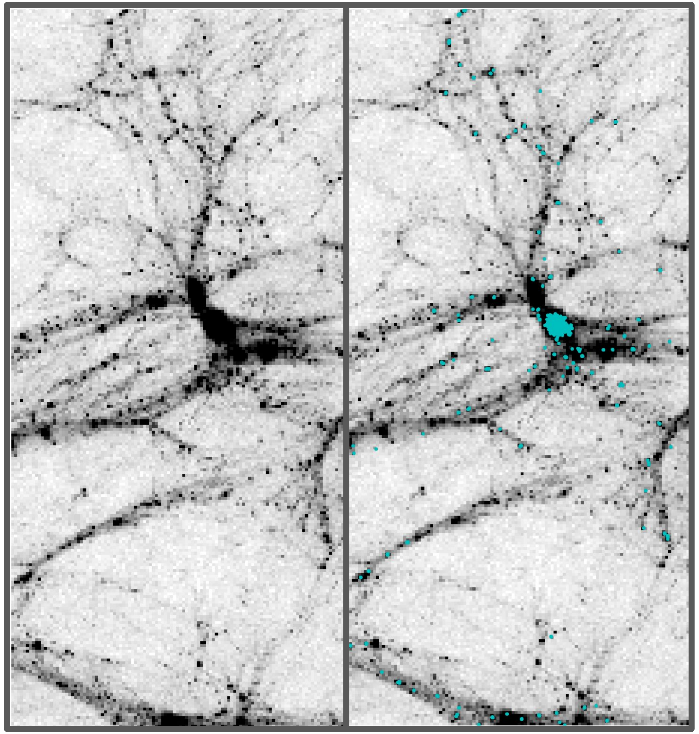

z = 0
M.C. Artale, Y. Bouffanis, M. Mapelli
Binary Black Hole mergers

clustering

Sarah Libanore

Simulations

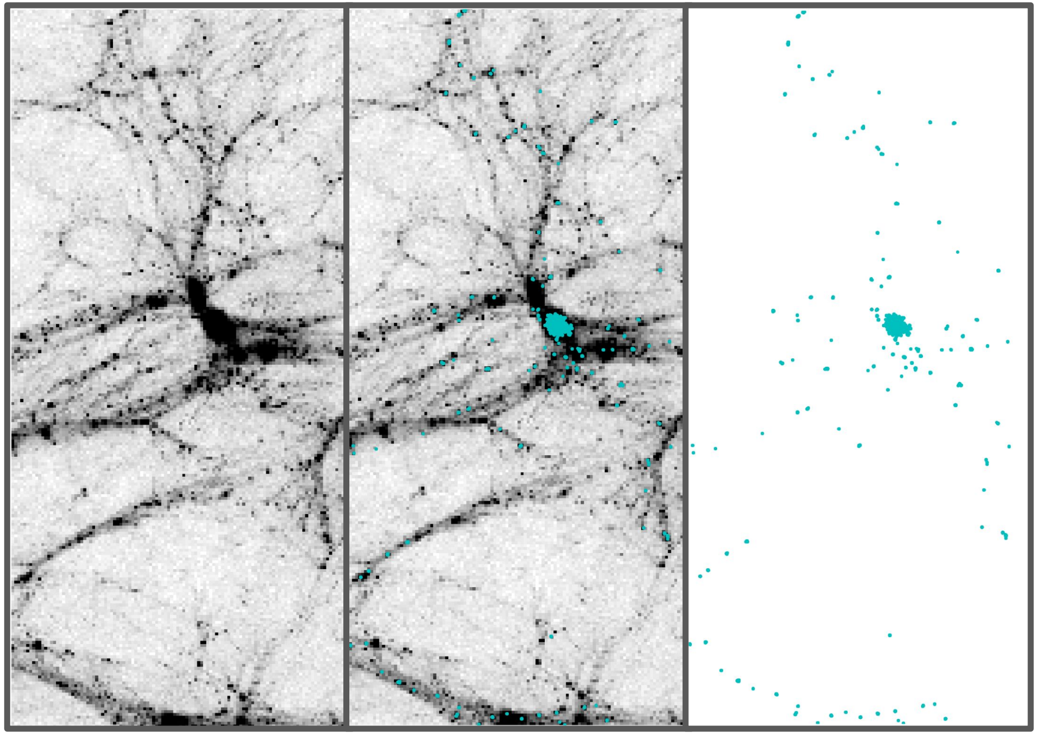

clustering

Biased observations

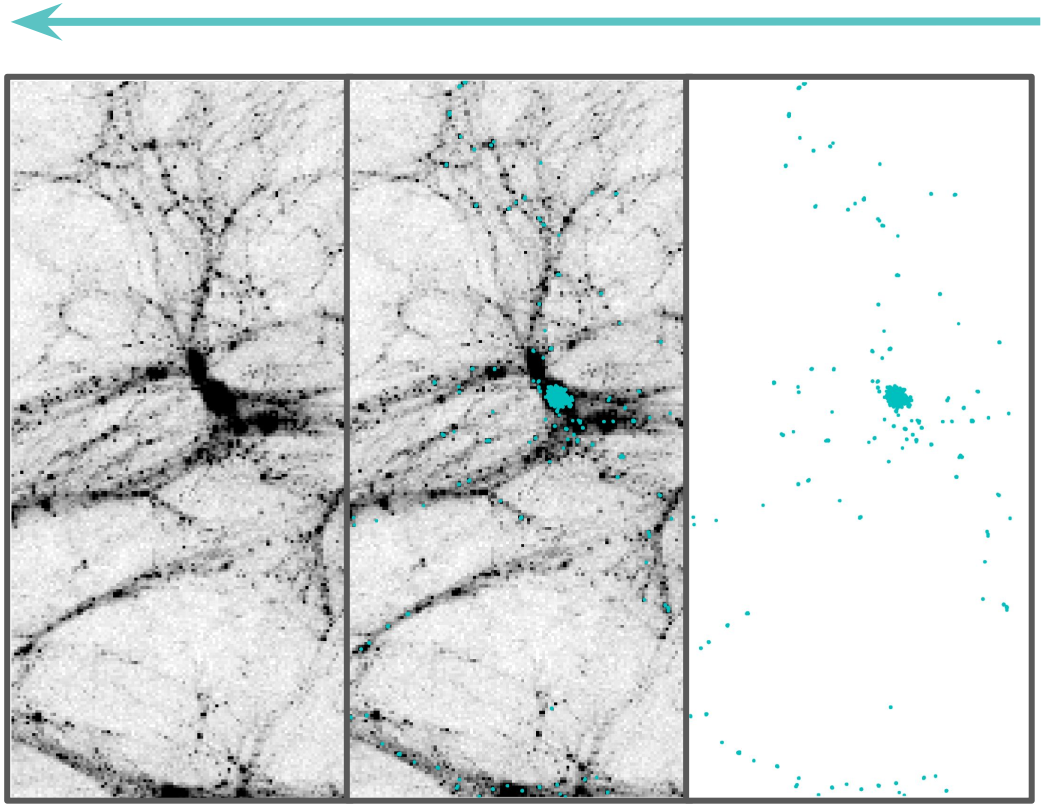

clustering

Degeneracy between progenitor masses and redshift
How to compute the source distance?

© LIGO Virgo Kagra Collaboration

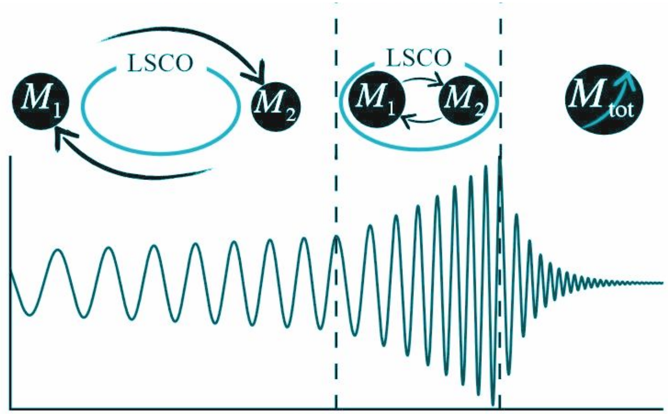

Sarah Libanore

Degeneracy between progenitor masses and redshift

How to compute the source distance?

© LIGO Virgo Kagra Collaboration

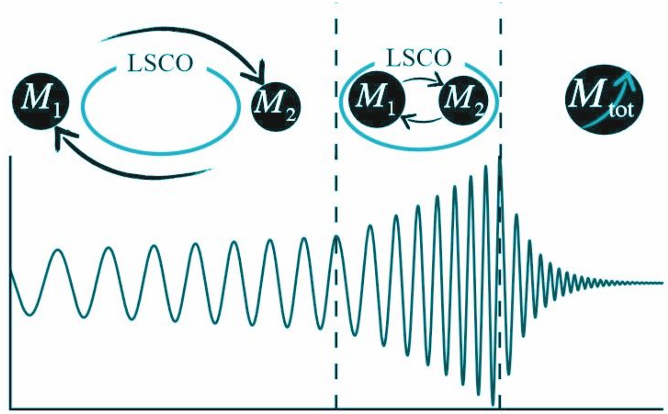

Binary mergers are

standard sirens

Luminosity distance

as radial coordinate

with no external data-sets required

Sarah Libanore

Einstein Telescope

Third generation interferometer, scheduled mid 2030s

Sensitivity ~10 times better than LIGO: ~10^6 events!

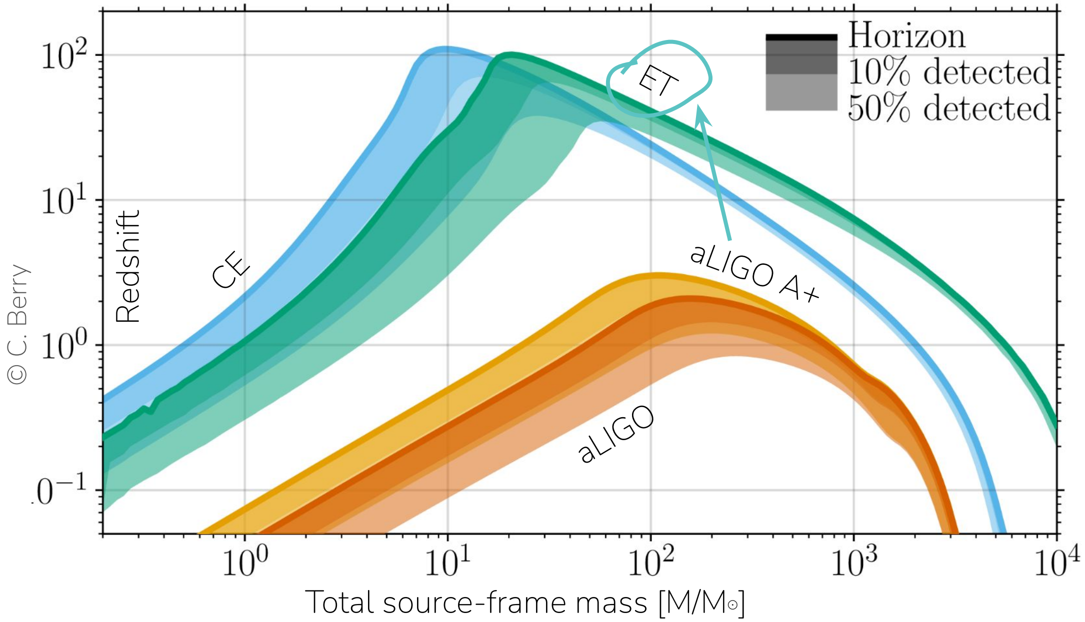

gravitational wave surveys

Forecasts to understand whether statistical analyses of future gravitational wave surveys can constrain...

constrain cosmology and astrophysics

Forecasts to understand whether statistical analyses of future gravitational wave surveys can constrain...

...*cosmological parameters*

High redshift and large volumes probed

Complementary to other tracers (galaxy surveys, intensity mapping...)

constrain cosmology and astrophysics

Forecasts to understand whether statistical analyses of future gravitational wave surveys can constrain...

...*cosmological parameters*

High redshift and large volumes probed

Complementary to other tracers (galaxy surveys, intensity mapping...)

...*bias parameters*

Only require the large scales

Understand formation channels and properties of the host galaxy

constrain cosmology and astrophysics

Sarah Libanore

Forecasts to understand whether statistical analyses of future gravitational wave surveys can constrain...

...*cosmological parameters*

High redshift and large volumes probed

Complementary to other tracers (galaxy surveys, intensity mapping...)

...*bias parameters*

Only require the large scales

Understand formation channels and properties of the host galaxy

constrain cosmology and astrophysics

Sarah Libanore

Merger clustering properties depend

on the *formation channel* of black hole binaries

constrain cosmology and astrophysics

Merger clustering properties depend
on the *formation channel* of black hole binaries

Astrophysical origin is related
with stellar evolution

Astrophysical Black Hole
mergers bias is linear
similarly to galaxy bias

constrain cosmology and astrophysics

Merger clustering properties depend

on the *formation channel* of black hole binaries

Astrophysical origin is related with stellar evolution

↓

Astrophysical Black Hole mergers bias is linear similarly to galaxy bias

In the Early Universe *Primordial Black Holes* can form from collapse of high density peaks

↓

If they bound in binaries and merge their *bias* will be different

constrain cosmology and astrophysics

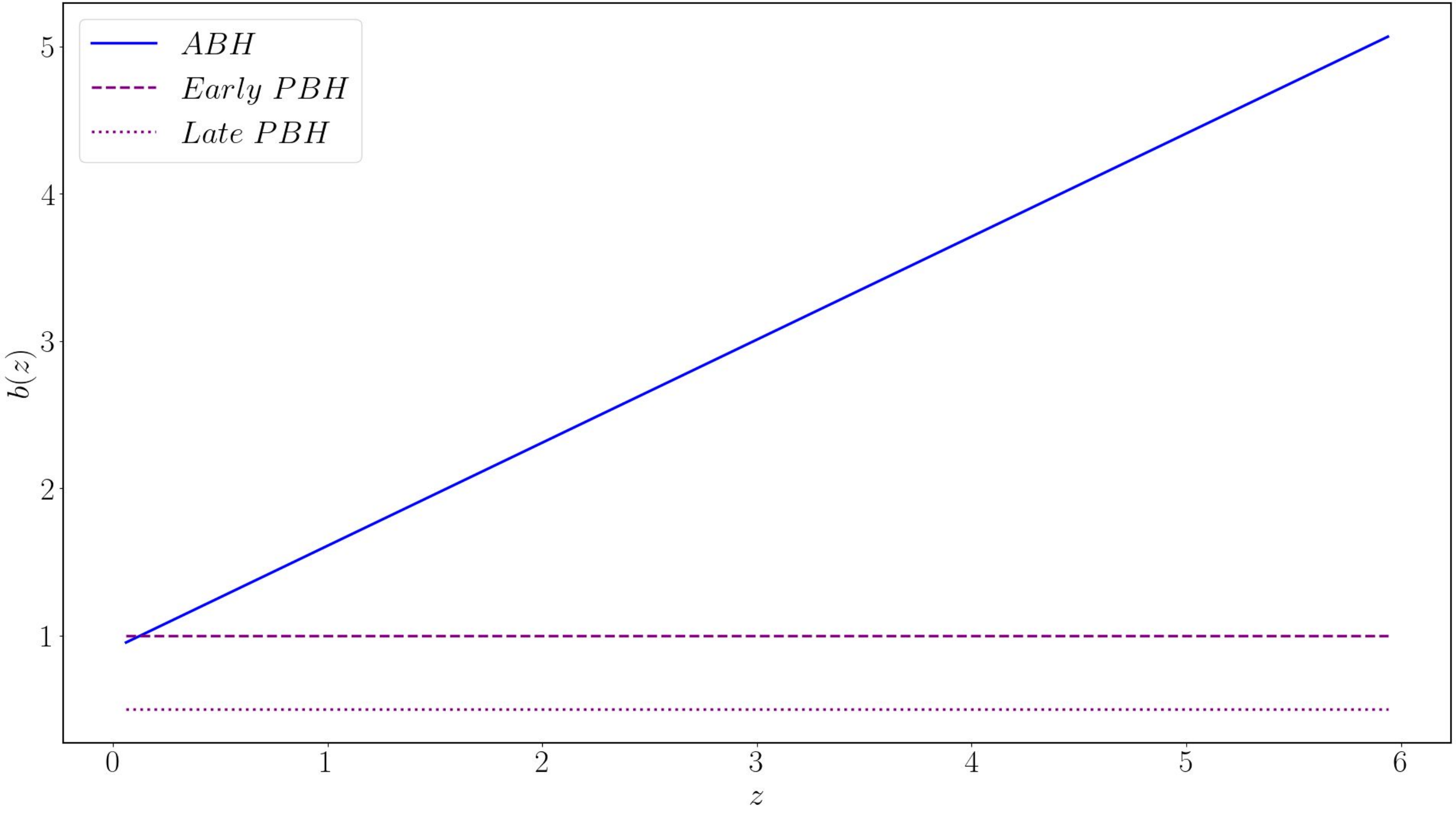

Libanore, Liguori, Raccanelli. in preparation

constrain cosmology and astrophysics

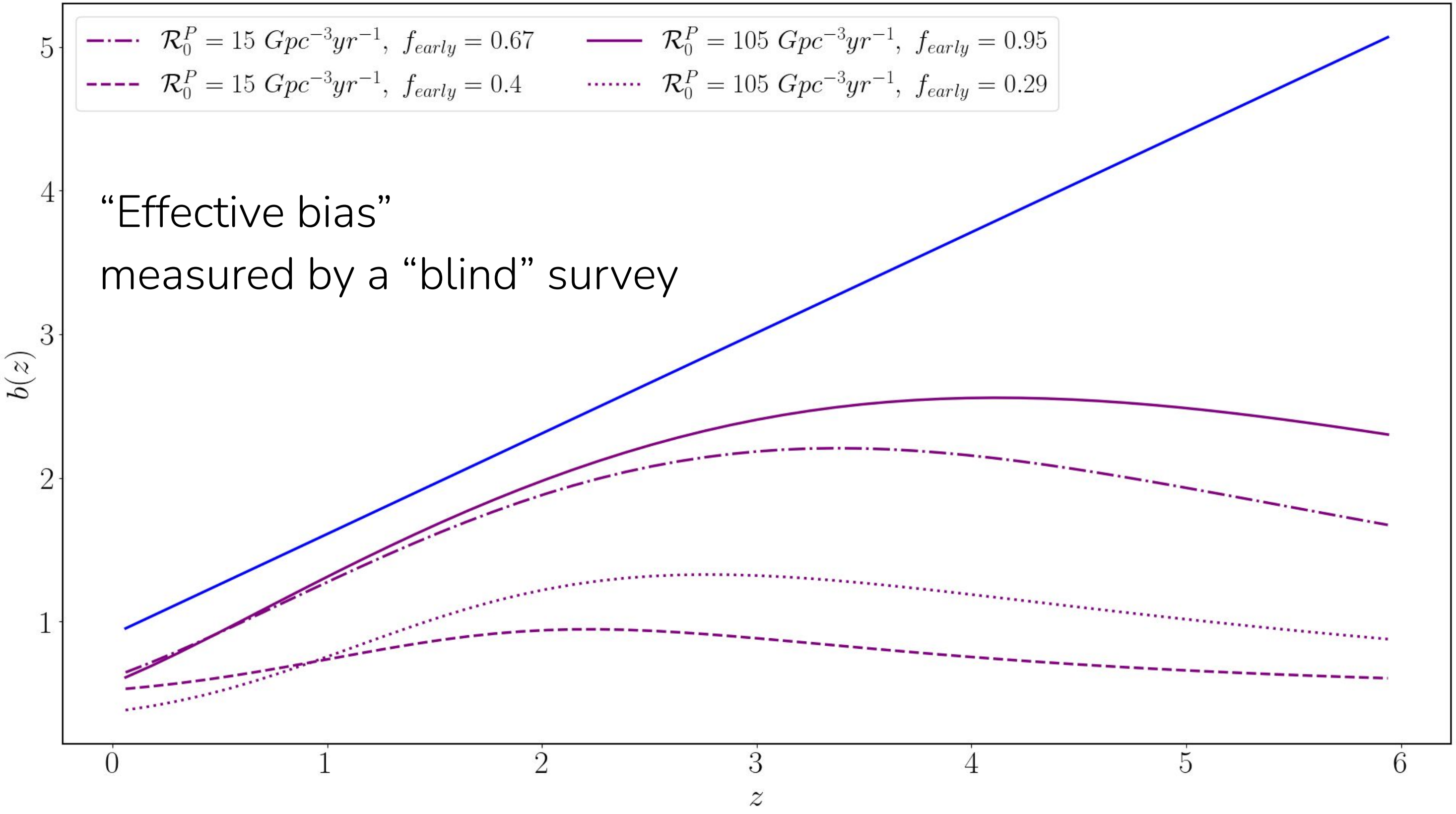

Libanore, Liguori, Raccanelli. in preparation

constrain cosmology and astrophysics

Sarah Libanore

The *clustering*

of future *gravitational wave surveys*

will be an effective tool to

constrain cosmology and astrophysics !

Thank you for your attention!

Sarah Libanore

Backup slides

Sarah Libanore

Estimated distances are perturbed
by the presence of large scale structures

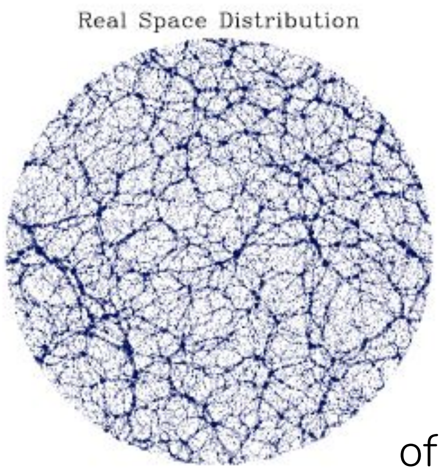

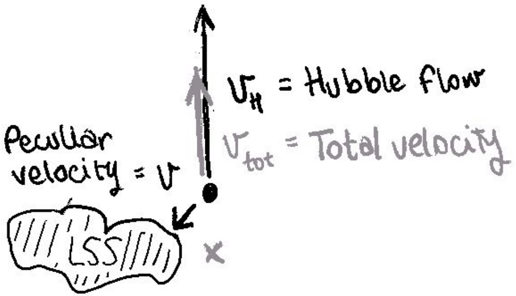

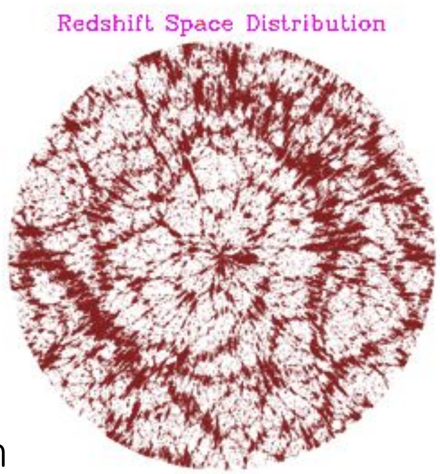

Tomographic analysis
of the angular power spectrum
requires a self-consistent computation of
luminosity distance space distortions

Backup slides

Sarah Libanore

$z = 0.7$

$z = 2.7$

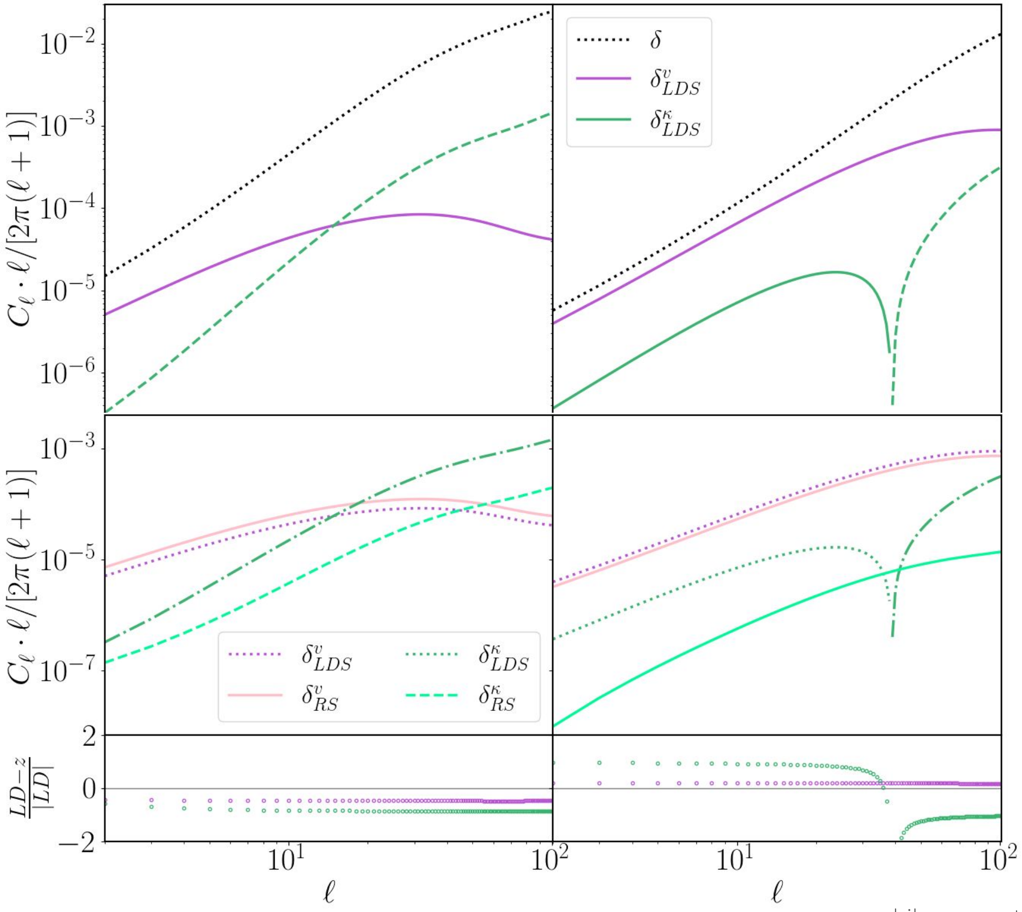

Libanore et al. JCAP02(2022)003

Backup slides

$$N_m^{\mathrm{SIM}}(z) = \sum_i \sum_j \langle N_m^{\mathrm{SIM}}(z) | M_*^i, SFR^j \rangle$$

$$N_m(z) \;=\; T^{\mathrm{OBS}} \frac{N_m^{\mathrm{SIM}}(z)}{T^{\mathrm{SIM}}(z)} \frac{dt^{\mathrm{SIM}}}{dt^{\mathrm{OBS}}} \;=\; T^{\mathrm{OBS}} \frac{N_m^{\mathrm{SIM}}(z)}{T^{\mathrm{SIM}}(z)} \frac{1}{1+z}$$

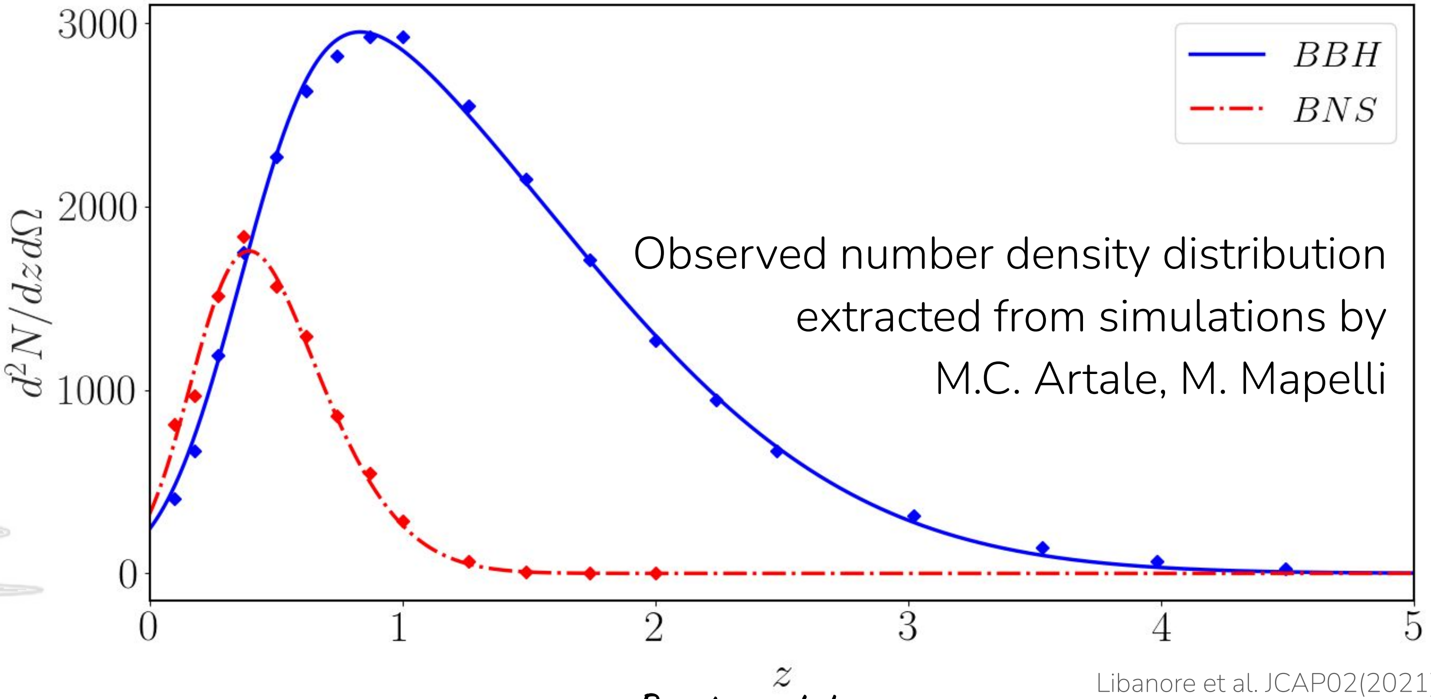

Observed number density distribution extracted from simulations by M.C. Artale, M. Mapelli

Libanore et al. JCAP02(2021)035

Backup slides

$$b_m(z) = \int_{M_*^{\min}}^{M_*^{\max}} dM_* \int_{SFR^{\min}}^{SFR^{\max}} dSFR\ n_g(z, M_*, SFR)\ b_g(z, M_*, SFR) \frac{\langle N_m(z) | M_*, SFR \rangle}{n_m(z)}$$

$$b_g(z, M_*, SFR) = \int_{M_h^{min,(*,SFR)}}^{+\infty} dM_h\ n_h(z, M_h)\ b_h(z, M_h) \frac{\langle N_g(M_*, SFR) | M_h \rangle}{n_g(z, M_*, SFR)}$$

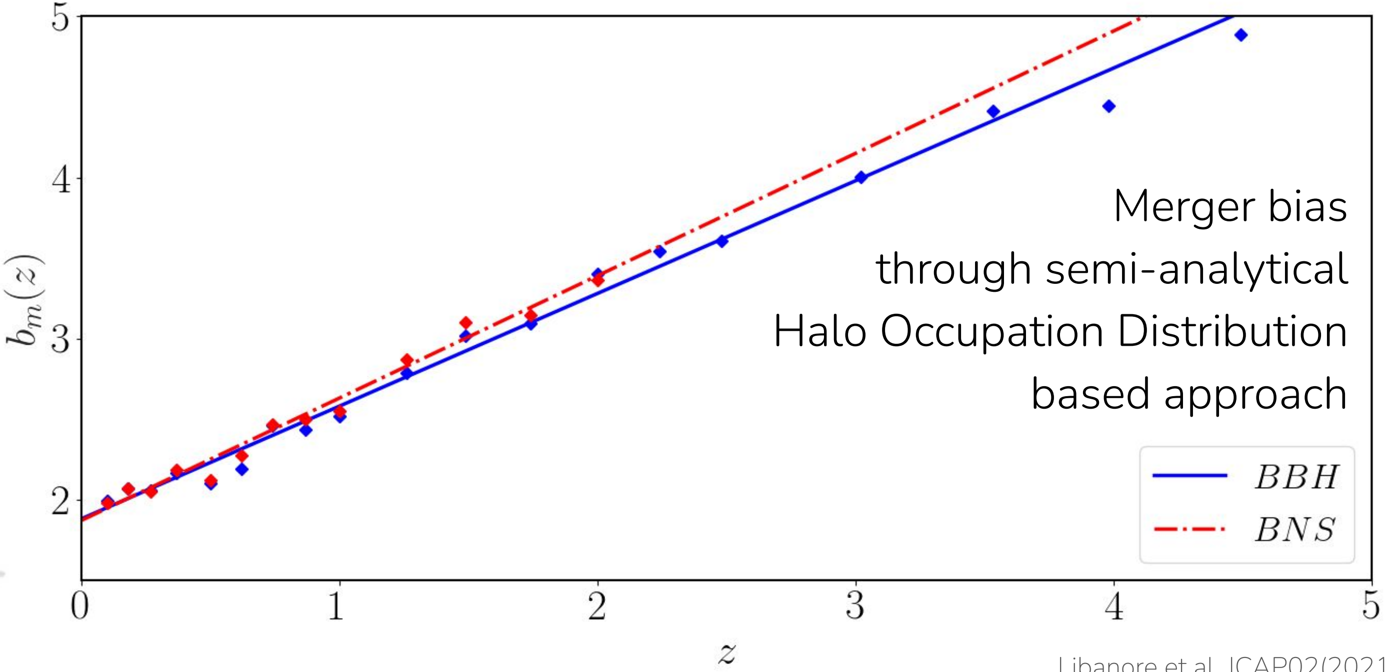

Libanore et al. JCAP02(2021)035

Backup slides

Merger bias
maximum likelihood
estimator
on mock data-sets

$$\tilde{b}^{lin}(k) \sim \sqrt{\frac{\tilde{P}_{merger}(k)}{\tilde{P}(k)}}$$

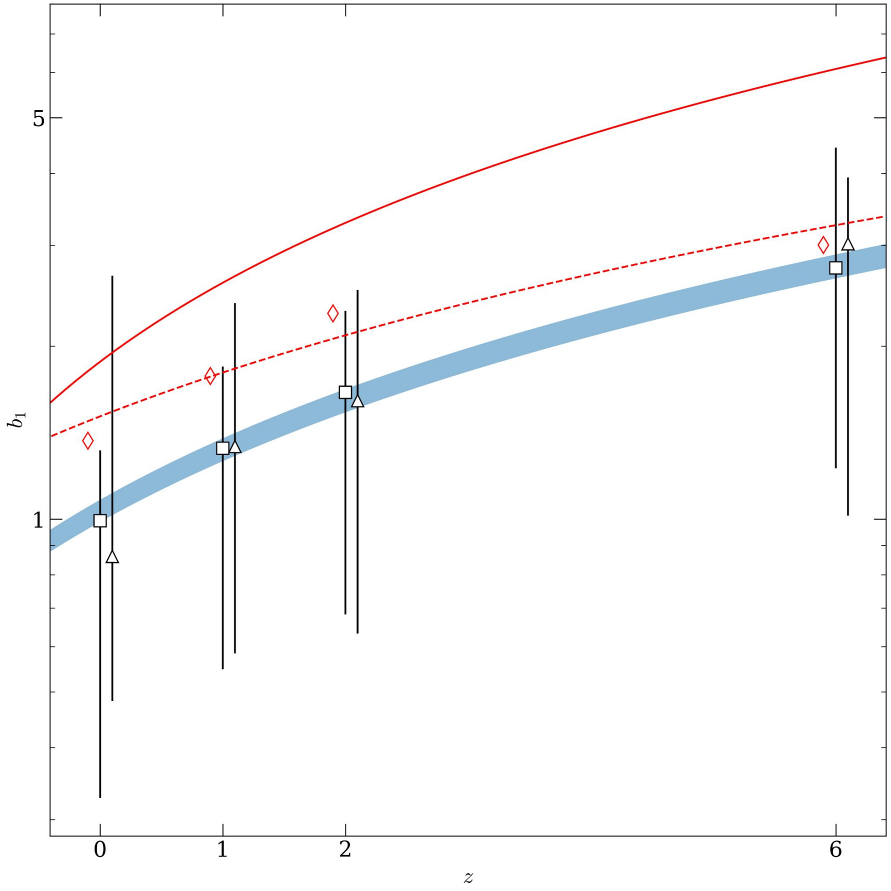

Peron, Libanore et al. in preparation

Backup slides

Observed Angular Power Spectra

Fisher matrix analysis

$$F_{\alpha\beta} = \sum_l \frac{2l+1}{2} f_{sky} \mathrm{Tr}\left[\partial_\alpha \mathbf{C}_l \, \Gamma_l^{-1} \partial_\beta \mathbf{C}_l \, \Gamma_l^{-1}\right]$$

Both single and multi tracer can be considered
to get cosmological and bias parameter constraints

[1]: $\Theta = [H_0, \Omega_c h^2, w_0, w_a, b_m^0, \ldots, b_m^n]$

[2]: $\Theta = [H_0, \Omega_c h^2, w_0, w_a, \Omega_b h^2, n_s, A_s, A_i, P_i]$

Einstein Telescope (x3)

Survey	Source	Area [deg^2]	$\Delta D_L/D_L$	$\Delta\Omega$ [deg^2]	z_{max}	T^{OBS}	N^{TOT}
ET	DNS BHNS DBH	Full sky	0.3 0.3 0.1	100	2 3 5	3yr	$10^{4.14}$ $10^{4.37}$ $10^{4.79}$
ET×3	DNS BHNS DBH	Full sky	0.3 0.3 0.1	10 10 3	2 3 5	3yr	$10^{4.14}$ $10^{4.37}$ $10^{4.79}$

Sarah Libanore

$$b_g(z, M_*, SFR) = \int_{M_h^{min,(*,SFR)}}^{+\infty} dM_h \; n_h(z, M_h) \; b_h(z, M_h) \frac{\langle N_g(M_*, SFR)|M_h \rangle}{n_g(z, M_*, SFR)}$$

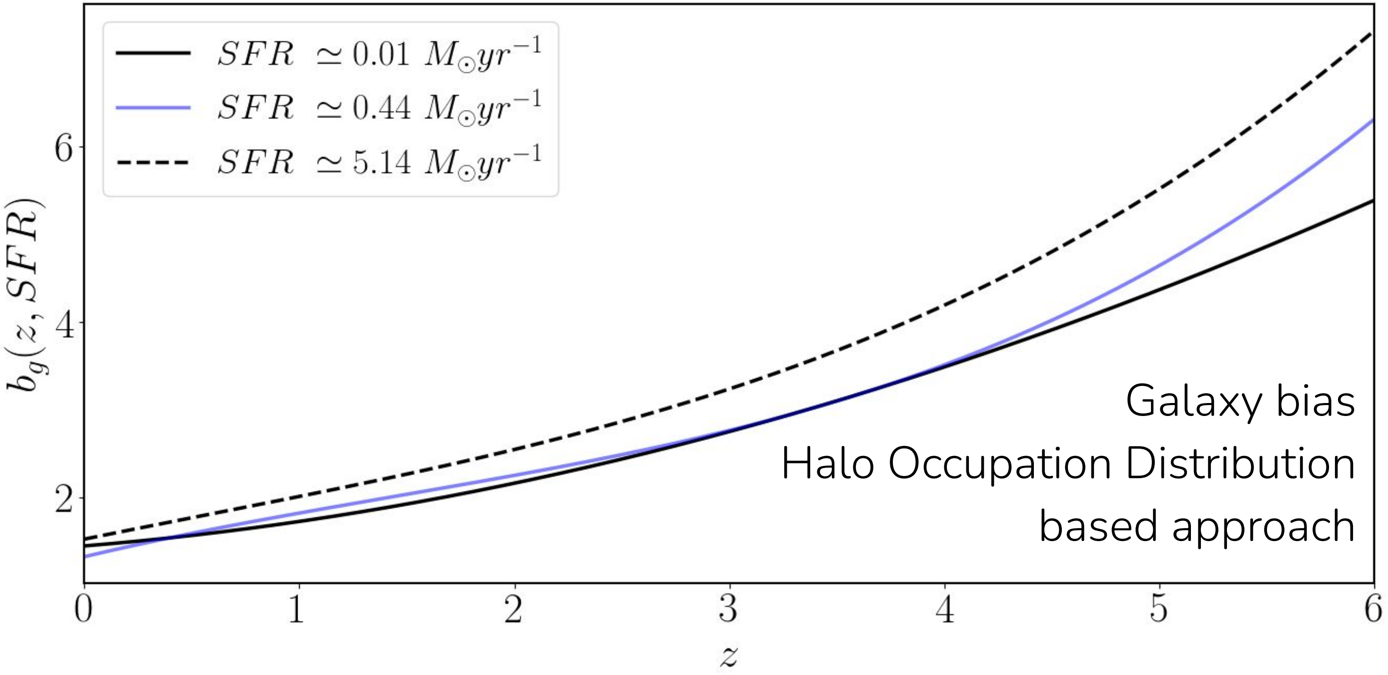

Galaxy bias

Halo Occupation Distribution based approach

Backup slides

Sarah Libanore

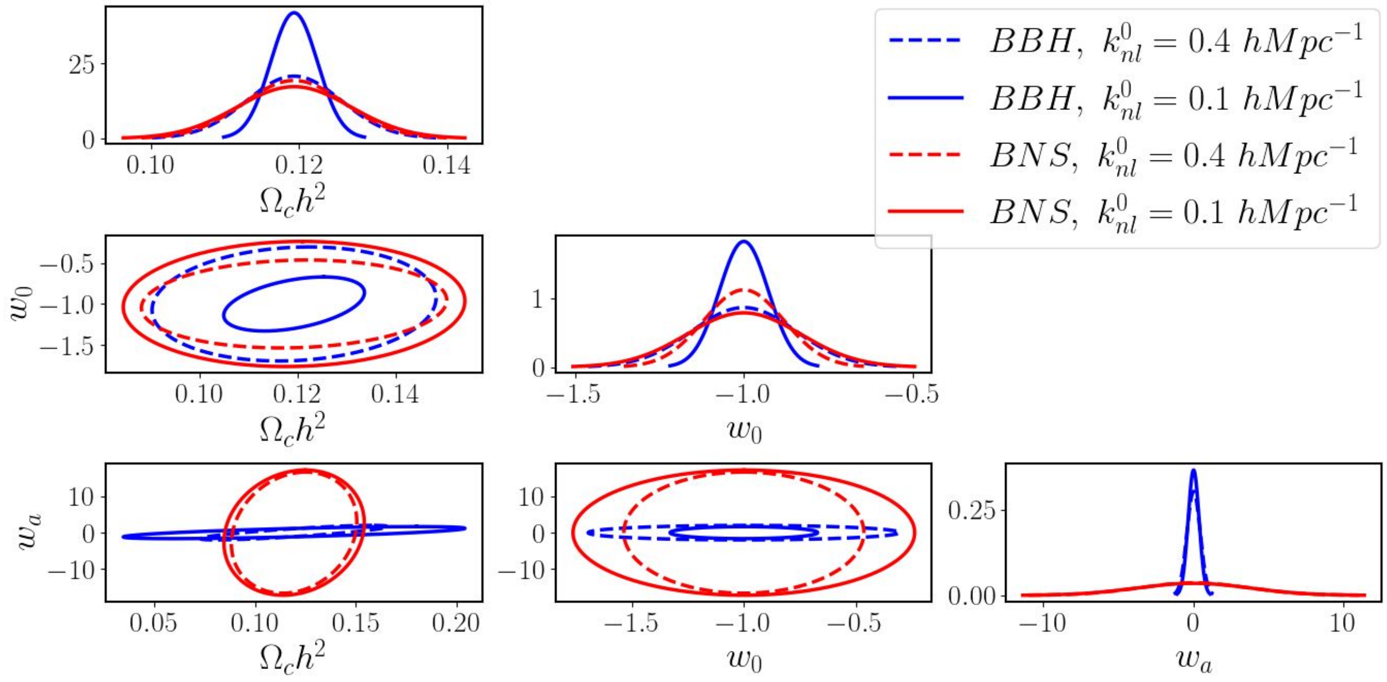

Backup slides

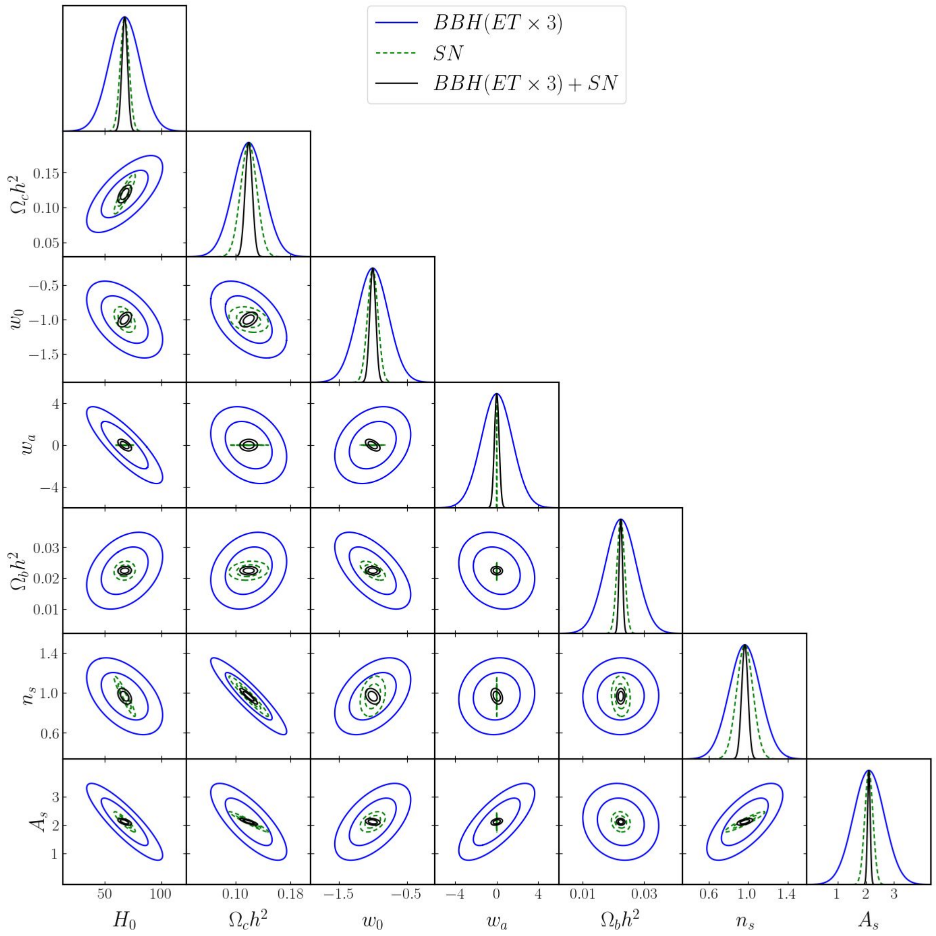

Backup slides

$$\Theta = [H_0, \Omega_c h^2, w_0, w_a, b_m^0, \ldots, b_m^n]$$

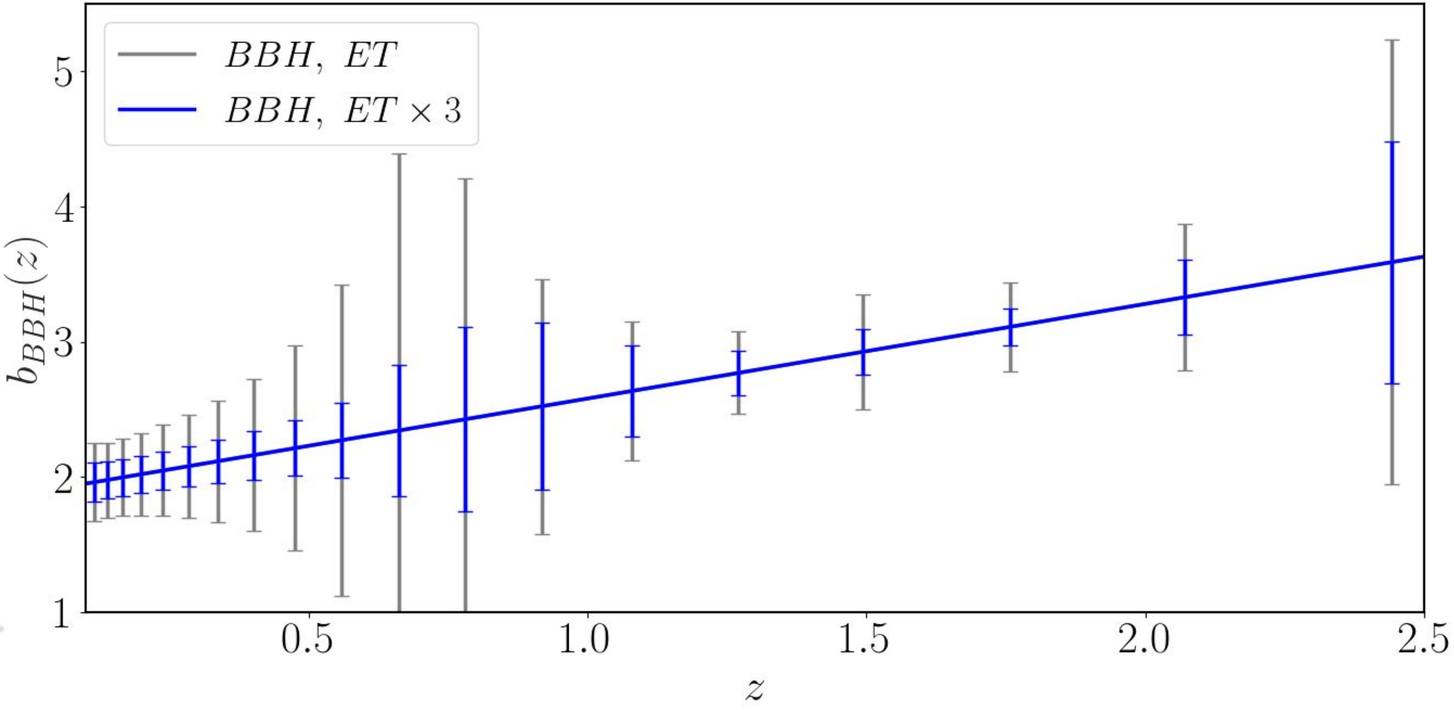

Libanore et al. JCAP02(2021)035

Backup slides

$$b_m(z) = A_m(z + B_m)^{P_m}$$

$$\Theta = [H_0, \Omega_c h^2, w_0, w_a, \Omega_b h^2, n_s, A_s, A_i, P_i]$$

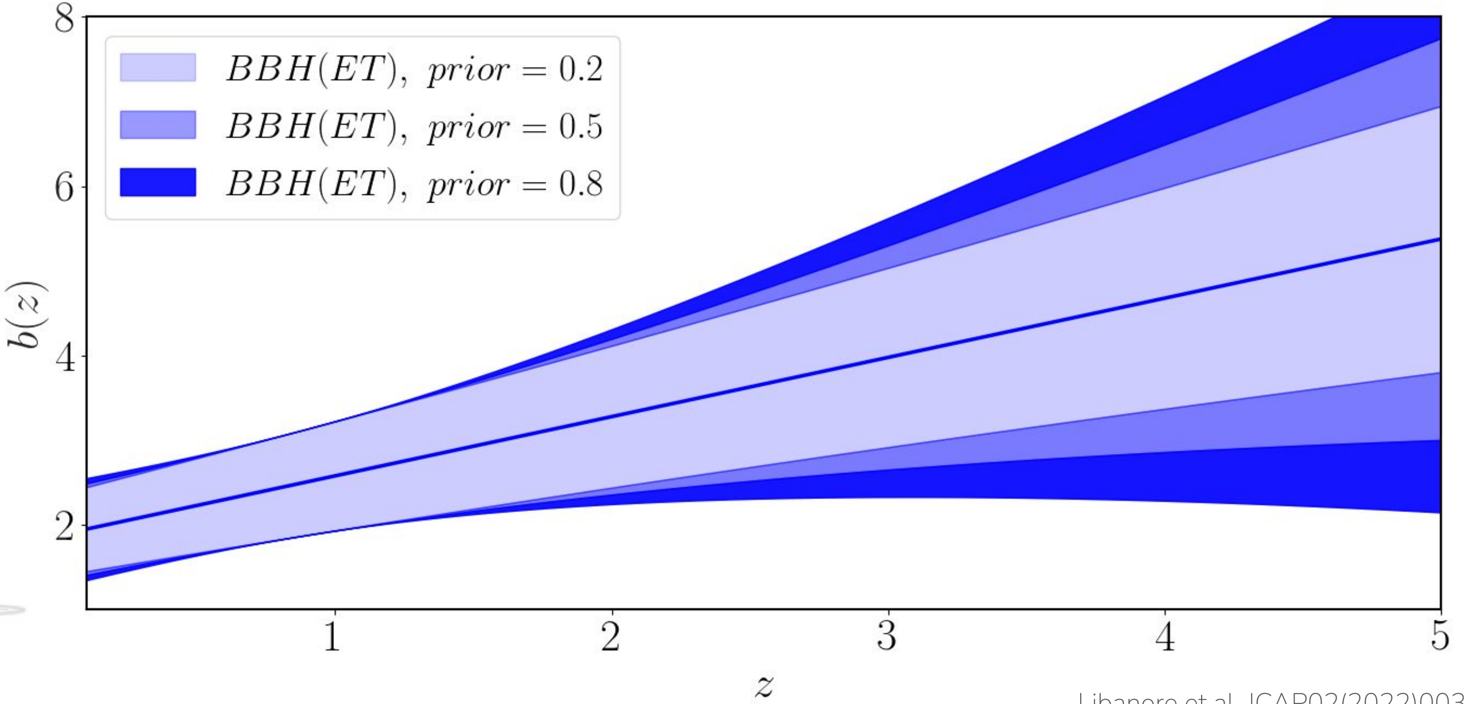

Libanore et al. JCAP02(2022)003

Backup slides

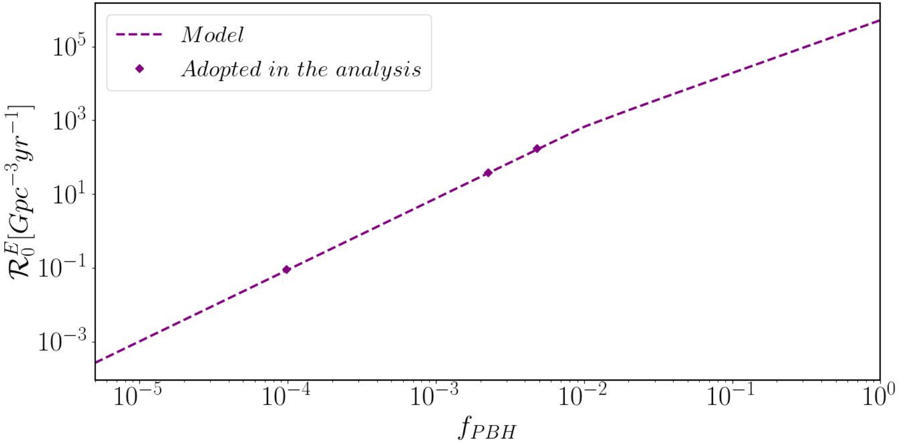

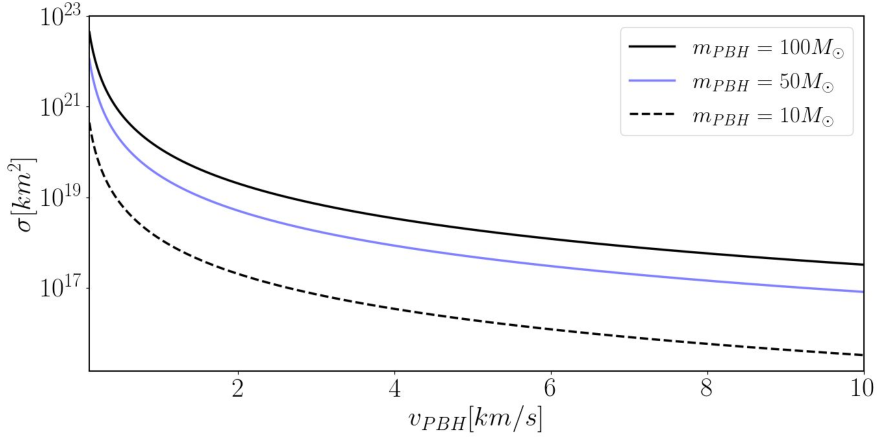

Early binaries

bound during radiation era
depending on the surrounding
dark matter content

Late binaries

dynamical capture
in small dark matter halos

Libanore, Liguori, Raccanelli. in preparation

Backup slides